MOIR, LEE A (2016) The use of thermoresponsive nanoparticles for targeting cancer cells. PhD thesis, University of Nottingham.

The Use of Thermoresponsive Nanoparticles for Targeting Cancer Cells

Lee A. Moir MChem (Hons.)

Thesis submitted to the University of Nottingham for the degree of Doctor of Philosophy

September 2015

Abstract

The aim of this thesis was to investigate a dual method of targeting cancer cells with a nanoparticle system containing both a thermoresponsive corona and folate tag. The nanoparticle system used a 'hide-and-reveal' motif whereby the folate tag would only be revealed above the transition temperature of the thermoresponsive corona.

There were difficulties encountered during the synthesis of poly(lactide-*co*-glycolide) (PLGA) for the further polymerisation of the thermoresponsive copolymer therefore poly(lactide) (PLA) was synthesized as an alternative. The initial thermoresponsive polymer library synthesised (PLGA-*b*-poly((polypropylene glycol methacrylate)-*stat*-(oligoethylene glycol methacrylate))) when assembled into nanoparticles had a transition temperature (T_t) of 40 – 65 °C and thus did not have a low enough T_t for the cell studies. A second polymer library (PLA-*b*-P((diethylene glycol methacrylate)-*stat*-(oligoethylene glycol methacrylate)), PLA-*b*-P(DEGMA-*stat*-OEGMA)) when assembled into NPs had a T_t of between 28 – 78 °C when the DEGMA:OEGMA ratio was altered from 100:0 to 50:50. In addition to the thermoresponsive polymer library, three folate tagged amphiphilic polymers were synthesised. The polymers were PLA-*b*-polyethylene glycol (PLA-PEG) with a terminal folate. Each of the three PLA-PEG$_x$ polymers were synthesised with a different length of PEG, PEG$_{450}$, PEG$_{3k}$ and PEG$_{10k}$.

A reproducible method of nanoparticle assembly was developed which produced nanoparticles of an average radius of ~100 nm when PLA-*b*-P(DEGMA-*stat*-OEGMA) polymers were used.

Three methods of controlling the overall aggregation temperature were put forward. By assembling NPs using one type of PLA-*b*-P(DEGMA-*stat*-OEGMA) the T_t of the NPs was dependent on the ratio of DEGMA:OEGMA. It was also possible to control the aggregation temperature by mixing two types of PLA-*b*-P(DEGMA-*stat*-OEGMA) polymers (provided the difference in DEGMA:OEGMA between the two polymers was between 0 − 10 %). In addition by mixing PLA-*b*-P(DEGMA-*stat*-OEGMA) preformed NPs the aggregation temperature could be controlled similar to that for polymer blend NPs.

The NPs were tested in both MCF-7 and HCT116 cell lines and were shown to have no adverse effect on the cell metabolism or membrane integrity when the NP concentration was below 4 mg/mL. It was found that there was in increase in uptake of the thermoresponsive NPs when incubation temperature was above the NPs T_t. When the PEG_{450} and PEG_{3k} linked folate was used an increased uptake was observed in MCF-7 cells however no difference in uptake was observed in HCT116 cell line.

Overall the 'hide-and-reveal' motif on this NP system was shown to be successful in enhancing the uptake in folate receptor positive cells.

Acknowledgements

Firstly, I would like to thank my supervisors from the University of Nottingham, Prof. Cameron Alexander, Dr. Jon Aylott and Dr. Sebastian Spain, and AstraZeneca, Dr. Marianne Ashford and Dr. Paul Gellert, for their help and support throughout my PhD; especially to Dr. Sebastian Spain for his help in the lab showing me how to actually make polymers! I would also like to thank all the members of B15 lab for keeping me going through the good times and the bad (as well as teaching me a couple of words of Italian). I am very grateful for the support offered by Dr. Laura Purdie and Mrs. Pamela Collier for help with the cell work and microscopy experiments.

I would like to acknowledge both the University of Nottingham American Football team, especially Coach Phil Wood for all that I have learnt, for not only the chance to represent the university in a sporting event, something I never thought I would do, but especially the chance to knock some heads when it had been a bad day/week in the lab!

A large amount of thanks goes to the CDT and especially my cohort (Andreea, Francesco, Jamie and Naim) for not only their academic support but also their social support! I would also like to thank my Mum, Dad and extended family who have supported me all the way through.

Finally the largest thanks go to my girlfriend Kathryn, who has had to put up with all the bad moods as well as the good. Without her support all the way

to the end I may well have faltered through those less than happy times that beset almost all PhD students along the way!

Table of Contents

Abbreviations

abs	Absorbance
AGET	Activator generated by electron transfer
ATRP	Atom transfer radical polymerisation
b	Block (copolymer)
cat.	Catalyst
CSP	Core-shell nanoparticle
Đ	Polydispersity (M_w/M_n)
Da	Dalton
DBU	1,8-Diazabicyclo[5.4.0]undec-7-ene
DEGMA	Diethylene glycol methacrylate
DLS	Dynamic light scattering
DMAc	Dimethylacetamide
DMF	Dimethylformamide
DMSO	Dimethyl sulfoxide
DNA	Deoxyribonucleic acid
DOX	Doxorubicin
DP	Degree of polymerisation
e.e.	Encapsulation efficiency
EDTA	Ethylenediaminetetraacetic acid
EH	2-ethylhexanoate
EPR	Enhanced permeation and retention
EtOAc	Ethyl acetate
FA	Folic acid
FR	Folate receptor
GPC	Gel permeation chromatography
HA	Hyaluronic acid
HBSS	Hank's balanced salt solution
HUVEC	Human umbilical vein endothelial cell
ini	Initiator

LCST	Lower critical solution temperature
LDH	Lactate dehydrogenase
M_n	Number average molecular weight
M_w	Weight average molecular weight
NAD	Nicotinamide adenine dinucleotide
NMR	Nuclear magnetic resonance
NP	Nanoparticle
OEGMA	Oligoethylene glycol methacrylate
PBS	Phosphate buffered saline
PEG	Polyethylene glycol
PFA	Paraformaldehyde
PLA	Poly(D,L-lactide)
PLGA	Poly(D,L-lactide-*co*-glycolide)
PNIPAM	Poly(*N*-isopropylacrylamide)
PPGMA	Polypropylene glycol methacrylate
PTX	Paclitaxel
r.p.m	revolutions per minute
RAFT	Reversible addition–fragmentation chain transfer
ROP	Ring opening polymerisation
RPMI	Roswell Park Memorial Institute (cell culture medium)
SPR	Surface plasmon resonance
stat	Statistical (copolymer)
TBD	1,5,7-Triazabicyclo[4.4.0]dec-5-ene
TEM	Transmission electron microscopy
T_t	Transition temperature
UCST	Upper critical solution temperature
VEGF	Vascular endothelial growth factor

1 Introduction

Recent research in drug delivery has led to the development of new and innovative delivery systems.[1] The need for these new systems stems from the ever increasing push to make drugs safer and more efficient. Various systems have been used for this purpose including liposomes, micelles, dendrimers and other polymeric particles. Many of these such types of nanoparticles have found a use within cancer treatments.[2]

In general, there are many hurdles a drug molecule and carrier must overcome before it can cause a therapeutic response at the relevant site. Macrophages and the reticuloendothelial system (RES), as well as organs such as the kidneys and liver, cause rapid excretion from the bloodstream and thus lower bioavailability of drugs. With solid tumours comes another type of challenge, how to get the drug molecule to the cells when they are in a hypoxic (low oxygen) environment. This is caused by the lack of blood vessels to the innermost regions of the tumour. This, though, can offer an advantage for drug delivery due to the type of blood vessels that grow into the tumour area. This so called 'leaky' architecture, part of the enhanced permeability and retention (EPR) effect,[3] allows for the accumulation of macromolecules, a possible target for nanoparticle drug delivery vehicles.

A core-shell nanoparticle (CSP) is one such type of drug delivery and in certain circumstances diagnostic vehicle that has been developed to overcome the hurdles mentioned above. CSPs consist of a core to allow for the encapsulation or attachment, by chemically bonding the drug to the core, of

hydrophobic/poorly-soluble drug molecules, whilst the shell is hydrophilic for transport around the body in the bloodstream. Therefore allowing for longer circulation times and in turn increasing the bio-availability.[4]

An advantage of these types of nanoparticles is that they are capable of being targeted both actively and passively.[5]

1.1 Passive targeting

Passive targeting of these drug delivery vehicles uses the EPR effect to allow large macromolecules and particles to be transported through the permeable vasculature surrounding solid tumours.[6] The EPR effect is a characteristic of solid tumours which have elevated levels of permeability factors, such as nitric oxide and bradykinin.[7,8] These permeability factors in conjunction with a proteinaceous vascular permeability factor (VPF) similar to vascular endothelial growth factor (VEGF),[9] leads to the formation of leaky vasculature around solid tumours. This so called 'leaky' nature of the vasculature results in the extravasation of plasma proteins and most importantly of all, for drug delivery purposes, macromolecules and lipid particles.

1.2 'Active' targeting

The so-called active targeting, where by a specific active site is targeted on the diseased cells using a ligand was first proposed over 100 years ago by Paul Ehrlich the founder of chemotherapy (for which he won the Nobel prize for Physiology or Medicine in 1908).[10] Ehrlich's proposed idea of using 'magic bullets' to seek out and treat only the diseased site has been the foundation for many research groups work over the last century.

The approach of active targeting is aimed at increasing the interactions between specific cells and the NPs targeting them, therefore enhancing the selectivity of the uptake and delivery of drugs without altering the overall biodistribution.[11,12]

Numerous cancerous tumours overexpress certain factors which can be taken advantage of to target nanoparticles for site-specific uptake and drug delivery. One such over expressed factor is the folate receptor. It has been shown that by conjugating folate to a macromolecule uptake of the NP into tumour cells increases.[13] This idea has been used by many research groups since this discovery and will be discussed later in this chapter.[14-19]

CSPs have found a niche in so called 'smart materials' where, with the use of certain types of materials, the CSPs respond to different stimuli whether they are applied externally or through changes within the body. This use of stimuli-responsive materials has allowed scientists to target the changes both within and surrounding tumour tissues as a method for treating the disease.

In this introduction some of the recent examples of the use of stimuli-responsive CSPs and the site specific targeting of said CSPs will be outlined.

1.3   Types of Core

There are 3 main types of core used for stimuli-responsive CSPs: iron (magnetic), gold and polymeric material, Figure 1. With each of these types of cores offering different characteristics dependant on what is required.
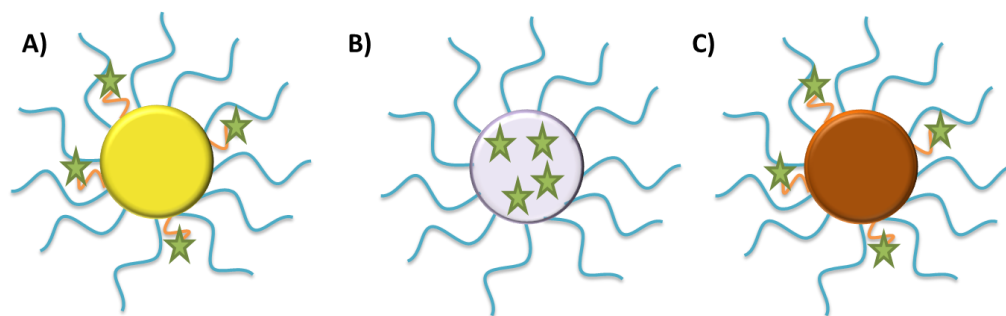
Figure 1 General schematic of three different types of CSPs. A) Gold CSP. B) Polymer CSP. C) Iron oxide CSP. Green star denotes drug/dye molecules.

1.3.1   Inorganic

1.3.1.1   Gold (Au NPs)

Au NPs have recently found themselves to be a promising tool as a delivery agent as they have many desirable characteristics. Gold itself is essentially inert, non-toxic and so making it biocompatible.[20,21] 2 key aspects of Au NPs are that, firstly, they can be fabricated relatively easily in a range of core-sizes from 1 - 150 nm.[22] Secondly, the high surface-to-volume ratio of Au NPs allows for incorporation of multiple shell types and targeting ligands.[23]

With the possibilities of controlling the structure of the Au NPs, either spheres or nanorods, there has been interest in determining how these two morphologies affect the cell uptake. Arnida *et al*. tested both rod and sphere type NPs with a PEG shell for their toxicity and uptake in human prostate cancer cells.[21] It was determined that neither morphologies had a detrimental effect on the cell viability however the smaller of the spheres (30 and 50 nm) were taken up to a higher extent than the larger (90 nm) spheres. For the rods the opposite was true whereby the larger of the rods (45 nm) showed an increased uptake when compared with the smaller (35 nm) rods. The group concluded that it was the core size and not the hydrodynamic volume that

determined the level of uptake. When similar particles were tested *in vivo* the nanorods with a PEG coating were taken up to a lesser extent by the liver than the PEGylated Au spheres.[24] The geometry of the particles also had an effect on the uptake by macrophages as the PEGylate nanorods showed a significantly lower uptake than the spheres.

Au NPs also offer an alternative option to other types of NPs as they can be heated due to a phenomenon known as surface plasmon resonance (SPR) whereby light energy is transformed into heat.[25] This is advantageous as a treatment with gold particles alone as they can be used for thermal ablation therapy. By using gold nanorods, shown above to offer advantages over their spherical counterparts, local hyperthermia at tumour sites can be achieved. By injecting gold nanorods into mice Dickerson *et al*. showed that tumour growth could be inhibited by simply heating the nanorods with near infra-red light.[26] Similar targeting and hyperthermia induced growth inhibition has been noted *in vitro* and *in vivo* by others as it becomes a burgeoning area for preclinical non-invasive cancer therapy.[27-29]

Au has shown to be susceptible to external stimuli when grafted with specific types of polymers to form a shell. PNIPAM,[30] thiol-terminal PEG,[31] poly(acrylic acid) to form star block copolymers,[32] and poly(vinyl pyridine)[33] have all been used to form a responsive shell. The possibility of heating Au NPs is also advantageous when NPs are coated with a thermoresponsive polymer coating. The opportunity of specifically inducing a temperature switch through the heating of the Au NPs has been exploited by Barhoumi *et al*. to

enhance the uptake of gold shell NPs.[34] By coating the gold shell with PNIPAM a peptide ligand attached to the gold surface could be revealed when the temperature was raised above the polymer's transition temperature, thus offering a heightened NP uptake compared to non-targeted versions.

Au NPs are never likely to offer long term use as a drug delivery vehicle due to a lack of hollow core and so removing the possibility of drug encapsulation. The need to chemically alter any drug molecules used in order to facilitate conjugation/adsorption to the Au surface or NP shell is also a weakness. The use of Au Ns in thermal treatments does however offer the possibility of this being a long term efficacious treatment without the need for small drug molecules to be attached.

A similar type of inorganic particle uses an iron core, although it has similar disadvantages as Au it does have one major advantage as it can be used for diagnostics as well as uses in therapeutic areas.

1.3.1.2 Iron Oxide (Magnetic)

CSPs using a magnetic core (MCSP) can be used for both targeting and imaging.[35,36] This stems for the recent increase in 'theranostic' agents, which allows both for the controlled release of a drug molecule and for imaging of the site using clinical techniques such as MRI[37] due to iron being an effective contrast agent.

As with for Au NPs, iron is used mostly as a solid core with the surface functionalised with different substances depending on what is required. Kievit

et al gave an example of using a drug loaded iron oxide NP coated with a PEG shell for the pH responsive delivery of DOX.[38] Huang *et al* showed the guiding of MCSP (using superparamagnetic iron oxide nanoparticles with a shell of Pluronic F127 and poly(DL-lactide)) was enhanced when an external magnetic field was applied.[39]

A recent alternative to the use of Fe as the entirety of the core is to use a poly(lactic-co-glycolic acid) (PLGA) core embedded with magnetite nanoparticles, thus offering the need for less iron to be present and using a biocompatible polymer for delivery.[40] The Nguyen group previously used CSPs to be used for drug delivery using poly(N-isopropylacrylamide–acrylamide–allylamine) (PNIPAAM-AAm-AH)-coated magnetic nanoparticles with PLGA as the shell.[41] However, the magnetic particles were not all contained in the core and a portion was present on the surface which led to uncontrolled drug release and an inefficient drug delivery vehicle. Nguyen *et al* successfully synthesised the magnetic CSPs using a layer-by-layer technique and carried out both *in-vitro* and *in-vivo* studies. It was found that by using the targeting of Gly-Arg-Gly-Asp-Ser (GRGDS) peptides the uptake was increased over the bare MCSPs. While *in-vivo* investigations showed that with the use of a magnet the MCSPs accumulated exclusively at the tumour in a mouse model.

The downside of using magnetic CSPs is using a magnet of sufficient strength to enable control at deep lying tumours can lead to adverse physiological effects.

To fulfil the potential of CSPs for use in the clinic organic/polymer core NPs offer the main route from benchtop to the hospital bed as the use of hollow cores can lead to higher drug transport than inorganic based CSPs.

1.3.2 Organic

There have been many different types of organic polymer materials used to make diverse forms of nanaoparticles over the last few decades.[42-45] When amphiphilic block copolymers are used a CSP can be formed, the hydrophilic polymer forms a protective shell over the hydrophobic section which can in turn house hydrophobic guests, such as drugs and dyes. The functionalisation of polymers allows for the attachment of both targeting ligands[14] and cell-penetrating peptides[46] to aid in the delivery.

The focus of the remainder of this chapter will be on the use of these polymer CSPs due to the advantages with using organic/polymer core materials and the use of these as stimuli-responsive drug delivery vehicles.

1.4   Types of Stimuli
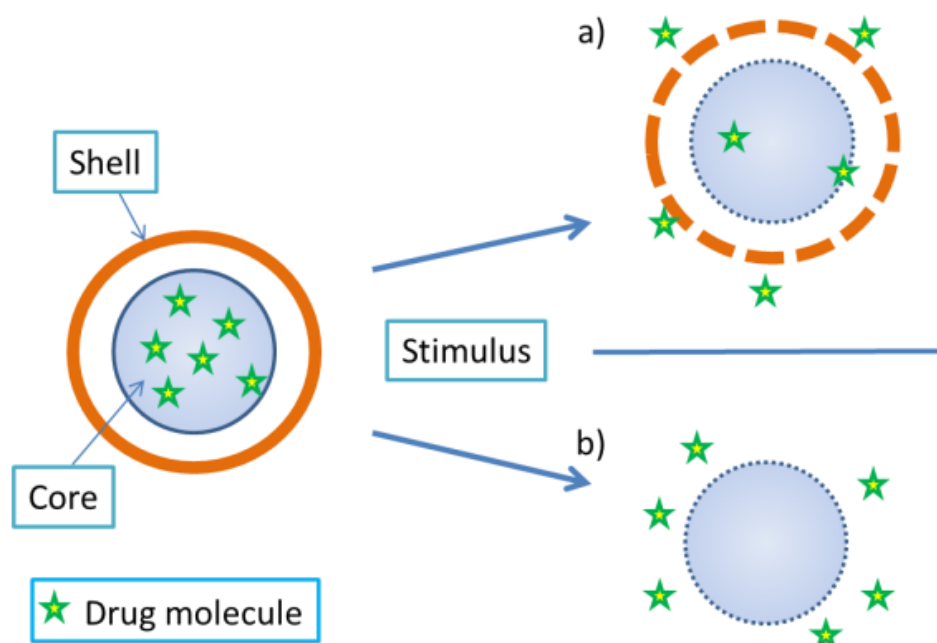
Figure 2 Depiction of a core-shell nanoparticle. **a) After a stimulus the shell becomes 'leaky' allowing for release of drug molecule. b) Complete degradation of shell to allow release of drug from core.**

There are many stimuli used to initiate a response from smart material, Table 1.

Table 1 Types of stimuli that can be used to initiate a response from 'smart' materials. [47]

Physical stimuli	Chemical and biochemical stimuli
Temperature	Specific ions
Ionic strength	Chemical agents
Solvents	Host–guest interaction
Magnetic field	Antigen–antibody interaction
Electric field	Enzyme substrates
Electromagnetic radiation (UV, visible)	Affinity ligands
Mechanism stress, strain	Other biochemical agents

Below we will focus on two of the types of local stimuli used to bring about the site specific release of CSPs cargo, temperature and local pH changes.

Both changes in temperature and pH can be brought about either by the clinician or by taking advantages of local changes of tumour tissue.

1.4.1   Temperature

Thermoresponsive polymers represent one of the most common sub-groups of 'smart' polymers; these possess an upper (UCST) and lower critical solution temperature (LCST) in aqueous media.[34,48,49] The LCST is the critical point at which the hydrogen bonds between the polymer and the surrounding water molecules break,[50] leading to a decrease in colloidal stability of the polymer chains and thus phase separation occurring in an entropy driven process due to the loss of water molecules. The phase separation results in the formation of a 'polymer-rich' and a 'polymer-poor' phase which can be characterised by the bulk aggregation of the polymer/particles present.

One such polymer is poly(*N*-isopropylacrylamide) (PNIPAM) and has been one of the most heavily researched thermoresponsive polymers due to a LCST close to body temperature, ~32 °C and that its LCST is relatively insensitive to environmental conditions; providing scope for PNIPAM use *in vivo* and the use of which has already been covered in numerous reviews.[51,52]

The Takao Aoyagi lab conducted a study using PNIPAM to open up a new possibility of effective and facile encapsulation targeting and triggered release of drugs.[53] Three series of copolymers with different polymer structures, all with PNIPAM as a common denominator, were successfully synthesised by reversible addition–fragmentation chain transfer (RAFT) polymerisation, Figure 3.
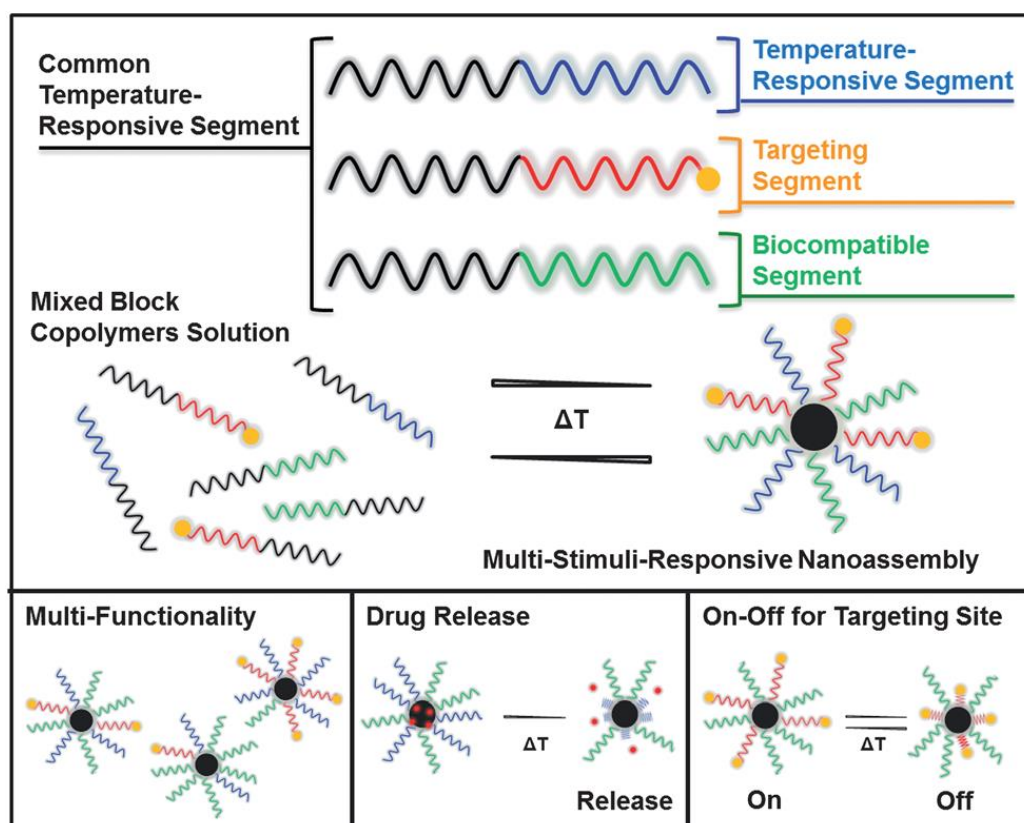
Figure 3 Schematic representation of the multi-stimuli-responsive nano- assembly by mixing of selected block copolymers with the common temperature-responsive segment and heating/cooling. [53]

They found that with simple mixing of the different block copolymers the distinct two-step temperature response behaviour, due to the different LCSTs of each block, made this system considerably advantageous over self-assembly of the one block copolymer system, Figure 4.
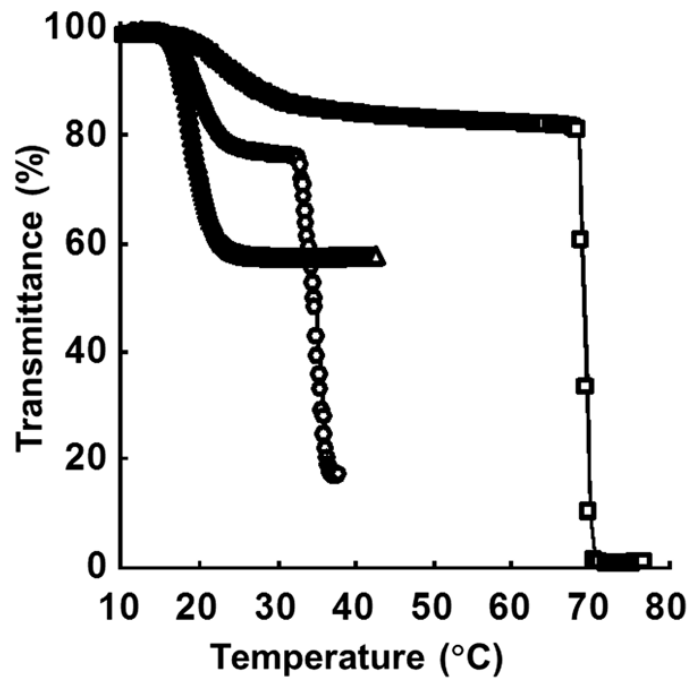
Figure 4 Temperature-dependent behavior of 0.1 w/v% aqueous solution of (O) P(NIPAAm$_{112}$-co-HMAAm$_{14}$)-b-P(NIPAAm$_{54}$-co-BMAAm$_{12}$), (Δ) PEO$_{113}$-b-P(NIPAAm$_{85}$-co-BMAAm$_{19}$), and (□) PLAMA$_2$-b- P(NIPAAm$_{79}$-co-HMAAm$_{35}$)-b-P(NIPAAm$_{28}$-co-BMAAm$_6$).[53]

Thermo- and pH-sensitive polyion complex (PIC) micelles were formed from two oppositely charged diblock copolymer based on PNIPAM by Guiying Li and colleagues.[54]
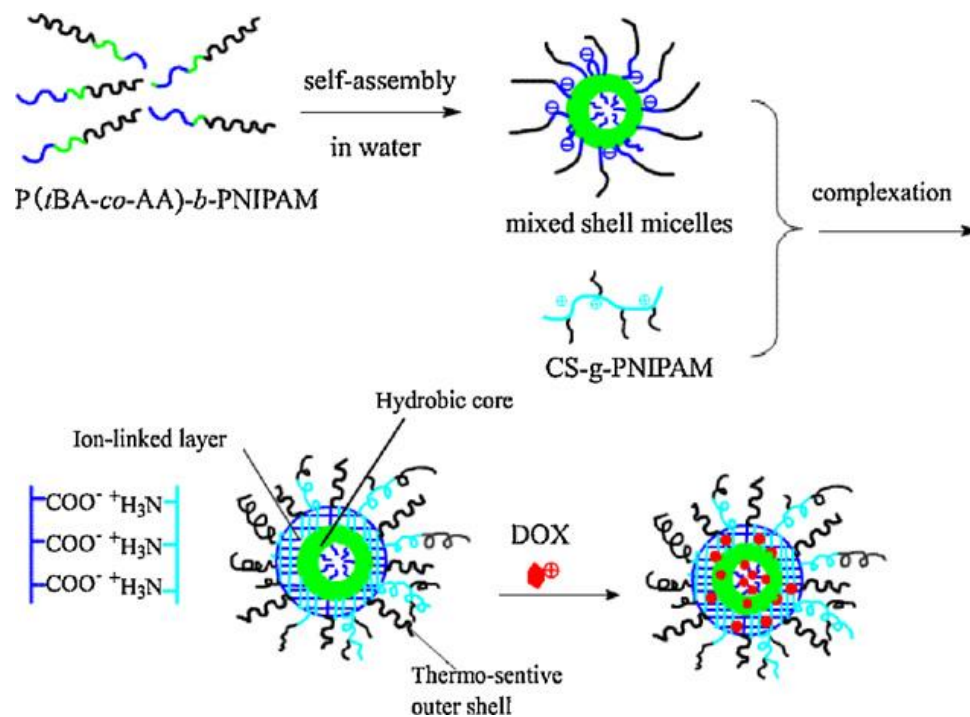
Figure 5 The proposed schematic representation of drug-loaded PIC micelles.[54]

The chitosan (CS)/poly acrylic acid (PAA) layer of these micelles, Figure 5, successfully protected the encapsulated doxorubicin (DOX) drug in neutral conditions. However, once the pH dropped or the temperature was raised above LCST the sensitive PNIPAM chains collapse, leading to the rapid sustained release of DOX due to the differences in electrostatic interactions between the micelles and the DOX; when these were minimised, upon PNIPAM collapse and low pH the DOX was released rapidly from the micelles.

Both of the above examples using PNIPAM show it to be an accomplished thermoresponsive polymer system. A possible drawback however is that the systems are responsive to both pH and temperature which could lead to insufficient control on the site specific delivery. As the advantage of PNIPAM is the readily altered LCST to a range needed which has led to multiple research groups choosing this polymer, it must be considered that questions

have been brought against it in relation to its possible cytotoxic effects, as well as phase transition hysteresis and a significant end group influence on thermal behaviour. [55-57]

As an alternative to PNIPAM, Wei *et al* synthesised a new type of monomer to form a thermoresponsive block copolymer.[58] Poly(*N-(N*-Boc-ethylenediamine)methacryloylglycylglycylamide) (PBEMAGG) was synthesised from MAGG-COOH and *N*-Boc-ethylenediamine and copolymerised with a PEG-chain transfer agent. It was found the precise control of the LCST could be regulated by altering the number of pendant BOC groups. When temperature is below the LCST, the hydrogen bonds between amide groups and water ensure the stability of the particles. When the temperature is above LCST, the hydrogen bonds are broken by tert-butyl groups which are hydrophobic groups in each PBEMAGG repeat unit, so the solubility of polymers declines.[59]
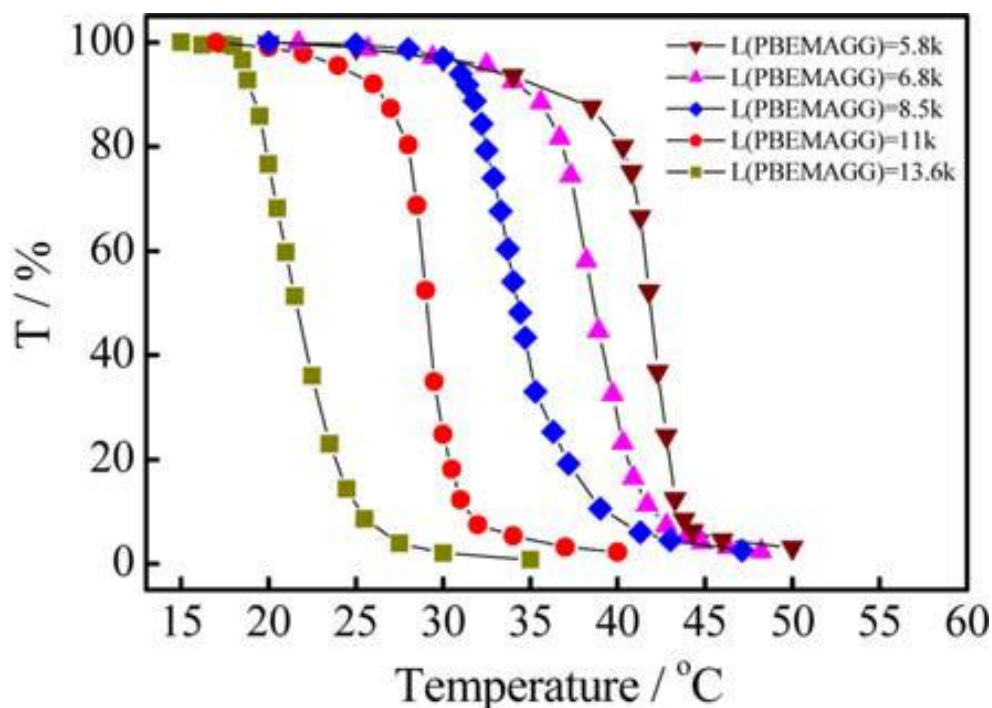
Figure 6 The UV transmission percentage of PEG$_{2k}$-*b*-PBEMAGG with different PBEMAGG block lengths at different temperatures. The UV wavelength is 400 nm. The concentration of sample is 1.5mg/mL in water. The PBEMAGG block length was denoted by its number-average molecular weight (M$_n$ determined by ^{1}H NMR analysis).[58]

As the temperature increases, the hydrophobicity of PBEMAGG increases; leading to the deformation of the micelle, thus the release of the drug cargo.

A more recent type of polymer containing an LCST suitable for *in vitro* and *in vivo* offering similar advantages to that of PNIPAM but with few of the drawbacks are combinations of oligo(ethylene glycol methacrylate) (OEGMA).[60,61] PNIPAM exhibits broad hysteresis on cooling, most likely as a result of the PNIPAM globules exhibiting intra- and intermolecular hydrogen bonding and high T$_g$; OEGMA based polymers though do not undergo any intermolecular hydrogen bonding and thus limited hysteresis is exhibited.[62] POEGMA offers further advantages over PNIPAM in that the molar mass of the polymer does not have a significant effect on the transition temperature.

It is the hydrophilic-hydrophobic balance of the OEGMA monomer units which allows for the precise control of the transition.[63]

The precise control of transition temperatures that is possible for POEGMA led to the synthesis of poly((diethylene glycol methacrylate)-*co*-OEGMA) (P(DEGMA-*co*-OEGMA)) brushes on silicon wafers.[64] When the polymer chains were extended at low temperatures a good resistance to protein adsorption was observed. Further anti-fouling properties were also observed by Chilkoti *et al.*;[65,66] this is a critical point if these polymers are to be used to enable long circulation time of NPs.

The use of OEGMA-based polymers within colloids has grown recently with various uses such as triggers for assembly/disassembly of dendritic elements,[67] vesicles as cell mimics[68] and drug delivery.[69]

Recent uses of POEGMA copolymerised with polycaprolactone in a star shape allowed for loose micelles to be formed with non-interacting cores.[70] These micellar NPs were capable of encapsulating doxorubicin and also shown to have no adverse reaction with human blood, in terms of whole blood viscosity, erythrocyte aggregation, and haemolysis. Much like most groups working in the drug delivery field enhancing the encapsulation of small molecule drugs was to be the focus of future research to enable improvement of this NP type as a drug delivery vehicle.

As well as the thermoresponsive nature of OEGMA-based polymers the addition of a disulfide crosslinking within NPs allows for dual-stimuli-

responsive drug delivery. Ulasan and co-workers developed a p(OEGMA-*co*-vinyl pyrrolidone) NP system using a disulfide-based cross-linker by surfactant-free emulsion polymerisation.[71] It was found that by using temperature as a trigger small molecular weight drug molecules could be released; then by the addition of dithiothreitol (DTT), to mimic cleavage of disulfide bond *in vivo*, larger drug molecules (PEG-alizarin dye as a model) could be released. This use of two stimuli for the controlled release of two different drugs offers an advantage for the delivery of large biomacromolecule drugs currently being developed (e.g. proteins, siRNA). The use of redox as a trigger for stimuli-responsive materials is further discussed below.

1.4.2   Glutathione (reducing conditions)

A further trigger used to good effect with stimuli-responsive material is the change in pH. A hallmark of tumour environment is the lowered extracellular pH caused by excess metabolic acids (CO_2 and lactic acid),[72] the pH can drop below 6.5 down from pH 7.4 in normal tissue. This pH gradient continues downward upon entry to the cell as within the intracellular organelles the pH can drop to 5.5 (endosomes) and below this in the lysosomes. This drop of almost 2 pH units is the cause for many anti-cancer drugs to be ineffective against solid tumours.[73] However, the local drop in pH can be taken advantage of to trigger a response from CSPs. In addition to the drop in pH, the intracellular concentration of glutathione, a thiol-containing tripeptide responsible for the cleavage of disulfide bonds, is much higher than

extracellular.[74] Many groups have taken advantage of this fact and used it to their advantage in designing of drug delivery vehicles.

One such strategy is to use the acidity to bring about disassembly of a nanoparticle assembly to release its cargo i.e. the drug of choice. This involves the cross-linking of a core of a micelle and allow it be susceptible to a reducing environment. The micelle allows for the encapsulation of drugs and dyes, for monitoring, into the inner area and once pH drops the release of the drug is contained within a local area.[75,76] Although this is not the typical idea of a CSP it does show that by taking this idea of disassembly and using it for CSPs it could be improved with the additional shell and targeting.

An advantage of using a CSP is shown by Guo *et al* whereby a CSP can be used to encompass a water insoluble drug.[77] Their 10 step synthesis afforded a mPEG-SS-PBLG (poly(benzyl L-glutamate)) diblock polymer which was able to form nano-scale micelles in aqueous media. These micelles could be loaded with a hydrophobic drug (SN-38) at encapsulation efficiency (e.e.) of 73.5% at a content of 10 wt%. The disulfide bond was used to attach the PEG shell so as to allow for the shedding of the shell upon entry to an environment with reducing conditions. This was successful and the CSPs themselves showed no inherent cytotoxicity. Although there were signs that there was a slight release of the drug in a non-reducing environment over time, this would have to be remedied but initial results look promising for this type of sheddable shell CSP.

Similar work to this by Jiang and co-workers showed comparable results with a different pH responsive block copolymer, poly((PEG-MEMA)-*co*-(Boc-Cyst-MMAm))-*block*-PEG.[78] Using the pH cleavable disulfide bond the micelle loaded with paclitaxel (PTX) (e.e. > 90%, high-loading up to 35 wt%) could deliver extremely rapid release after exposure to an reducing environment and so improving the cytotoxicity of free PTX, Figure 7.
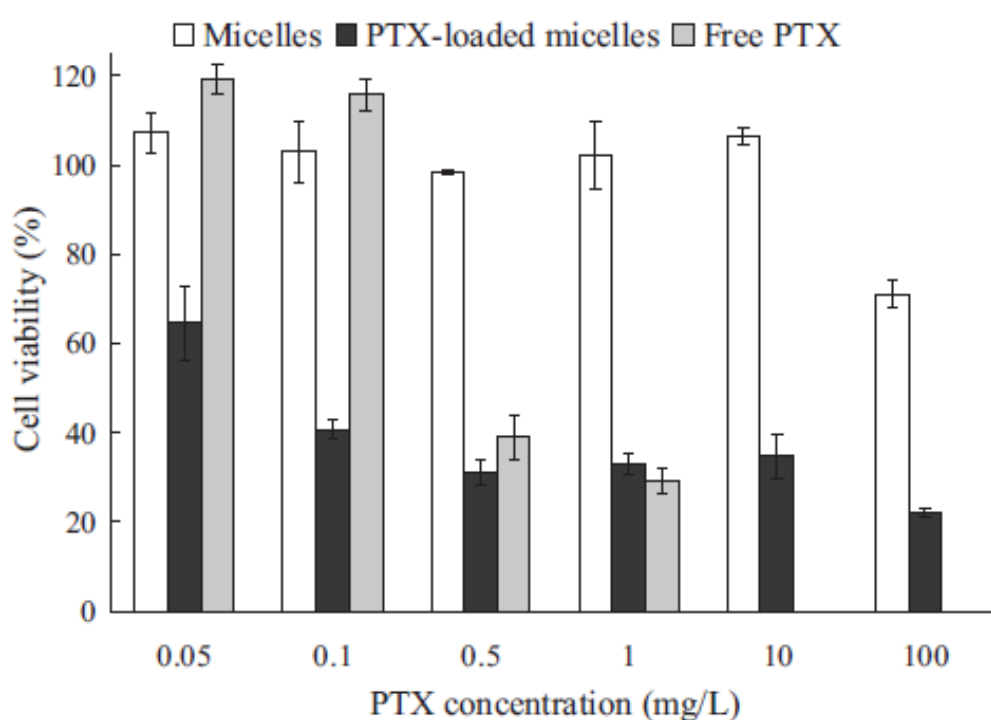
Figure 7. In vitro cytotoxicity of PTX-loaded PEG-P-SS-HP1 micelles (LC 9.9%, black bars) on HepG2 cells after 48h of incubation in comparison with empty micelles (left white bars) and free PTX (right gray bars). Data represent the mean and standard deviation of four independent experiments.[78]

To enhance what are promising signs of an anticancer drug delivery vehicle, Jiang *et al* are investigation the adaptation of their design to incorporate an active targeting ligand to benefit the possibilities of this as a suitable drug delivery vehicle.

The motif of a sheddable shell, similar to Guo and coworkers, upon response to a reducing environment is something that groups are beginning to further develop. Cui *et al* used the same type of PEG shell as Guo *et al* but this time attaching it to a silica NP core.[79] The silica core allows for the accommodation of guests, such as drugs or dyes, and the PEG shell was attached *via* a disulfide bond which is cleavable in reducing conditions (i.e. glutathione (GSH) rich environment which occurs around solid tumours). The group showed that there was a rapid release of the dye upon contact with GSH compared with no GSH present. Cell cytotoxicity studies using a MTT assay showed no adverse effects of the use of these CSPs, although only one cell line was tested, Figure 8.
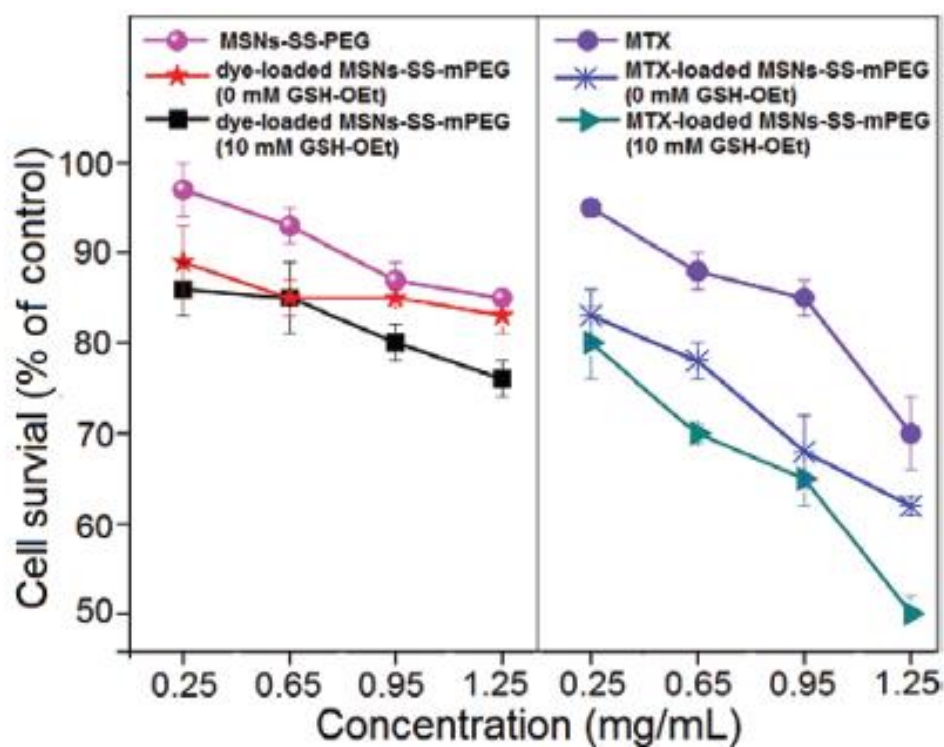
Figure 8 Cell survival of MCF-7 cells incubated with different concentrations of MSNs-SS-mPEG alone, Dye-loaded MSNs-SS- mPEG, MTX alone, and MTX-loaded MSNs-SS-mPEG nanoparticles after 24 h incubation.[79]

The group aims to push on from these results and carry out further testing using various types of human cancer cell lines and how different pore-sizes of the silica core affects the release patterns.

Sheddable outer shells promote the intracellular delivery of hydrophobic drugs which, without this motif, find it problematic to be delivered to the internal areas of cells. This is also shown by Sun *et al*, whereby dextran-SS-poly (caprolactone) was used to incorporate DOX within self-assembled micelle.[80] The release of DOX was compared with micelles not containing the disulfide bond which allowed for the shedding of the hydrophilic outer shell and the results shown, Figure 9.
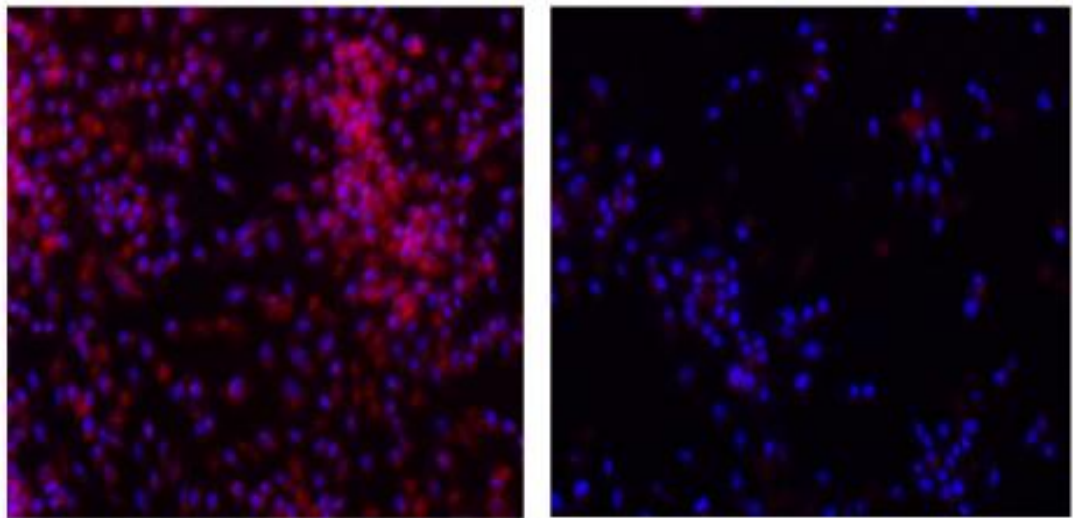
Figure 9 Fluorescence images of macrophage RAW264.7 cells incubated for 4 h with DOX loaded Dex-SS-PCL micelles (left) and DOX loaded Dex-PCL micelles (right). The DOX dosage was 12.5 μg/mL. Red: DOX fluorescence; Blue: cell nuclei stained by DAPI.[80]

There is a marked increase in quantity of DOX present in cells when the release can be accelerated with the use of this sheddable shell compared to the standard micelle lacking in the disulfide bond.

All of these shell sheddable forms of drug delivery show promise as an efficient way of enhancing the treatment of cancers. However, as the *in-vitro* testing is only carried out on selected cell-lines it cannot be determined how well the targeting of these vehicles are. It can be theorised that they all could take advantage of the EPR effect as passive targeting, but, with an added active targeting ligand the potential could rise even further.

1.5 Receptor Targeting

Receptor targeting when used in combination with stimuli-responsive material can only improve upon the selectivity of drug delivery. As outlined previously targeting the folate receptor is just one way of exploiting the over expressed receptors common among certain cancers. Two such types of receptor targeting are outlined below.

1.5.1 CD44

One such receptor is the CD44 receptor which has been found to be overexpressed in certain cancers (breast, colon and ovarian).[81,82] CD44 is a receptor of hyaluronic acid (HA) which is regarded as an excellent bio-inert material due to the immunoneutral, biocompatible and biodegradable nature of the material.[83,84] It has been reported that HA-paclitaxel conjugates enter cells *via* receptor-mediated endocytosis.[83] Previous work concentrated on using HA to form a prodrug by conjugating HA backbone directly to a drug molecule.[85]

Jeong and co-workers used the idea of HA targeting of the CD44 receptor as a basis for their research. A CSP was synthesised with HA for targeting and a core of PLGA (HAbLG).[86] Proton NMR was used to confirm the presence of the

HA as a hydrophilic shell covering the core of PLGA upon precipitation, with DOX incorporated in the core. HAbLG was found to have particle size of under 200 nm which is favourable for consideration for drug targeting.[87] To determine the efficiency of the targeting HCT-116 (a human colon carcinoma cell line[88]) was used as it is found to overexpress the CD44 receptor. It was shown that when the CD44 receptor was not blocked there was strong fluorescence from DOX within the cells showing successful entry *via* receptor mediated endocytosis. This was confirmed by blocking the receptor and exposing the cells the HAbLG-DOX once again. On this occasion the fluorescence was very small confirming the hypothesis of cell entry and successful intracellular administration of DOX.

In the same vein as that of Jeong *et al*, Ki Young Choi and colleagues used the targeting of potential of HA to synthesise a theranostic device.[89] This group had previously demonstrated that poly(ethylene glycol) (PEG)-conjugated hyaluronic acid nanoparticles (P-HA-NPs) upon systemic administration resulted in accumulation in tumour tissue.[90,91] It was noted that these P-HA-NPs accumulated not only due to the EPR effect like many other NPs but also because of the CD44 receptor targeting, as above. As previous work confirmed the effectiveness of this type of CSP as a delivery agent, this study was concerned with evaluating the prospect as a theranostic system. P-HA-NP was conjugated with Cy5.5 and loaded with IRT (a hydrophobic anticancer treatment). The resulting CSP was then administered to mice and the tumours monitored, Figure 10.
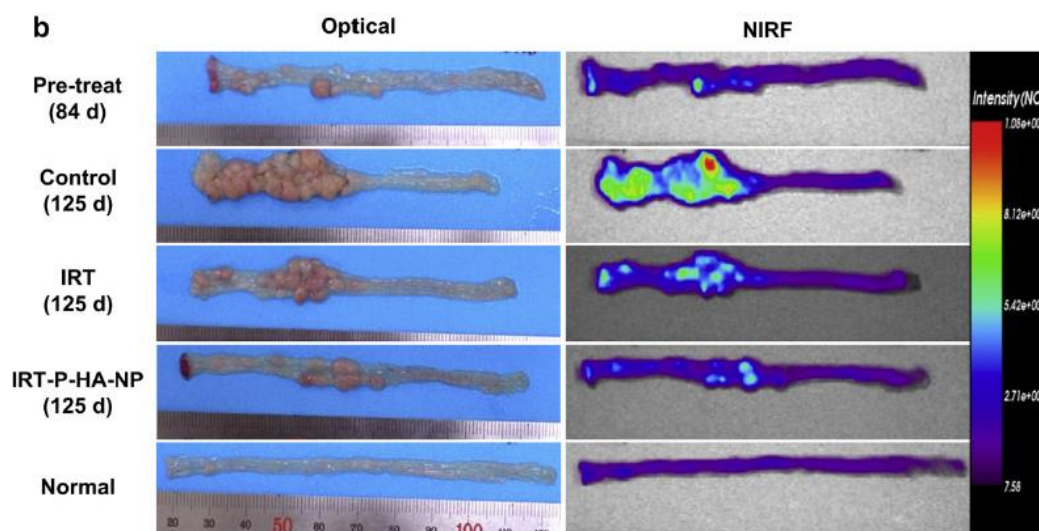
Figure 10 Representative colon images of AOM/DSS-induced orthotopic colon cancer models that were pre-treated or treated with saline, IRT or IRT-P-HA-NPs. Images acquired at 6 h after intravenous injection of Cy5.5-P-HA-NPs.

It was determined that the dye allowed for early stage detection of the colon cancer with the delivery of the drug causing a reduction on the size of the tumours.

As colon cancer is very difficult to be detected with the miss rate being as high as 27 % for small, flat and depressed neoplasms[92] which in turn can lead to further metastases;[93] any improvement in aiding the treatment and detection is a positive step.

1.5.2   Folate Receptor

Folate targeting has garnered much attention after Kamen and Capdevila reported that folates entered cells *via* a receptor-mediated endocytic process.[94] The vitamin folic acid displays extremely high affinity (K_D ~10^{-10} M) for its cell surface-orientated receptor[95] which is overexpressed in some forms of cancer.[96] This makes it a more than suitable target to aim for when targeting tumour cells. It has already been shown that different types of

agents have been delivered to cells *via* this mechanism, from MRI agents [97], small molecule drugs[98] and liposomes with entrapped drugs.[99] With this process already been shown to work there should be no reason why this cannot be applied successfully to CSPs.

Indeed, Zhao *et al* showed that with a PTX loaded folic acid modified PLGA-PEG CSP, a higher cytotoxicity was achieved than when PTX was used alone.[100] Upon intravenous administration of the CSPs to mice tumours showed signs of regression and improvement of animal survival, compared with that observed when Taxol® was used. Similar results were obtained by Ming Shen and co-workers when polymethacrylates (PMA)-grafted poly(amidoamine) (PAMAM) CSPs were used with folate-PEGylation.[101] It was found that this type of CSP not only had enhanced targeting abilities due to the presence of the folate receptor and help from the EPR effect but also that the lower pH in intra-tumoral spaces stimulated the release of the drug molecule. This led to *in-vivo* results that showed strong inhibition of tumour growth, Figure 11.
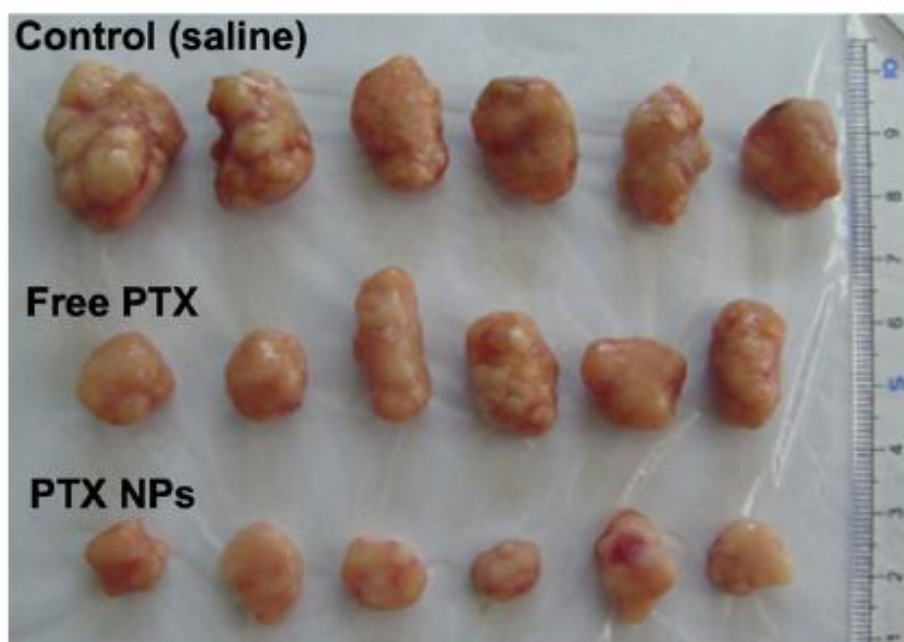
Figure 11 Tumours after the 15th injection with PTX injection, FA-PEG-PMA-PAMAM-NPs (1 mg/kg) and saline group (n=6).[101]

Recently two groups have shown the advantages of combining multiple active targeting on one type of particle. By conjugating both glucose and folic acid to gold nanoparticles the uptake of the NPs was increased by 3.9 fold and 12.7 fold when compared with AuNPs with only the folate or glucose ligands respectively.[102] A similar study also targeted the folate receptor and included an anti-EGFR (epidermal receptor growth factor) on a single AuNP core.[103] The Au NPs were shown to be taken up to a high degree in cell types expressing one of the receptors and if both receptors were over-expressed the ability of the dual targeted NP system to be taken up was enhanced further. The use of two targeting ligands is clearly advantageous for targeting disease sites where more than one type of receptor is over-expressed; however careful consideration must be made when designing these multi-targeted NPs to ensure no off-site targeting would occur.

The examples above for receptor targeting outline how the increase in accumulation of CSPs in tumour tissue can increase the therapeutic value of drugs over the dose of the free drug and result in higher accumulation of CSPs. The encapsulation of a drug with the CSP not only allows for the improved targeting of the drug but, with the added extra of having stimuli-responsive material within the CSP allows for site specific release of the drug and longer circulation times.

1.6   Adoption of Nanoparticle Delivery Systems in the Clinic

As shown above there has been a large amount of progress made in the design and synthesis of drug delivery systems however the take up within the clinic has not followed this ever increasing trajectory of development preclinically. The main type of delivery system that has been developed is based on polymeric particles and liposomes. Currently there are only six clinically approved nanoparticle-based cancer therapies currently on the market, Table 2; these include polymer formulations Genexol-PM and liposomal formulations such as Doxil and Myocet.

Table 2 Examples of Nanomedicines for cancer approved by FDA [104]

Drug Product	Active Ingredient	Formulation type	Treatment Area	FDA approved date
Doxil	doxorubicin	PEGylated liposome	Ovarian/breast cancer	1995
Abraxane	Paclitaxel	Nanospheres	Various cancers	2005
Myocet	doxorubicin	Liposome	Breast cancer	2000 (EU and Canada)
DaunoXome	Daunorubicin	Liposome	HIV-related Kaposi sarcoma	1996
Marqibo	Vincristine	Liposome	Philadelphia chromosomenegative lymphoblastic leukemia	2012
Genexol-PM	Paclitaxel	Polymer micelle	Breast cancer/small cell lung cancer	Marketed in Europe

Doxil was the first FDA approved nanodrug treatment for cancer (AIDS-related Kaposi's sarcoma and metastatic ovarian and breast cancer). The treatment consists of unilamellar liposome with a PEG coating to allow shielding from the reticuloendothelial system and reduce clearance times, thus improving its pharmacokinetic profile.[105] Following this the remaining five formulations have been introduced into the clinic with the Marqibo being last formulation to hit the market in 2012.

To date there are no stimuli-responsive or actively targeted nanocarriers currently approved by the FDA. There are however two currently in clinical

trials, ThermoDox®, a thermoresponsive liposome treatment, and BIND-014 an actively targeted polymeric NP.

ThermoDox® is a heat-sensitive liposome which is used to encapsulate doxorubicin and deliver it in a burst effect when the temperature is raised to a specific temperature. At this temperature the liposome rapidly changes its structure which allows the doxorubicin to escape.[106] This treatment has reached phase 3 clinical trials and has shown efficacy against primary liver cancer.

BIND-014 consists of a hydrophobic biodegradable core (consisting of PLA or PLGA) with a PEG shell. With the addition of a *S,S*-2-[3-[5-amino-1-carboxypentyl]-ureido]-pentanedioic acid (ACUPA) ligand the NP system was capable of targeting the prostate-specific membrane antigen (PSMA).[107] PSMA is a clinically validated transmembrane receptor which is overexpressed on the surface of prostate cancer cells and in the neovasculature of nearly all non-prostate solid tumours.[108] During the development of BIND-014 more than 100 different NP compositions were thoroughly investigated in order to ensure that the highest possible drug loading of docetaxel and most stable NPs were formulated, the outcome of this investigation is shown in Figure 12. After impressing in preclinical trials the formulation is currently in phase 2 clinical trials. To date it has been shown that BIND-014 is well tolerated and the anti-tumour activity measured is meaningfully lower at lower dose than that for conventional docetaxel dosing.[109]
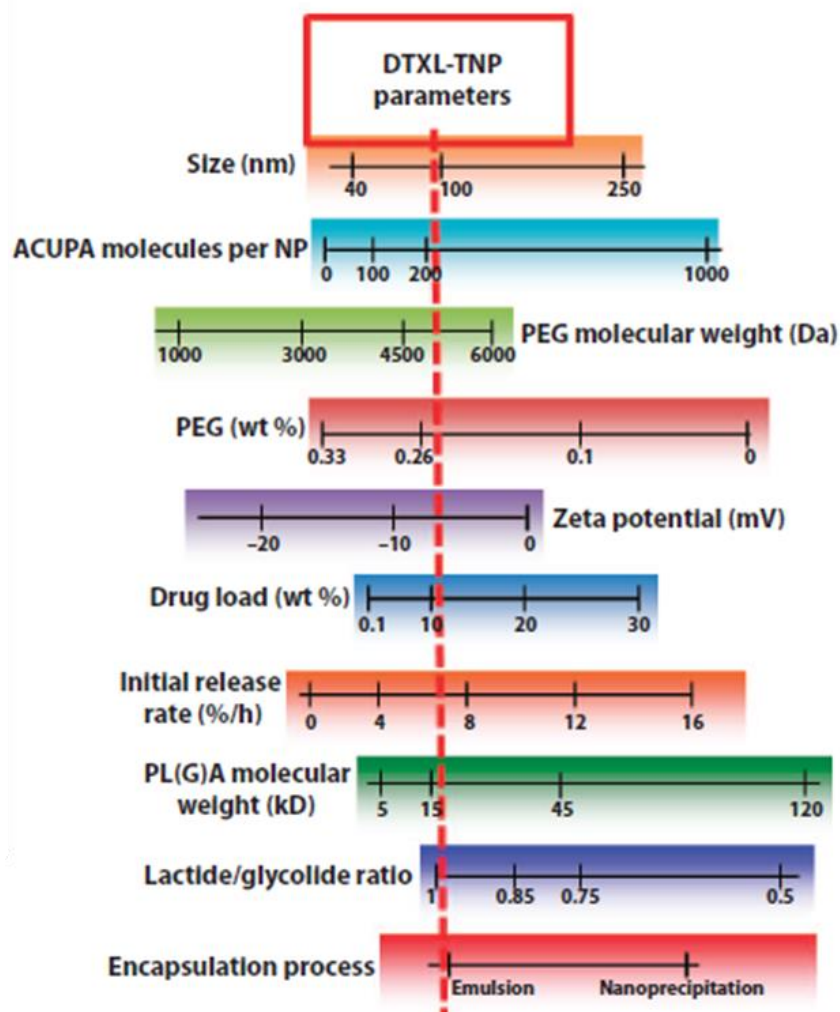
Figure 12 Range of formulation parameters and NP physicochemical properties evaluated during development of BIND-014, with optimized parameters and target properties indicated by the red dotted line.[107]

With the success these types of stimuli-responsive nanoparticle delivery systems are having in clinical trials it is hopefully only a short time until they are available for treatment.

1.7   Conclusion

It is hoped that the reader has been informed on some of the recent developments in the field of stimuli-responsive NPs and the development of NPs as drug delivery formulations. As to date there are only six approved nanoparticle delivery vehicles in the clinic[104,110] there is still a long journey to

cover before NP drug delivery is common place. That said the promise of these CSPs as an effective and efficient delivery of anti-cancer drugs cannot be overlooked; with continued high quality research more and more of these NPs will find their place amongst a clinician's arsenal for the fight against cancer.

1.8   Project aims:

This introduction has outlined the potential for polymer nanoparticles to be used as a targeted drug delivery vehicle to aid in cancer treatment. There has been progress made in the development of both stimuli responsive and receptor targeted NPs however very little work has been carried out in the combination of both into one formulation. Previous investigations have shown merit in both approaches for targeting nanoparticles to cancerous cells.

1.8.1   Principal aims:

The overall aim of this thesis was to develop a thermoresponsive polymer nanoparticle formulation that was capable of targeting cancer cells *in vitro*. The nanoparticle formulation was to contain a 'hide-and-reveal' motif designed to only reveal a folate targeting ligand upon heating the formulation beyond its transition temperature. The premise behind the 'hide-and-reveal' motif was to minimise off-site targeting by the folate ligand whilst maximising uptake within cancer cells which overexpress the folate receptor. To succeed in accomplishing this aim, the thesis is divided into the following experimental chapters:

Chapter 2: The design and synthesis of the polymers required for the assembly of the targeted nanoparticles. Selection of a suitable thermoresponsive polymer for *in vitro* testing and synthesis of polymers tagged with folate ligand for receptor targeting.

Chapter 3: Development of a reproducible method for nanoparticle assembly.

Chapter 4: Tuning the aggregation temperature of thermoresponsive nanoparticles.

Chapter 5: Assessing the targeting capabilities of the thermoresponsive nanoparticle system *in vitro*.

2 Design and Synthesis of the Polymers for the Assembly of Targeted Nanoparticles

2.1 Introduction

Many possible reactions exist for the synthesis of polymers;[14,111-114] each type capable of assembling multiple types of polymer with a wide variety of potential structural motifs.

Ring-opening polymerisation (ROP); for which there are three main routes of initiation: radical, ionic (anionic or cationic) and metathesis, is one of the most documented polymerisation methods, with over 2,600 papers published in 2015 alone,[115] due to their simple set-up and ease of use.

In this work anionic ROP was employed for the quick, controlled and reproducible assembly of polymers. The simplicity of the method, which requires only the presence of a catalyst, such as a tin[14] or aluminium[116] cation, and a nucleophilic initiator, which in this case was an alcohol, was a major factor in choosing this technique. For the remainder of this chapter anionic ROP will hereby be denoted by the abbreviation ROP.

ROP has garnered much attention in recent years, with many groups attempting to dissect the intricate mechanism. Tin(II) 2-ethylhexanoate is a frequently used catalyst yet there still remains uncertainty as to its mechanism of action. One theory supports tin(II) coordinating with the initiator with the retention of the ethylhexanoate ligands (EH)[117], whilst another suggests that the EH ligands are liberated upon coordination with

initiator.[118] More recently, support for the coordination-insertion mechanism has been obtained.[119] Using methanol as the reacting alcohol, two molecules of methanol were found to coordinate to $Sn(OAc)_2$, as a model for $Sn(EH)_2$, and the two ethylhexanoate moieties were found to be retained. The alcohol ligand is subsequently converted to an alkoxide which reacts with cyclic monomers *via* nucleophilic attack.

A more complex set of reactions, when directly compared with ROP, free radical polymerisations necessitates highly controlled environments. The system is required to be completely void of air (oxygen) for the reaction to proceed. These types of polymerisations often require specialist equipment and make producing the desired polymers challenging.

To overcome the aforementioned problems, new methods of polymerisation have been discovered that enable synthesis of polymers without the imposition of these strict conditions. One such type of polymerisation is Atom Transfer Radical Polymerisation (ATRP) which itself can be sub-categorised into a number of methods that are finding themselves common place amongst many polymer chemistry laboratories due to their flexibilities in terms of both monomer choice and catalysts used.[120-124] One of these methods, which will feature heavily in this work is the activator generated by electron transfer (AGET) ATRP.

AGET ATRP was first reported by the Matyjaszewski group in 2005.[125] This technique uses relatively air stable complexes, such as copper (II), with the active catalyst being generated *in situ.* The general mechanism is shown in

Scheme 1; the copper(II) catalyst is reduced by tin (II) 2-ethylhexanoate to Cu (I), the Cu (I) is then used to form the initiator radical which reacts with the methacrylate monomers in solution *via* a step-wise process to form the desired polymer. The degree of polymerisation can be easily controlled by altering the monomer to initiator ratio as well as the duration of the reaction. The advantage of this type of polymerisation is the increased tolerability of the catalysts to air, allowing for small amounts of oxygen to be present without interfering with the reaction progression, either by affecting the catalyst or reaction intermediates.
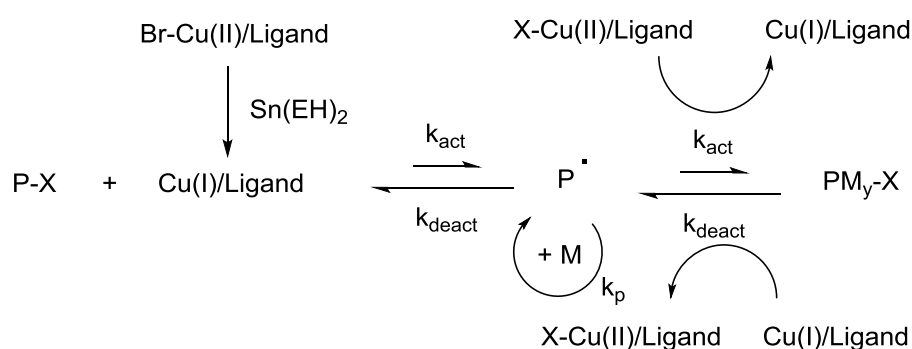
Scheme 1 AGET ATRP schematic. The Cu (II) is reduced by Sn(EH)$_2$ to produce the active catalyst Cu (I), this produces the initiator radical (P) which reacts with the acrylate/methacrylate monomers (M) to form the random block copolymer. To form a more ordered copolymer the monomers can be added in batches.

The polymers used for the targeted nanoparticle assembly were synthesised using both ROP and AGET ATRP as polymerisation techniques. Firstly, ROP was utilised to synthesise the hydrophobic core, comprising either a poly(lactide-*co*-glycolide) (PLGA) or polylactide (PLA). PL(G)A was chosen as a core material due to its attractive properties for clinical use, such as biodegradability and biocompatibility, its well described formulation methods for drug encapsulation and its approval for use by the FDA and EMA.[126] The

introduction of hydrophobicity also allows for the complete encapsulation of poorly soluble drug molecules in the future allowing for PL(G)As use as a drug delivery vehicle.

The PL(G)A core was further functionalised with a hydrophilic thermoresponsive shell, synthesised *via* AGET ATRP, capable of forming stable self-assembled nanoparticles (NPs). Within this thermoresponsive NP a 'hide-and-reveal' motif was included with the intention of enhancing targeting of the NPs to cancerous tumour cells; accordingly, a folate tagged PLA-PEG polymer was included within the NP. The folate tag was designed to be "visible" to the cell receptor only upon raising the temperature of the tumour/cell environment beyond the transition temperature of the thermoresponsive shell, as shown in Figure 13.
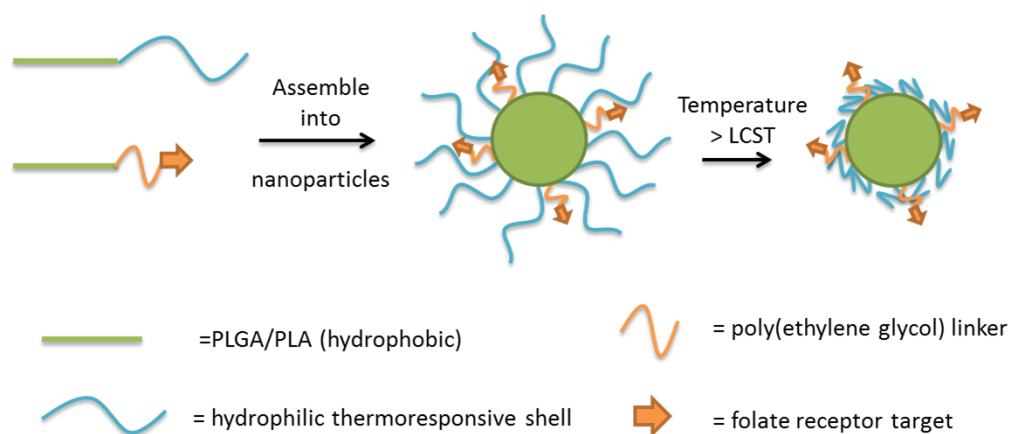
Figure 13 Design of the "hide-and-reveal" folate targeted thermoresponsive nanoparticles

2.2 Methods

For full details of all materials and equipment used consult Chapter 7. All GPC was carried out in chloroform and NMR was carried out in deuterated chloroform unless otherwise stated.

2.2.1 *O*-(2 -Bromoisobutyryl)tetraethylene glycol (ROP initiator) synthesis

Tetraethylene glycol (10.0 g, 51.5 mmol) was dried by azeotropic distillation of its solution in toluene (100 mL) twice then dissolved in CH_2Cl_2 (100 mL). $NaHCO_3$ (10 g, 119 mmol) was added followed by drop-wise addition of 2-bromoisobutyryl bromide (13.0 g, 7.0 mL, 56.6 mmol). The resulting suspension was stirred under N_2 overnight after which complete consumption of the acyl bromide was confirmed by TLC. Solids were removed by filtration and volatiles removed *in vacuo*. The resulting oil was purified by flash column chromatography (silica gel, 60 Å, 35–70 μm) with EtOAc as the eluent to yield O-(2 -bromoisobutyryl)tetraethylene glycol (**1**) as a clear viscous liquid.

Yield: 2.2 g (12.5 %)

^{1}H NMR – δ / ppm (d_6-DMSO): 1.90 (s, 6H, C$\underline{H}_3$), 3.40-3.70 (m, 14H, O-C$\underline{H}_2$-C$\underline{H}_2$), 4.25 (s, O$\underline{H}$).

2.2.2 PLGA Synthesis

2.2.2.1 50:50 PLGA

2.2.2.1.1 Sn(II) catalysed ROP

Glycolide (2.42 g, 21 mmol), D,L-lactide (3.0 g, 21 mmol) and initiator (**1**) (0.18 mg, 0.52 mmol) were added together with a stirrer bar to a round bottom flask. The mixture was stirred under nitrogen for 10 min at 50 °C before temperature was raised to 130 °C, after which tin (II) ethylhexanoate (42 mg, 0.1 mmol) was added and stirred overnight. The product formed was

dissolved in CH_2Cl_2 prior to being precipitated three times in cold hexane. The resulting precipitate was dissolved in CH_2Cl_2 and recovered *in vacuo*. Yield: 2.08 g. (38 %)

GPC: M_n 2307 Da, Đ 2.33

^{1}H NMR – δ / ppm (CDCl$_3$): 1.25-2.0 (m, 87.53H, lactide C$\underline{H}_3$), 2.25 (s, 3H, C$\underline{H}_3$), 3.47-3.80 (m, 6.95H C$\underline{H}_2$C$\underline{H}_2$O), 4.58-4.98 (m, 86.94H, glycolide C$\underline{H}_2$), 5.03-5.39 (m, 38.55H, lactide C$\underline{H}$).

2.2.2.1.2   1,5,7-Triazabicyclo[4.4.0]dec-5-ene (TBD) catalysed ROP

Glycolide (0.5 g, 4.3 mmol), D,L-lactide (0.62 g, 4.3 mmol) and initiator (**1**) (60 mg, 0.175 mmol) were dissolved in CH_2Cl_2 (10 mL) in a round bottom flask. The mixture was stirred under nitrogen for 10 min at 50 °C to aid dissolution, after which TBD (10 mg, 0.07 mmol) in CH_2Cl_2 (1.5 mL) was added and stirred for 0.5 h. The reaction solution was precipitated three times in cold hexane. The resulting precipitate was dissolved in CH_2Cl_2 and recovered *in vacuo*. Yield: 0.8 g (71 %).

GPC: M_n 1100 Da, Đ 2.31

^{1}H NMR – δ / ppm (d$_6$-DMSO): 1.33-1.57 (d, 8.1H, lactide C$\underline{H}_3$), 2.5 (s, 2.9H, C$\underline{H}_3$), 3.08-3.59 (br s, 18.5H C$\underline{H}_2$C$\underline{H}_2$O), 5.05 (s, 1H, glycolide C$\underline{H}_2$), 5.45 (q, 2.56H, lactide C$\underline{H}$).

2.2.2.2   65:35 PLGA

Glycolide (3.25 g, 28 mmol), D,L-lactide (7.49 g, 52 mmol) and initiator (**1**) (273 mg, 0.8 mmol) were added together with a stirrer bar to a round bottom flask. The mixture was stirred under nitrogen for 10 min at 50 °C before the

temperature was raised to 130 °C after which tin (II) ethylhexanoate (65 mg, 0.16 mmol) was added and stirred for 30 minutes. The product formed was dissolved in CH_2Cl_2 prior to being precipitated three times in cold hexane. The resulting precipitate was dissolved in CH_2Cl_2 and recovered *in vacuo*. Yield: 9.15 g (85 %).

GPC: M_n 18100 Da, Đ 1.56

^{1}H NMR – δ / ppm (CDCl$_3$): 1.46-1.68 (m, 156.45H, lactide C$\underline{H}_3$), 1.95 (s, 3H, C$\underline{H}_3$), 3.62-3.81 (m, 7.12H C$\underline{H}_2$C$\underline{H}_2$O), 4.61-4.97 (m, 63.34H, glycolide C$\underline{H}_2$), 5.11-5.31 (m, 46.24H, lactide C$\underline{H}$).

$M_{n, NMR}$: 7300 Da

Lactide:glycolide 62:38 (by ^{1}H NMR)

2.2.2.3   75:25 PLGA

Glycolide (2.15 g, 18.5 mmol) and D,L-lactide (80 g, 55.5 mmol) were combined with **1** (273 mg, 0.8 mmol) in a round-bottomed flask, the remainder of reaction was repeated as for 65:35 PLGA-Br. Yield: 9.10 g (90 %).

GPC: M_n 19500 Da, Đ 1.89

^{1}H NMR – δ / ppm (CDCl$_3$): 1.26-1.80 (m, 201.3H, lactide C$\underline{H}_3$), 1.95 (s, 3H, C$\underline{H}_3$), 3.56-3.83 (m, 5.18H C$\underline{H}_2$C$\underline{H}_2$O), 4.56-5.01 (m, 44.4H, glycolide C$\underline{H}_2$), 5.09-5.50 (m, 67.81H, lactide C$\underline{H}$).

$M_{n, NMR}$: 12700 Da

Lactide:glycolide 74:26 (by ^{1}H NMR)

2.2.3 PLA synthesis

2.2.3.1 Sn (II) catalysed

Initiator (**1**) (500 mg, 1.45 mmol) and D,L-lactide (30.0 g, 0.2 mol) were added to a RBF together with a stir bar and heated to melt (130 °C) under nitrogen for 30 min. Tin (II) ethylhexanoate (200 mg, 0.49 mmol) was added using a syringe. The reaction was left to stir under nitrogen for 1 h. The product formed was dissolved in CH_2Cl_2 prior to being precipitated three times in cold hexane. The resulting precipitate was dissolved in CH_2Cl_2 and recovered *in vacuo*. Yield: 29.5 g (98 %)

GPC: M_n 13300 Da, Đ 1.77

^{1}H NMR – δ / ppm ($CDCl_3$): 1.50-1.66 (m, 472.2H, lactide C$\underline{H}_3$), 1.95 (s, 3H, C$\underline{H}_3$), 3.59-3.82 (m, 6.4H C$\underline{H}_2$C$\underline{H}_2$O), 5.12-5.30 (m, 139.55H, lactide C$\underline{H}$).

$M_{n, NMR}$: 15600 Da

2.2.3.2 TBD catalysed

Compound **1** (1.7 g, 4.88 mmol) and D,L-lactide (34.0 g, 0.23 mol) were dissolved in dry CH_2Cl_2 (160 mL). TBD (680 mg, 4.88 mmol) was dissolved in 10 mL CH_2Cl_2 and added upon complete dissolution of monomers and left to stir for 30 minutes to ensure complete polymerisation. The reaction mixture was precipitated into cold hexane twice and polymer recovered *in vacuo*. Yield 33.9 g (99 %).

GPC: M_n 16100 Da, Đ 1.87

^{1}H NMR – δ / ppm (CDCl$_3$): 1.42-1.74 (m, 757H, lactide C$\underline{H}_3$), 1.95 (s, 3H, C$\underline{H}_3$), 3.62-3.82 (m, 2.33H C$\underline{H}_2$CH$_2$O), 5.11-5.30 (m, 246.77H, lactide C$\underline{H}$).

M$_{n, NMR}$: 26600 Da

2.2.4 Poly(lactide-co-glycolide)-*block*-((polypropylene glycol methacrylate)-*stat*-(oligo(ethylene glycol) methacrylate) (PLGA-*b*-(PPGMA-*stat*-OEGMA))

To a round-bottom flask PLGA-Br (0.1 mmol), PMDTA (21 µL, 0.1 mmol) and CuBr$_2$ (23 mg, 0.1 mmol) were added. To the mixture, varying amounts of the two co-monomers, PPGMA$_{375}$ and OEGMA$_{475}$, were added in order to give polymers with different thermoresponsive properties. All the materials were dissolved in 15 mL of 2-butanone. The mixture was degassed by flushing with Ar or N$_2$ and stirred for 1 h. Tin (II) 2-ethyl-hexanoate (0.1 mmol) was added as the AGET reducing agent under Ar. The reaction was heated to 60 °C and stirred for 3-6 h (until 60-70% monomer conversion). The polymerization was stopped by opening the flask and exposing the contents to air. The reaction mixture was precipitated three times into an excess of hexane: diethyl ether (1:1) mixture. The precipitate was then dissolved with CH$_2$Cl$_2$ and passed through an aluminium oxide column. The resulting co-polymer was obtained by evaporating to dryness *in vacuo*.

^{1}H NMR – δ / ppm (CDCl$_3$): (P1) 1.50-1.68 (m, 14.19H, lactide C$\underline{H}_3$), 3.40 (s, 3H, OEGMA C$\underline{H}_3$), 3.86-4.20 (m, 4.87H, OEGMA CH$_2$, PPGMA CH), 4.63-4.98 (m, 4.8H, glycolide C$\underline{H}_2$), 5.11-5.39 (m, 5.02H, lactide C$\underline{H}$).

(P2): 1.50-1.68 (m, 10.44H, lactide C$\underline{H}_3$), 3.40 (s, 3H, OEGMA C$\underline{H}_3$), 3.86-4.20 (m, 533H, OEGMA C$\underline{H}_2$, PPGMA C$\underline{H}$), 4.63-4.98 (m, 5.4H, glycolide C$\underline{H}_2$), 5.11-5.39 (m, 3.99H, lactide C$\underline{H}$).

(P3): 1.50-1.68 (m, 12.17H, lactide C$\underline{H}_3$), 3.40 (s, 3H, OEGMA C$\underline{H}_3$), 3.86-4.20 (m, 2.4H, OEGMA C$\underline{H}_2$, PPGMA C$\underline{H}$), 4.63-4.98 (m, 3.98H, glycolide C$\underline{H}_2$), 5.11-5.39 (m, 3.91H, lactide C$\underline{H}$).

(P4): 1.50-1.68 (m, 9.92H, lactide C$\underline{H}_3$), 3.40 (s, 3H, OEGMA C$\underline{H}_3$), 3.86-4.20 (m, 2.6H, OEGMA C$\underline{H}_2$, PPGMA C$\underline{H}$), 4.63-4.98 (m, 4.58H, glycolide C$\underline{H}_2$), 5.11-5.39 (m, 3.25H, lactide C$\underline{H}$).

 (P5): 1.5-1.64 (m, 18.83H, lactide C$\underline{H}_3$), 3.40 (s, 3H, OEGMA C$\underline{H}_3$), 3.87-4.20 (m, 3.65H, OEGMA C$\underline{H}_2$, PPGMA C$\underline{H}$), 4.63-4.98 (m, 5.16H, glycolide C$\underline{H}_2$), 5.11-5.39 (m, 6.04H, lactide C$\underline{H}$).

2.2.5   Poly(lactide)-*block*-((2-methoxyethoxy)ethylmethacrylate)-*stat*-(oligo(ethylene glycol) methacrylate) (PLA-PEGMA)

To a round bottom flask, a poly(lactide) macroinitiator (0.1 mmol), PMDTA (21 µL, 0.1 mmol) and CuBr$_2$ (23 mg, 0.1 mmol) were added. To the mixture varying amounts of the two co-monomers, DEGMA and OEGMA$_{475}$, were used to give polymers with different properties. All the materials were dissolved in 15 mL of 2-butanone. The mixture was degassed by 3 cycles of freeze-pump-thaw prior to being backfilled with Ar. Tin (II) 2-ethyl hexanoate (40.5 mg, 0.1 mmol) was added as the AGET reducing agent under Ar. The reaction was heated to 60 °C and stirred for 3 − 6 h to achieve 60-70% monomer

conversion. The polymerisation was stopped by opening the flask and exposing the contents to air. The reaction mixture was precipitated three times into an excess of cold hexane. The precipitate was then dissolved with CH_2Cl_2 and passed through an aluminium oxide column to remove copper. The resulting co-polymer was obtained by evaporating to dryness *in vacuo*. ^{1}H NMR – δ / ppm (CDCl$_3$): (P6) 1.46-1.69 (m, 11.07H, lactide C$\underline{H}_3$), 3.42 (s, 3H, D/OEGMA C$\underline{H}_3$), 3.49-4.29 (m, 8H, D/OEGMA C$\underline{H}_2$), 5.08-5.30 (m, 3.6H, lactide C$\underline{H}$).

(P7): 1.46-1.69 (m, 10.34H, lactide C$\underline{H}_3$), 3.42 (s, 3H, D/OEGMA C$\underline{H}_3$), 3.49-4.29 (m, 8.58H, D/OEGMA C$\underline{H}_2$), 5.08-5.30 (m, 2.98H, lactide C$\underline{H}$).

(P8): 1.46-1.69 (m, 11.18H, lactide C$\underline{H}_3$), 3.42 (s, 3H, D/OEGMA C$\underline{H}_3$), 3.49-4.29 (m, 10.08H, D/OEGMA C$\underline{H}_2$), 5.08-5.30 (m, 3.5H, lactide C$\underline{H}$).

(P9): 1.46-1.69 (m, 10.8H, lactide C$\underline{H}_3$), 3.42 (m, 3H, D/OEGMA C$\underline{H}_3$), 3.49-4.29 (m, 12.3H, D/OEGMA C$\underline{H}_2$), 5.08-5.30 (m, 3.35H, lactide C$\underline{H}$)

(P10): 1.46-1.69 (m, 12.38H, lactide C$\underline{H}_3$), 3.42 (m, 3H, D/OEGMA C$\underline{H}_3$), 3.49-4.29 (m, 17.42H, D/OEGMA C$\underline{H}_2$), 5.08-5.30 (m, 3.97H, lactide C$\underline{H}$)

(P11): 1.46-1.69 (m, 12.16H, lactide C$\underline{H}_3$), 3.42 (m, 3H, D/OEGMA C$\underline{H}_3$), 3.49-4.29 (m, 21.9H, D/OEGMA C$\underline{H}_2$), 5.08-5.30 (m, 3.88H, lactide C$\underline{H}$)

2.2.6 Fluorescent PLA-PEGMA synthesis

To a round bottom flask, a poly(lactide) macroinitiator (1 mmol), PMDTA (210 µL, 1 mmol), CuBr$_2$ (230 mg, 1 mmol) and rhodamine methacrylate (25.6 mg, 0.0375 mmol) were added. To the mixture varying amounts of the two co-

monomers, DEGMA and OEGMA$_{475}$, were used to give polymers with different properties. All the materials were dissolved in 25 mL of 2-butanone. The mixture was degassed by 3 cycles of freeze-pump-thaw prior to being backfilled with Ar. Tin (II) 2-ethyl hexanoate (405 mg, 1 mmol) was added as the AGET reducing agent under Ar. The reaction was heated to 60 °C and stirred for 3 – 6 h to achieve 60-70% monomer conversion. The polymerisation was stopped by opening the flask and exposing the contents to air. The reaction mixture was precipitated three times into an excess of cold hexane. The precipitate was then dissolved with CH_2Cl_2 and passed through an aluminium oxide column to remove copper. The resulting co-polymer was obtained by evaporating to dryness *in vacuo*.

(P12): 1.51-1.64 (m, 8.24H, lactide C$\underline{H}_3$), 3.42 (m, 3H, D/OEGMA C$\underline{H}_3$), 3.49-4.29 (m, 9.22H, D/OEGMA C$\underline{H}_2$), 5.08-5.30 (m, 2.68H, lactide C$\underline{H}$)

(P13): 1.51-1.64 (m, 17.78H, lactide C$\underline{H}_3$), 3.42 (m, 3H, D/OEGMA C$\underline{H}_3$), 3.49-4.29 (m, 11H, D/OEGMA C$\underline{H}_2$), 5.08-5.30 (m, 5.63H, lactide C$\underline{H}$)

2.2.7   2-(4-(((2-amino-4-oxo-3,4-dihydropteridin-6-yl)methyl)amino)benzoyl)-5-(prop-2-yn-1-yl)glutamine (Propargyl folate) synthesis

Folic acid (1 g, 2.2 mmol), *N*-hydroxysuccinimide (260 mg, 2.5 mmol) was dissolved in 10 mL anhydrous DMF and cooled to 0 °C before adding 1-ethyl-3-(3-dimethylaminopropyl)carbodiimide (440 mg, 2.5 mmol). Reaction mixture was left to stir for 30 minutes until white precipitate had formed. Propargyl amine (124 mg, 22.5 mmol) in 5 mL anhydrous DMF was added and the reaction warmed to room temperature. After 24 h the product was

precipitated in 100 mL water. Precipitate was filtered and washed with acetone before drying. Yield 781 mg (81.7%, orange solid)

MS (m/z): $[M+H]^+$ 479.1779

$[M+K]^+$ 517.1387
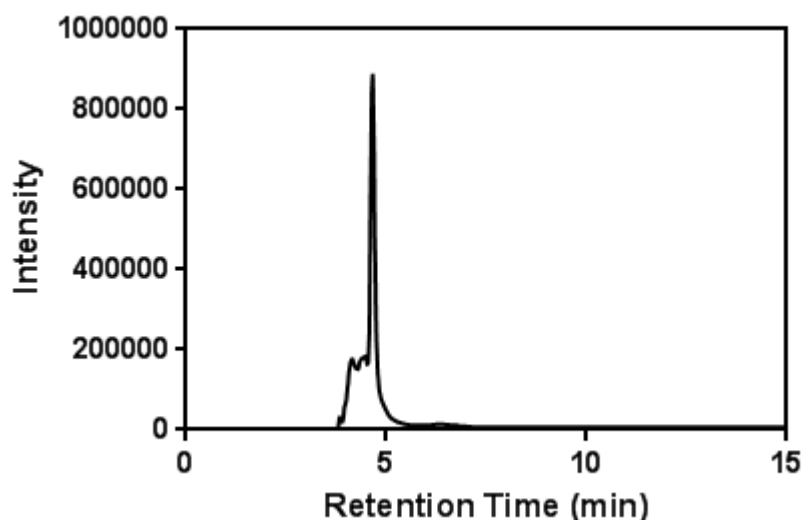
Figure 14 HPLC chromatogram of propargyl folate. Observed Peak shows β-substitution (main peak) and α-substitution (shoulder of peak). Sample prepared in DMSO diluted with water. HPLC method: 10%-20% MeCN over 17 minutes, UV detection at 363 nm.

2.2.8   2-(4-(((2-amino-4-oxo-3,4-dihydropteridin-6-yl)methyl)amino)benzoyl)-5-diazoglutamine (Azido-folate) synthesis

Folic acid (250 mg, 0.56 mmol) 2-(2-(2-azidoethoxy)ethoxy ethanol (90 µL, 0.588 mmol), DCC (231 mg, 1.12 mmol) and DMAP (1.7 mg, 0.014 mmol,) were dissolved in 25 mL DMSO under nitrogen. The reaction was stirred under nitrogen for 30 minutes until complete dissolution of the folic acid. The reaction proceeded at room temperature for 18 h under stirring. Upon completion the product was precipitated into pure water and product was recovered by centrifugation and freeze-drying. Yield: 215 mg (64.2%, pale yellow solid)

MS (m/z):   [M+H]$^+$ 599.2058
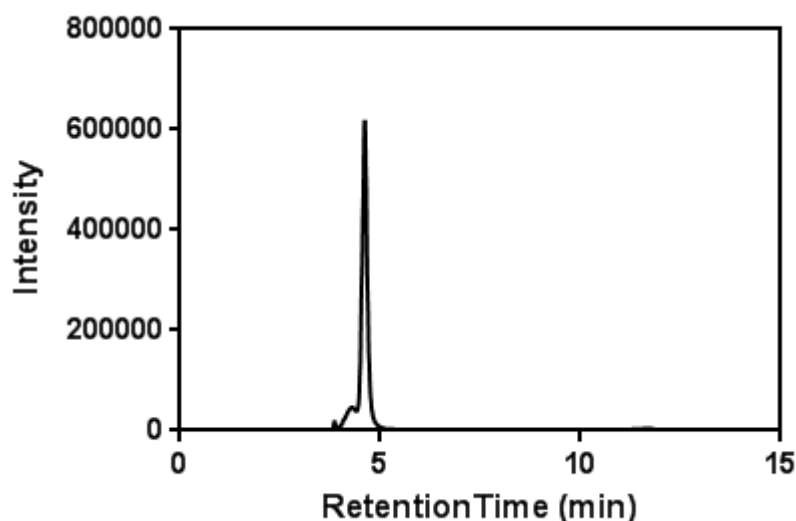
Figure 15 HPLC chromatogram of azido-folate. Observed Peak shows β-substitution (main peak) and α-substitution (shoulder of peak). Sample prepared in DMSO diluted with water. HPLC method: 10%-20% MeCN over 17 minutes, UV detection at 363 nm.

2.2.9   PLA-PEG synthesis

2.2.9.1   PEG$_{450}$:

D,L-Lactide (5.18 g, 36 mmol) and *O*-(2-aminoethyl)-*O'*-(2-azidoethyl)nonaethylene glycol (95 mg, 0.18 mmol) were heated to 120 °C under nitrogen then tin (II) ethylhexanoate (50 mg, 0.12 mmol) was added. The reaction was left to stir for 1 h before cooling. The product formed was dissolved in CH_2Cl_2 prior to being precipitated three times in cold hexane. The resulting precipitate was dissolved in CH_2Cl_2 and recovered *in vacuo.* Yield: 4.78 g (90 %)

GPC: M$_n$ 19000 Da, Đ 1.51

2.2.9.2   PEG$_{3k}$:

D,L-Lactide (1.44 g, 10 mmol) and amino-PEG$_{3k}$-alkyne (67 mg, 0.02 mmol) were heated to 120 °C under nitrogen then tin (II) ethylhexanoate (2.5 mg,

0.006 mmol) was added. The reaction was left to stir for 1 h before cooling. The product formed was dissolved in CH_2Cl_2 prior to being precipitated three times in cold hexane. The resulting precipitate was dissolved in CH_2Cl_2 and recovered *in vacuo.* Yield: 930 mg (64 %).

GPC: M_n 19100 Da, Đ 1.89

2.2.9.3   PEG$_{10k}$:

D,L-Lactide (972 mg, 6.75 mmol) and amino-PEG$_{10k}$-alkyne (450 mg, 0.048 mmol) were heated to 120 °C under nitrogen then tin (II) ethylhexanoate (10 mg, 0.024 mmol) was added. The reaction was left to stir for 1 h before cooling. The product formed was dissolved in CH_2Cl_2 prior to being precipitated three times in cold hexane. The resulting precipitate was dissolved in CH_2Cl_2 and recovered *in vacuo*. Yield: 830 mg (58 %).

GPC: M_n 20400 Da, Đ 1.86

2.2.10 PLA-PEG-Folate synthesis

PLA-PEG-N_3 (0.5 g, 0.026 mmol), propargyl folate (20 mg, 0.039 mmol), copper (I) bromide (5 mg, 0.03 mmol) and 2-2'-bipyridyl (6.2 mg, 0.04 mmol) were dissolved in 4.5 mL dry dimethylacetamide (DMAc) and stirred under argon for 30 min. The reaction was stirred for 3 days at room temperature prior to dilution with 10 mL DMAc and precipitated into ice cold diethyl ether. The precipitate was obtained by centrifugation, dissolved in minimal CH_2Cl_2 and passed through an alumina plug to remove excess copper.

Yield: 429 mg (86 %).

GPC: M_n 19400 Da, Đ 1.19.

2.3 Results

The synthesis of the polymers required to form the targeted nanoparticles occurred in three steps

1. PLGA/PLA synthesis

2. Thermoresponsive polymer synthesis using the PLGA/PLA macro-initiator

3. Folate tagged polymer synthesis

Each step in turn of the synthesis will be discussed in detail below.

2.3.1 Step one: PLGA/PLA synthesis

2.3.1.1 PLGA synthesis

PLGA was to be used to form the hydrophobic block of the thermoresponsive copolymer and as the following step employed atom transfer radical polymerisation (ATRP), PLGA would need to be synthesised with a bromine end group.

The terminal bromine atom was incorporated into PLGA using a bromine containing initiator *O*-(2-bromoisobutyryl)tetraethylene glycol (**1**) for the ROP of both lactide and glycolide monomers, Scheme 2.
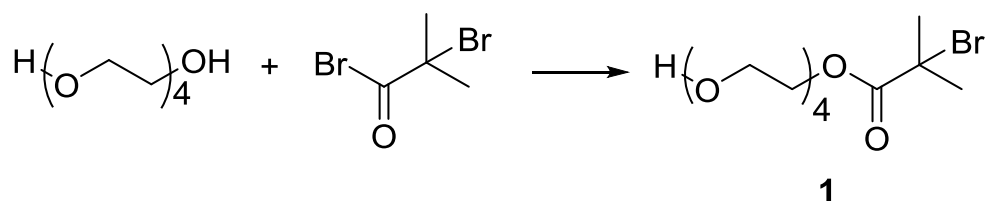
Scheme 2 Synthetic scheme for the synthesis of *O*-(2-bromoisobutyryl)tetraethylene glycol. Reaction conditions: NaHCO₃, 0°C – RT, overnight.

The bromide-containing initiator was synthesised by the nucleophilic substitution of tetraethylene glycol with 2-bromoisobutyryl bromide, achieving a final yield of 2.2 g (12.5 %) to be used in the ROP of lactide and glycolide, Scheme 2. The low yield can be attributed to the limited selectivity between reactants; the tetraethylene glycol has two terminal nucleophilic hydroxyl groups capable of reacting with the carbonyl of the acyl bromide and thus both mono- and di-substituted tetraethylene glycol are obtained. As only the mono-substituted initiator is required for the ROP, the di-substituted product (plus any unreacted materials) was removed by silica column chromatography.

Initial research aims required synthesis of polymers containing 50:50 PLGA (lactide-glycolide) as previous work within the group proposed these polymers as a good foundation for a thermoresponsive polymer NP.[127]

The synthesis of the 50:50 (lactide-glycolide) NPs was carried out under solvent free conditions with tin (II) chosen as an appropriate catalyst for the ROP, Scheme 3. However, initial attempts yielded polymers with both high polydispersity (Đ ≈3) and low M_n <5000 Da, indicating that there was scope for method optimisation. The method was further investigated in order to yield more defined polymers for ATRP, i.e. with M_n 10-20 kDa and Đ < 2.[127]
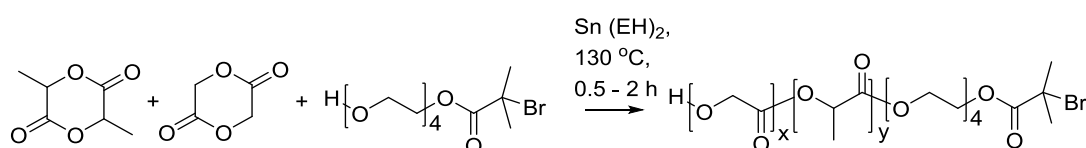
Scheme 3 Synthetic scheme for PLGA formation *via* ROP

The first approach was to introduce an alternative catalyst. Recent advances in organo-catalyst research led to the development of metal free catalysed ring opening polymerisations which offered an alternative to the more commonly reported inorganic catalysed ROP.[128]

Three organic catalysts were chosen for this optimisation reaction; 1,5,7-Triazabicyclo[4.4.0]dec-5-ene (TBD) (**3**),[129] 1,8-Diazabicyclo[5.4.0]undec-7-ene (DBU) (**4**),[130] and 1-(3,5-bis(trifluoromethyl)phenyl)-3-cyclohexylthiourea (**5**)[131,132] with dimethylaminopyridine as co-catalyst, Figure 16.
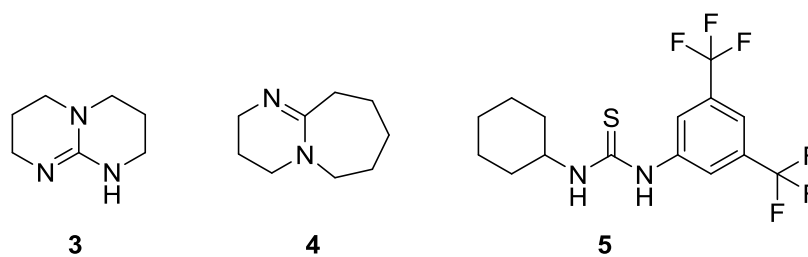
Figure 16 Organic catalysts used for ROP. 3: TBD. 4: DBU. 5: 1-(3,5-bis(trifluoromethyl)phenyl)-3-cyclohexylthiourea

These catalysts have previously been used for the ROP of cyclic esters,[128] including lactide, however not for the co-ROP of lactide and glycolide to form PLGA. The ROP with the organo-catalysts was investigated in both the melt and solution phases, but unfortunately none of the catalysts were found to produce PLGA with the desired M_n or polydispersity, affording an average M_n of 1000 – 3000 Da; significantly less than the M_n of the PLGA formed using the previous tin (II) catalyst. This can be explained by a possible lack of reactivity with the chosen co-monomers. Due to the lack of reactivity and inherent insolubility of the polymers produced, the decision to decrease the quantity of glycolide present in the PLGA was taken. Further optimisation of the

reaction was carried out by altering the ratio of lactide to glycolide to generate polymers with both greater M_n and solubility.

2.3.1.1.1 65:35 and 75:25 PLGA synthesis

As a proof of concept, initial studies to determine the effect of monomer ratio was carried out using only the 75:25 PLGA synthesis.

ROP on a 500 mg scale yielded approximately 325 mg of polymer after 2 h, however the calculated M_n for the resulting polymer was less than 1000 Da with a Đ of 2. The large Đ and low M_n was thought to be due to inefficient stirring of the monomers. As the polymer formed, the melt became overly viscous, decreasing the likelihood that the monomers were homogenously mixed. With a lack of stirring the polymer that formed was not able to come in contact with all the monomer present thus the low M_n observed.

To overcome the problem with mixing, the reaction was scaled up (2.5 g), increasing the final volume of the system, this allows for more efficient mixing using a stirrer bar ensuring that the melted monomers were able to form a homogenous mix with the initiator and catalyst. Under these conditions the catalyst was found to be well mixed with the monomers and initiator which enabled the reaction to proceed more efficiently, yielding a 75:25 PLGA polymer with M_n of 8 kDa. The Đ of this polymer was 2.7 however following purification it was possible to remove the lower molecular mass fractions. As this was the largest M_n achieved, it was thought that using a larger reaction scale would enhance the outcome of the polymerisation and potentially lead to the formation of a polymer with the desired properties, i.e. M_n, closer to

10-20 kDa and Đ , 2. The increased reaction scale also provided the additional benefit of allowing a large quantity of PLGA to be synthesised in one pot, ensuring batch-to-batch variability was minimised for consistency during further polymerisations.

To validate the robustness of the synthetic protocol the reaction was scaled up further to both 10 g and 30 g for 65:35 and 75:25 PLGA. Table 1 reports the observed M_n and Đ values calculated from the 75:25 polymerisation reactions, however, the values reported for 10 g and 30 g are representative of the values also obtained in the polymerisation of 65:35 PLGA.

Table 3 Properties of 75:25 PLGA-Br achieved from reaction scale-up

Reaction scale (g)	Reaction time (h)	M_n (Da)	Đ
0.5	2	920	2.01
2.5	2	8300	2.76
10	0.5	13900	1.49
30	0.5	19500	1.89

The scale up to 10 g and 30 g generated PLGA in sufficient M_n and Đ (10 - 20 kDa and Đ < 2). This method was therefore progressed through to subsequent steps in the synthesis of the thermoresponsive polymers.

As demonstrated above, the synthesis of a reproducible PLGA proved to be very challenging both in terms of time and yields. It was not until larger scale reactions were implemented and reduced quantities of glycolide were used that PLGA of desired quality was obtained. Thus, it was thought that removing

glycolide as a contributing co-monomer could potentially enhance the reaction even further. The following section reports synthesis of a polylactide (PLA) homopolymer.

2.3.1.2 The loss of glycolide: PLA synthesis

The omission of glycolide was considered to provide a two-fold advantage: firstly, it would alleviate any concern over ensuring the ratio of glycolide to lactide remained consistent batch-to-batch. Secondly, by only using lactide as the monomer more scope was afforded to the type of catalysts that could be used to synthesise the polymer. Both inorganic catalysts, such as Sn^{2+}, and organocatalysts, such as TBD and DBU, have been shown to polymerise lactide effectively. Initially both Sn^{2+} and TBD (**3**) were re-evaluated as suitable catalysts for the synthesis of PLA, to determine which method produced PLA of the highest quality. NMR scale reactions showed **3** was a suitable catalyst affording PLA with a M_n of 15 kDa and Đ of 1.7 following a 5 min reaction time. Sn^{2+} was investigated also to determine if an improvement in the Đ could be achieved. Using the conditions mentioned above for the synthesis of PLGA, this method was found to produce PLA with a M_n and Đ similar to those formed when **3** was used. Both methods were found to be scalable, up to 30 g tested, however, there was a slight increase in the observed polydispersity (from 1.5 to 1.7) when TBD was used. Thus, both TBD and Sn^{2+} were validated as viable catalysts for PLA synthesis.

With the confirmation that both 65:35 and 75:25 PLGA could be synthesised using a Sn^{2+} catalyst and that PLA could be synthesised with ease using either Sn^{2+} or **3**, the foundation was provided for the synthesis of the block copolymers that would make up the thermoresponsive shell of the NPs.

2.3.2 Step two: Thermoresponsive polymer synthesis

Polymerisation from the formed PLGA macro-initiator was achieved activator generated by electron transfer atom transfer radical polymerisation (AGET ATRP).

Poly(1-hydroxypropan-2-yl) methacrylate (PPGMA) and poly(2-methoxyethyl) methacrylate (OEGMA) were used to impart thermoresponsive properties to the polymer, as shown in Figure 17. These monomers were chosen as they had previously been shown to produce thermoresponsive polymers with a variable transition temperature (T_t) of 31 – 84 °C dependent on the monomer ratio.[127]
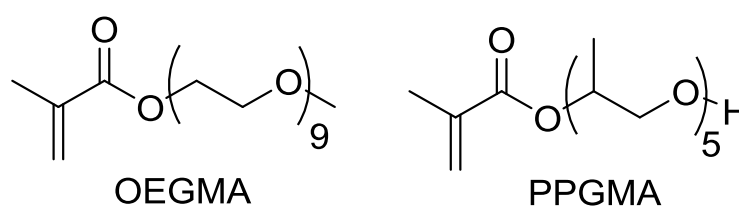
Figure 17 OEGMA$_{475}$ and PPGMA$_{375}$ monomers used for the synthesis of thermoresponsive polymers from PLGA

By varying the ratio of these two monomers the amphiphilicity of the resulting polymer can be controlled, thus enabling fine tuning of the T_t; the more hydrophilic the outer shell of the NP the higher the T_t and vice versa.

OEGMA is the more hydrophilic monomer, containing nine ethylene glycol

repeat units and thus presents more opportunity to hydrogen bond to water

in solution. The greater the number of sites capable of hydrogen bonding to

water the larger the amount of energy (by heating) that needs to be put into

the system to break these hydrogen bonds and bring about the phase

separation into polymer rich and polymer poor phases. As phase separation

occurs there is a loss of colloidal stability when these thermoresponsive

polymers are on the corona of nanoparticles.
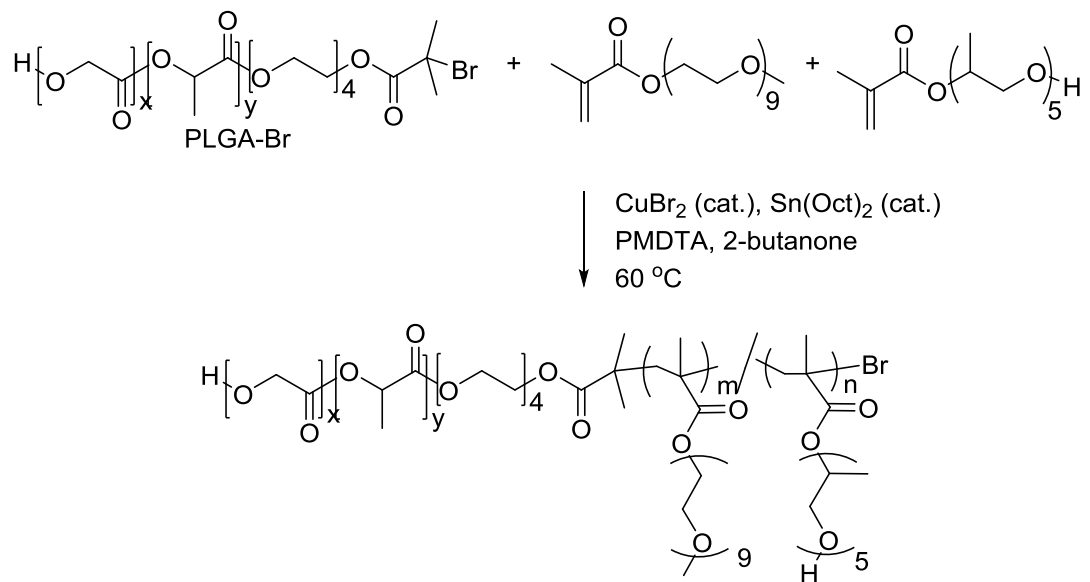
**Scheme 4 Reaction scheme for the synthesis of PLGA-*b*-P((PPGMA)-*stat*-(OEGMA)) by AGET
ATRP**

A small library of thermoresponsive PLGA-*b*-P((PPGMA)-*stat*-(OEGMA))

polymers was synthesised as shown in Table 4. Each of the polymers P1-P5

were synthesised using both the 65:35 and 75:25 PLGA macro-initiator,

Scheme 4.

Table 4 Feed ratio of monomers for the synthesis of PPGMA-OEGMA copolymers

Polymer	PPGMA:OEGMA	PPGMA (mmol)	OEGMA (mmol)
P1	3:1	5.63	1.87
P2	2:1	5	2.5
P3	1:1	3.75	3.75
P4	3:2	4.5	3
P5	4:1	6	1.5

Synthesis was carried out on a 0.1 mmol scale (initiator) with 1:1:75 [Ini.]:[cat.]:[monomer]. It was found that the average yield of each polymer was between 1.3-1.5 g with similar M_n and polydispersity values recorded. The mass analysis for each polymer synthesised was consistent (except for **P5a** and **P5b**, for which a different batch of PLGA with higher M_n was used) and therefore the Đ was found to be decreased for each (< 1.5). The data is in agreement with those figures previously published for similar polymers.[127]

Table 5 GPC results for copolymer synthesis (*M_n is larger for these two results due to a different batch of PLGA-Br which had a larger M_n itself.)

Polymer		M_n (kDa, GPC)	Đ
65:35 core	**P1a**	21.0	1.35
	P2a	17.9	1.44
	P3a	18.3	1.39
	P4a	15.5	1.49
	P5a	37.0*	1.28
75:25 core	**P1b**	21.0	1.30
	P2b	19.3	1.31
	P3b	18.7	1.33
	P4b	19.3	1.31
	P5b	40.1*	1.36

Upon completion of this library of polymers, NPs were assembled and tested for their thermoresponsive properties.

2.3.2.1 Thermoresponsive properties of P1-P5

For the NPs to progress through to *in vitro* testing a T_t of 30 – 35 °C was required. Maintaining this temperature would ensure the NPs existed only in their corona-collapsed/hydrophobic state whilst at 37 °C (standard incubator temperature) thus ensuring *in vitro* cell uptake could be efficiently monitored without concerns over an unintended change of state.

To determine the T_t of each polymer, UV-vis spectrophotometry was utilised, with T_t approximated *via* determination of the cloud point of the NP

suspension. The cloud point is referred to as the point at which the NPs lose their colloidal stability and begin to phase separate. Although the cloud point is not a quantitative representation of the LCST, it is a close and reliable approximation. This is because the cloud point is the bulk representation of the precipitation caused by the phase separation of polymers when the temperature of the solution reaches the polymer LCST.

The cloud points were measured by heating NP suspensions at a constant rate (0.5 °C/min) and reading the optical density measured at 550 nm. For **P1-4** for both 65:35 and 75:25 PLGA core T_t ranged from 42 – 64 °C, Figure 18. The two different cores had a negligible effect on the T_t of each NP, the only exception seen in **P4** which demonstrated an increase of 2.5 °C between the 65:35 and 75:25 cores.
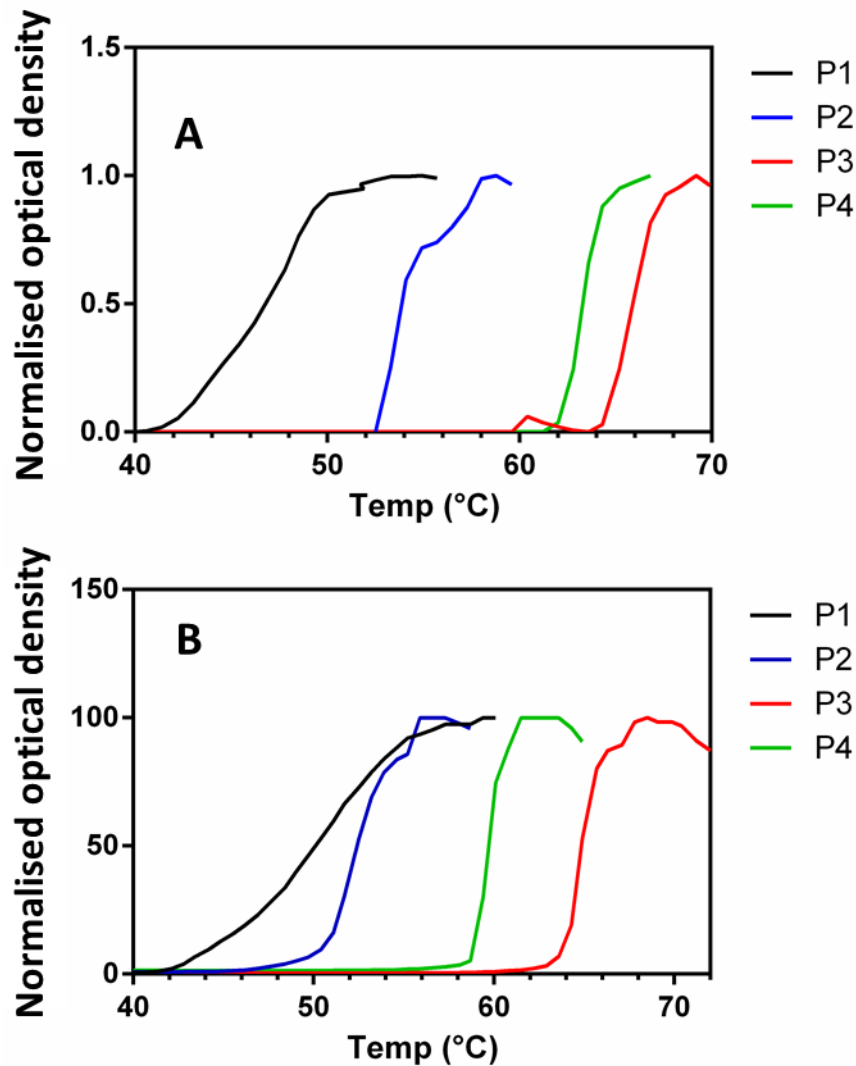
Figure 18 T_t data for P1-P4. A) 65:35 PLGA core P1-4. B) 75:25 PLGA core P1-P4. The inflection point in the optical density data denotes the T_t of each NP. The OD data was recorded at 550 nm from samples heated at 0.5 °C/min. Concentration of each NP sample was 10 mg/mL.

As the cloud point is a measure of when the bulk suspension loses colloidal stability it is possible that the measurement would be susceptible to concentration changes. It is possible that when the concentration of NPs is lowered the rate at which the NPs will aggregate together upon chain collapse will be slower, due to their being less NPs in the vicinity of each to aggregate quickly. If this was indeed the case then it would take a longer time period to cause a measureable change in the OD. To understand how much this would

affect **P1-P4**, the cloud point of **P1** was measured at 5 and 10 mg/mL in both water and phosphate buffered saline (PBS) as a more biologically relevant medium, Figure 19. There was no observable difference in the cloud point for **P1** NPs when the concentration of the suspension was halved, however when the NPs were in PBS the cloud point was observed at 3 °C lower that the sample prepared in water. This shows that the PPGMA-OEGMA corona NPs do not have a concentration dependant cloud point. The reason for the reduction in T_t when the NPs are suspended in PBS is due to the salting effect.[133] The salts in PBS, of which NaCl is the main constituent, interferes with the hydrogen bonding sites of the water by binding to the O atoms of the PPGMA and OEGMA. This causes there to be less energy needed to break these hydrogen bonds and thus facilitate phase separation. Recent molecular dynamics on poly(*N*-isopropylacrylamide) showed that when NaCl, NaBr, NaI and KCl salt solutions were used the cations had a strong affinity for the amide O and this was what lowered the observed LCST in the presence of salts.[134]
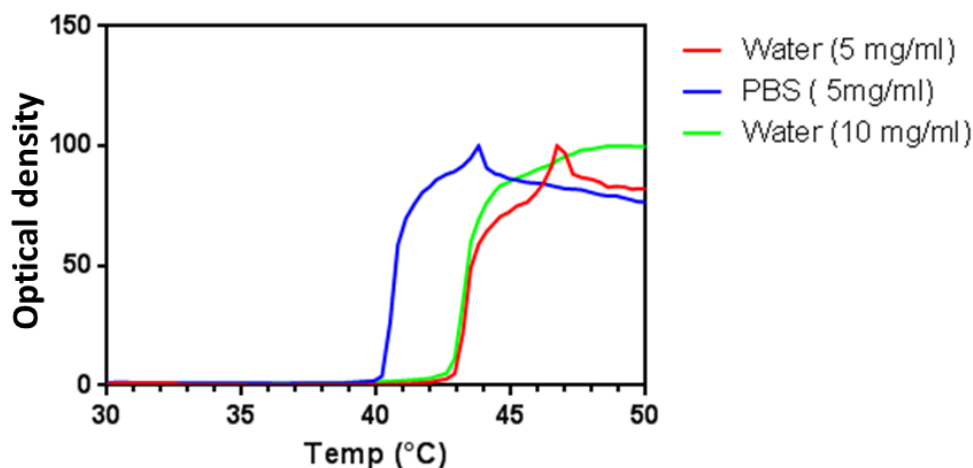
Figure 19 T_t data for P1 in water at 5 and 10 mg/mL and PBS at 5 mg/mL

The decrease in T_t observed when the NPs were suspended in salt containing solutions is something that needs to be considered when NPs are taken *in vitro/in vivo* and therefore needs thoroughly tested.

Although it has been shown that the T_t could be altered by simply modifying the ratio of PPGMA to OEGMA$_{475}$ the lowest observed T_t in each of these instances was 40 °C; when the NPs were assembled in PBS, 6 °C higher than the desired range for the T_t. These temperatures also contradicted those T_t's previously reported (31 – 55 °C).[127] The reasons behind the conflicting T_t results have yet to be determined as the synthesised polymers had very similar M_n and Đ values.

Given the observed increase in T_t, the PPGMA monomer was substituted for DEGMA (similar to the OEGMA monomer but with only two ethylene glycol repeat units). Lutz *et al* have shown that when copolymers were synthesised using these monomers the T_t could be finely controlled and that the degree of polymerisation (DP) had no effect on the T_t.[60] In addition to substituting

PPGMA for DEGMA, it was chosen at this point to only use PLA as the macroinitiator both due to the ease of synthesis and reproducibility of synthesis, i.e. no lactide:glycolide inconsistencies.
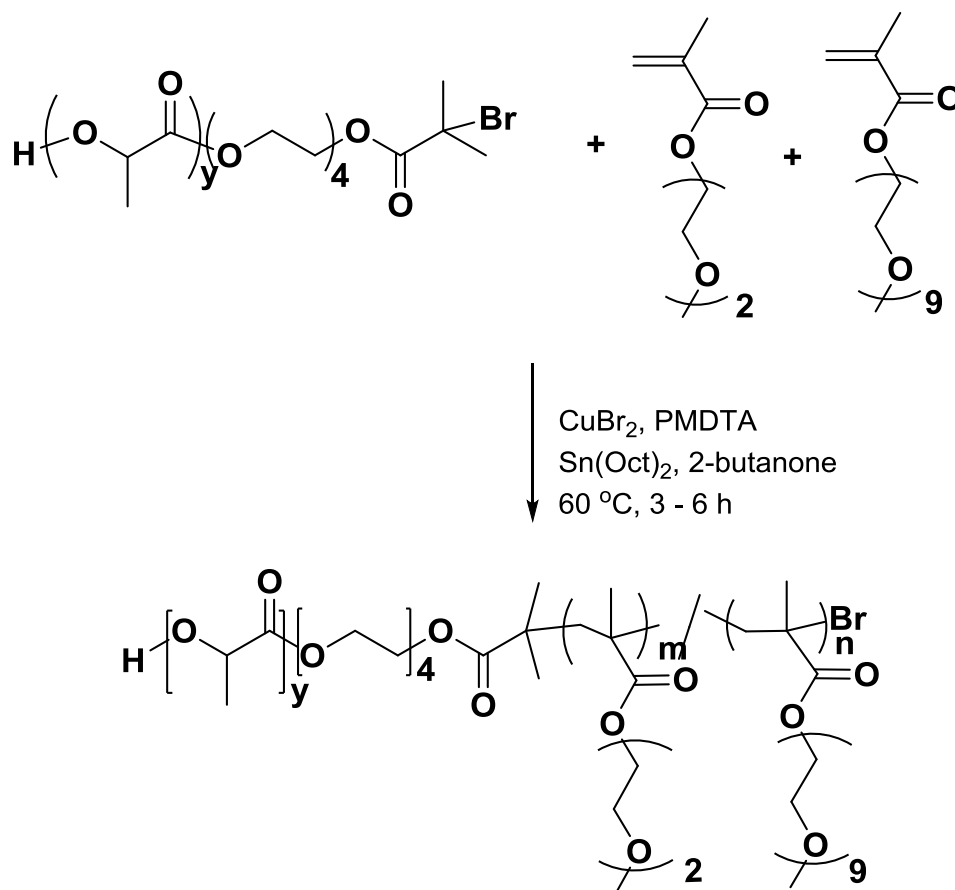
Scheme 5 PLA-*b*-((DEGMA)-*stat*-(OEGMA)) polymer synthetic scheme using AGET ATRP.

The PLA-*b*-((DEGMA)-*stat*-(OEGMA)) thermoresponsive polymers were synthesised as previously reported for the PLGA-*b*-((PPGMA)-*stat*-(OEGMA)) thermoresponsive polymers, **Scheme 5**. Using this method, a variety of polymers were assembled with varying ratios of DEGMA to OEGMA, a selection of which are shown in Table 6.

Table 6 Reaction and mass information for PLA-*b*-((DEGMA)-*stat*-(OEGMA)) polymers.

Polymer	PLA M_n (kDa)	Total $M_{n,GPC}$ (kDa)	$Đ_{GPC}$	M_n (kDa)$_{NMR}$	OEG$_9$MA, theoretical (mol%)	OEG$_9$MA content (mol%)$_{NMR}$	NP T_t (°C)
P6	14.7	37.3	1.32	34.8	0	0	28
P7	14.7	50.2	1.29	38.7	5	6	35
P8	14.7	52.1	1.26	37.4	10	8	42
P9	14.7	41.7	1.38	39.7	20	17	50
P10	13.1	36.6	1.45	28.7	35	30	64
P11	13.1	47.5	1.46	30.5	50	44	78

GPC: CHCl$_3$ mobile phase flow rate: 1 mL/min. Oven temp: 30 °C Samples dissolved in CHCl$_3$ prior to analysis. NMR: Bruker 400 Ultrashield at 400MHz and 25 °C.

As the data in Table 6 shows, the results are similar to those from the previous PLGA thermoresponsive polymers with all displaying a low Đ (< 1.5) and a consistent M_n across the series, Figure 20.
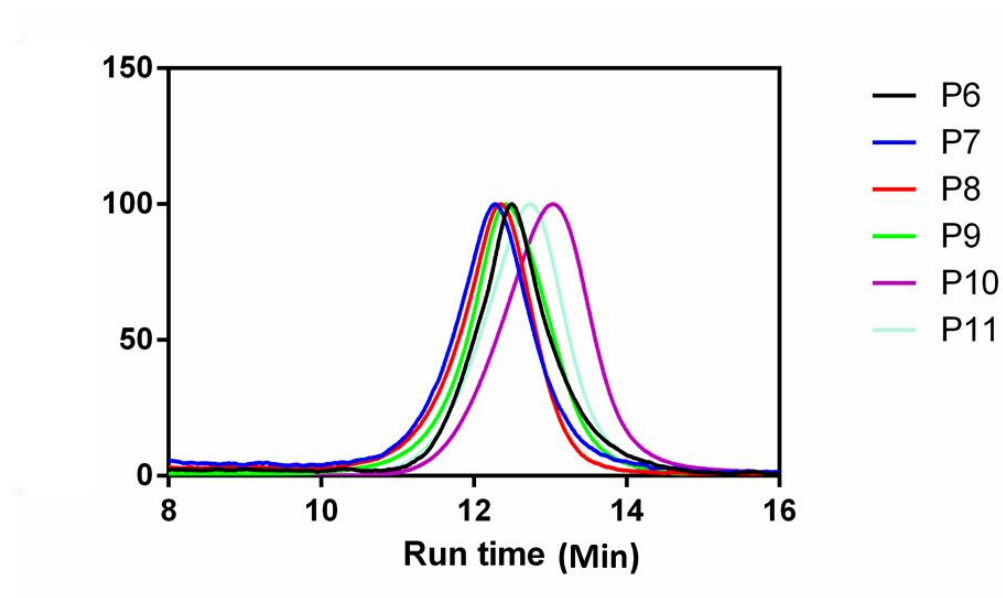
Figure 20 GPC traces overlaid for P6-11. Solvent: chloroform.

The important aspect of these polymers is that the resultant OEGMA content is agreeable with that of the feed ratio as this controls the transition temperature of the NPs. When the polymers were analysed by ^{1}H NMR it was possible to calculate the percentage content of OEGMA (with the remainder made up of DEGMA) in each polymer. For each polymer **P6-P11** the calculated OEGMA content mostly agreed with the theoretical content; there was a maximum 6 % difference between calculated and theoretical OEGMA for **P11**. To ascertain whether the change from PPGMA to DEGMA resulted in a drop in recorded T_t, NPs of **P6-P11** were assembled and tested.

2.3.3 Thermoresponsive properties of P6 – P11

The NP T_t for **P6-11** was determined using the method previously described for **P1**-**P5**.
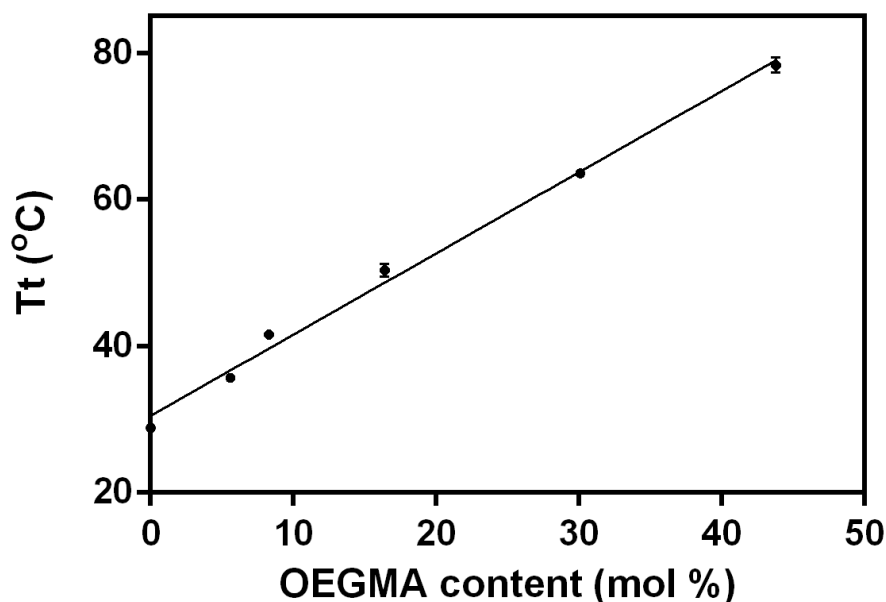
Figure 21 Comparison of the T_t of NP vs OEGMA content in the NP corona. Each data point is the mean of N=3 experiments.

The T_t of **P6-P11** NPs was compared with the OEGMA content and was found to exhibit a positive linear relationship across the entire series of polymers, Figure 21. The T_t of each of these polymers was in the range that was expected, i.e. from 28 °C for **P6** through to 78 °C for **P11**. The data agreed with that previously reported for p(DEGMA-*b*-OEGMA). For 5 % OEGMA the T_t would be 32 °C,[60] and the observed T_t for **P7** (6 % OEGMA) was 35 °C. As there was little difference in the T_t it can be concluded that the addition of PLA to p(DEGMA-*b*-OEGMA) had no effect on the resultant T_t of the NPs, as expected.

This result allows for a specific T_t to be selected and the associated ratio of OEGMA:DEGMA to be determined, without the need for multiple syntheses.

For the aforementioned NPs to be used as a drug delivery vehicle *in-vivo* the transition of the NPs between their colloidally stable and unstable states would need to be reversible. This w`ould limit any potential off target effects by ensuring the NPs remained in the hydrophilic, chain extended state when the NPs are not being heat activated.
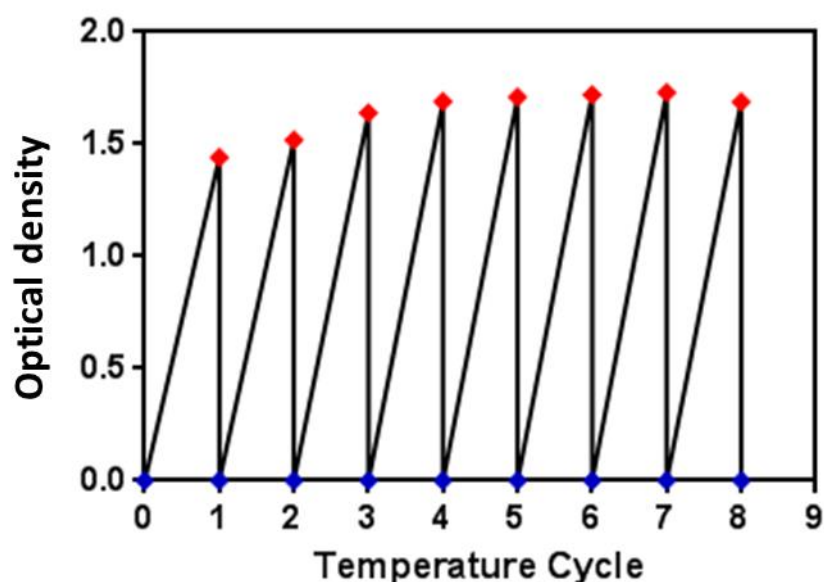
Figure 22 Reversibility in polymer collapse as shown by 8 heat/cool cycles where a large increase in optical density was measured upon each heating cycle.

To test the reversibility of the NP transition a sample of **P7** NPs were heated to 45 °C (beyond T_t) and cooled to 20 °C (below T_t) at 1 °C/min intervals and the change in optical density (550 nm) measured during each cycle, Figure 22. For each heat/cool cycle the optical density increased upon heating and reduced upon cooling as would be expected for NPs switching from colloidally unstable (high temp.) to stable states (low temp.).

The T_t data acquired for the PLA-*b*-((DEGMA)-*stat*-(OEGMA)) polymers confirmed this system as ideal for further study due to a defined and reversible T_t. From the library of polymers, two polymers with 5 % and 12 % OEGMA, respectively were synthesised to contain an additional red fluorescent rhodamine B tag for testing *in-vitro*.

2.3.4 Fluorescent thermoresponsive polymer synthesis for *in-vitro* studies
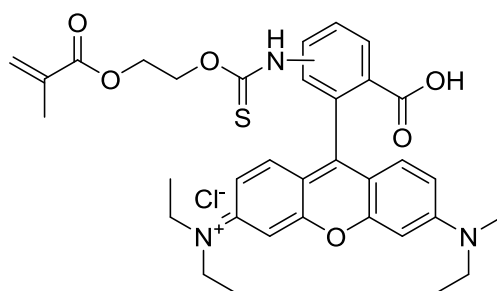
Figure 23 rhodamine B methacrylate dye

The addition of rhodamine B methacrylate dye ([dye]:[monomer], 1:1000) during the AGET ATRP process enabled the NPs formed to be fluorescent and thus visible for microscopy and flow cytometry experiments. The aim was for the T_t of each polymer when assembled into NPs to be in the region of 35 °C and 45 °C respectively, below and above body/incubator temperature, 37 °C, for *in-vitro* testing.

Table 7 Reaction and mass information for PLA-*b*-((DEGMA)-*stat*-(OEGMA)) polymers to be used for *in-vitro* studies.

Polymer	PLA M_n (kDa)	Total $M_{n, GPC}$ (kDa)	Đ$_{GPC}$	M_n (kDa)$_{NMR}$	OEG$_9$MA, theoretical (mol%)	OEG$_9$MA content (mol%)$_{NMR}$	NP T_t (°C)
P12	14	42	1.44	35	5	5	27

| P13 | 14 | 39 | 1.37 | 27 | 12 | 10 | 39 |

The two polymers were synthesised successfully with an OEGMA content in line with that desired, 5 and 10 mol% respectively, with a T_t of 27 °C for the first of the synthesised polymers, **P12**, and 39 °C for the second, **P13**. Although the measured T_t was slightly lower than desired they were in the range considered acceptable for further *in-vitro* testing.

Thus far only the thermoresponsive element of the drug delivery vehicle had been investigated, once the two rhodamine tagged polymers of desired T_t had been generated the remaining element of the 'hide-and-reveal' motif was synthesised.

2.3.5   Step Three: Folate tagged polymer synthesis

To add the hide-and-reveal motif of these NPs three amphiphilic polymers were synthesised with 3 different lengths of PEG linkers, each with a terminal folate group for targeting.

PEG_{400}, PEG_{3k} and PEG_{10k} were chosen to act as spacers between the PLA core and the folate tag. This polymer once assembled would then be mixed in with the thermoresponsive polymer and mixed NPs would be assembled with the hide-and-reveal motif.

The three different length spacers would facilitate the folate being situated at a certain distance from the core of the PLA, so may or may not be shielded by the thermoresponsive corona depending on the length of linker.

If we assume that all the polymers are in their linear elongated structure, the lengths of each polymer can be calculated using cosine rule. I.e. using PEG as an example:
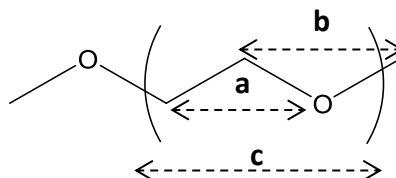
Figure 24 determining the length of PEG using the cosine rule

Each repeat unit of PEG consists of C-C-O triangle and C-O-C triangle, denoted in Figure 24 by **a** and **b**, respectively. To determine the length of one repeat unit:

$$\mathbf{c} = \mathbf{a} + 0.5\mathbf{b}$$

Using cosine rule:

$$a^2 = 0.154^2 + 0.14^2 - 2(0.154 \times 0.14)cos\ 109.5°$$

$$a = 0.240\ nm$$

$$b^2 = 0.14^2 + 0.14^2 - 2(0.14 \times 0.14)\ cos104°$$

$$b = 0.229\ nm$$

$$c = 0.355\ nm$$

Therefore with **c** being the length of one repeat unit, by multiplying this be the DP the lengths of each polymer can be determined, Table 8. It is also possible to calculate the freely-jointed random walk end to end distance if the polymers are assumed to be in their theta solvent:

$$r_f^2 = nl^2$$

Where r_f is the random walk end to end distance, n is the number of bonds in the chain and l is the length of bond.[135] The random walk end to end distance is however unrealistic as it does not take into account any bond angles or the interaction between the chain elements and thus the rigidity of the polymer chains; however this can serve as a minimum size for the purposes of the comparison between polymer chains. By comparing the two results together it can be postulated that the actual length of the polymers will be part way between these minimum and maximum distances.

Table 8 Length of polymers used for hide-and-reveal motif. Polymers were assumed to be in theta solvent and thus in their fully elongated structure

Polymer	Length of thermoresponsive corona (nm)		Length of PEG$_x$ linker (nm)	
	Fully elongated	**Random walk (end to end)**	**Fully elongated**	**Random walk (end to end)**
P12	37.7	3.8		
P13	20.0	2.7		
PEG$_{400}$			3.2	1.1
PEG$_{3k}$			24.1	2.9
PEG$_{10k}$			80.2	5.3

From the 3 PEG linkers, two, PEG$_{400}$ and PEG$_{3k}$ should have their folate tag 'hidden' when the thermoresponsive corona is in its fully hydrated state however, PEG$_{10k}$ has length larger than the thermoresponsive corona and so should be protruding from the surface of the NP corona and 'visible' at all

times. This would give the option of comparing the 3 types of folate tagged NPs and whether the length of linker has any significant effect on the uptake, this will be investigated in Chapter 4.

All 3 polymers were synthesised in the same manner. The PEG linker was purchased with a terminal amine and either a terminal alkyne or azide. The free amine was used for the ROP of lactide to form PLA-PEG$_x$-alkyne/azide, followed by copper catalysed cycloaddition to attach the folate molecule to the terminus of the chain, Scheme 6.
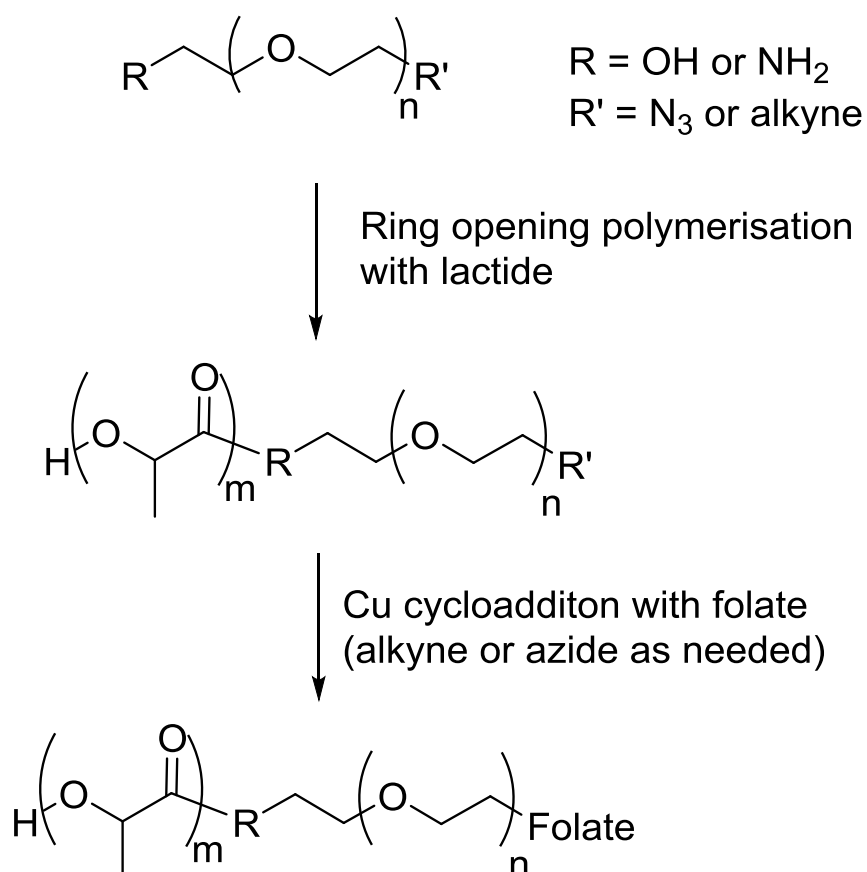
Scheme 6 Synthetic scheme for synthesis of PLA-PEG$_x$-folate

Table 9 Mass information for PLA-PEG$_x$-folate targeting polymers

Polymer	$M_{n,GPC}$ kDa	Đ $_{GPC}$

PLA-*b*-PEG$_{400}$-folate	19.5	1.19
PLA-*b*-PEG$_{3k}$-folate	17.2	1.34
PLA-*b*-PEG$_{10k}$-folate	22.5	1.45

Each PLA-PEG$_x$-folate was successfully synthesised with a consistent M$_n$ and low Đ and taken forward for further testing which will be discussed further in Chapter 4.

2.4   Conclusions

Many issues were encountered during the synthesis of a 50:50 PLGA suitable for further ATRP synthesis both in terms of achieving a desirable M$_n$ and with a required solubility. Establishing a system in which the glycolide was the minor component (65:35, 75:25 and 100:0) PL(G)A was successfully synthesised to the required M$_n$ for the thermoresponsive synthesis.

Although a library of PLGA-*b*-((PPGMA)-*stat*-(OEG$_{8-9}$MA)) was successfully synthesised the T$_t$ of NPs assembled for each was too high for further testing (> 40 °C). PLA-*b*-((DEGMA)-*stat*-(OEGMA)) however showed T$_t$ from 28-78 °C. Two types of the PLA-*b*-((DEGMA)-*stat*-(OEGMA)) were then chosen (5% and 12% OEGMA) for taking forward to further testing. The formulation of these NPs is investigated in Chapter 2. Three PLA-PEG$_x$-folate polymers were also synthesised, with different lengths of PEG, for mixing with thermoresponsive polymer to make NPs with the 'hide-and-reveal' motif. These were further tested *in vitro* and the results are discussed in Chapter 4.

3   Development of a reproducible method for nanoparticle assembly

3.1   Introduction

In Chapter 1 the synthesis of thirteen polymers (**P1-P13**) was reported. For these polymers to be considered as a suitable foundation for the targeted drug delivery device under investigation it must first be possible to formulate the polymers into nanoparticles (NPs). The NP formulation process must adhere to two criteria; firstly, it must be robust, allowing for the reproducible production of NPs within a precise size range, secondly, the NPs must be capable of encapsulating hydrophobic drug molecules

A common method of assembling nanoparticles is nanoprecipitation, or interfacial deposition. This method involves the addition of a polymer rich, water miscible, organic solution to water or predominantly aqueous phase. As the organic phase disperses and the polymer comes into contact with the aqueous phase, the hydrophobic block of the polymer forms the inner core of the NP, with the hydrophilic block forming the outer shell/corona, Figure 25.
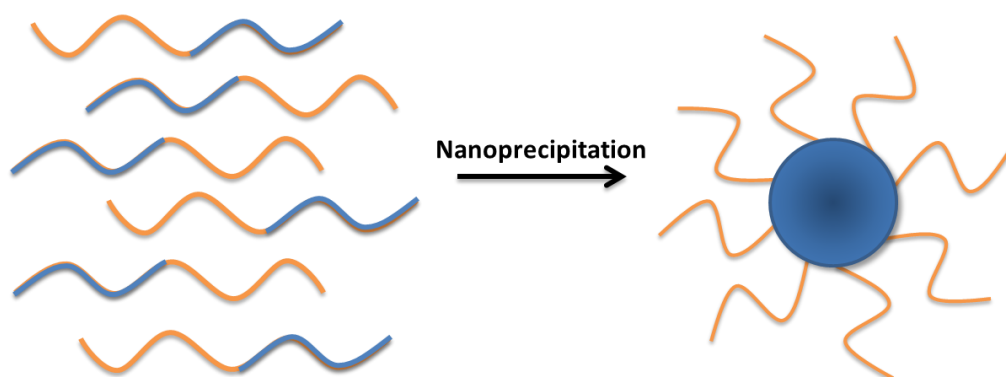
Figure 25 General schematic of nanoprecipitation. Free polymer on right hand side in organic solvent formed into NPs by adding to aqueous solution, hydrophobic (blue) section of polymer forms core of NP with hydrophilic (orange) section forming the corona.

This technique is typically executed by adding the polymer rich solution to a stirred aqueous solution using a dropper, e.g. pipette or dropping funnel, [136,137] and is one of the most commonly reported methods due to its ease of use without the requirement for any specialised equipment.

More recently however, the use of microfluidics for NP assembly has become an increasingly common technique for a variety of NP formulations, such as inorganic core-shell NPs[138-140] and polymeric NPs.[141-143] This technique allows fine control over solvent flow with mixing at the milli- to microsecond range possible.[140] This technique generally involves the assembly of microfluidic chambers or chips to house channels capable of holding nano- to microlitre volumes. A disadvantage of this technique is that it can only be used for preparing NPs for *in vitro* studies as the low volumes and flow rates protract the length of time taken to assemble the necessary quantity of NPs for *in vivo* experiments. It has been suggested that the use of parallel microfluidics would retain the structured and reproducible assembly of NPs but increase the quantity of NPs produced at a time.[144]

The recent advancement in microfluidic technology for the controlled assembly of NPs is here applied using a very similar strategy for the assembly of PLGA and PLA core NPs.

3.2 Methods

Polymers used for this formulation study are described in Chapter 1 (**P1 – P13**).

A)

B)
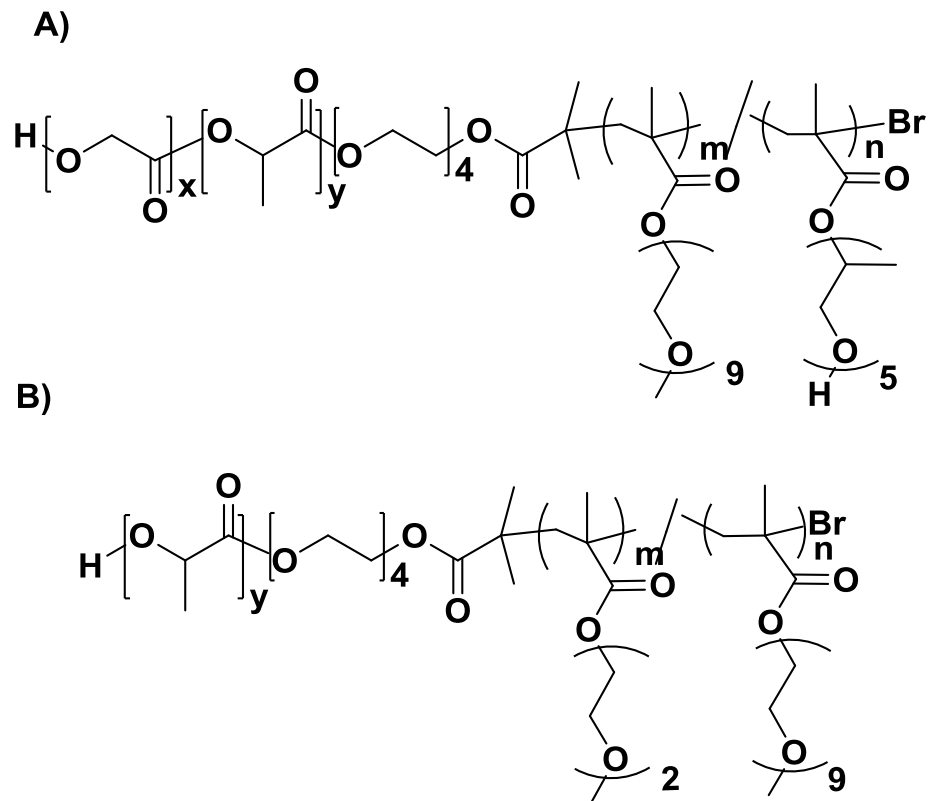
Figure 26 A) Structure of PLGA-*b*-p(PPGMA-*stat*-OEGMA) (P1-P5). B) Structure of PLA-*b*-p(DEGMA-*stat*-OEGMA) (P6-P13).

Table 10 Polymers used for the optimisation of NP assembly. For synthesis information consult Chapter 1. Polymers denoted with 'a' have 65:35 PLGA core, 'b' are 75:25 PLGA core.

Polymer	Type of core	PPGMA:OEGMA	mol% OEGMA	NP size (DLS – nm)
P1a/b	PLGA	3:1		34 ± 6
P2a/b	PLGA	2:1		39 ± 3
P3a/b	PLGA	1:1		29 ± 4
P4a/b	PLGA	3:2		41 ± 7
P5a/b	PLGA	4:1		30 ± 2
P6	PLA		0	60 ± 2
P7	PLA		6	75 ± 3
P8	PLA		8	102 ± 12
P9	PLA		17	86 ± 8
P10	PLA		30	78 ± 4
P11	PLA		44	92 ± 7
P12	PLA		5	78 ± 6
P13	PLA		10	93 ± 5

3.2.1 Solvent drop method

A known concentration of polymer in acetone (10 mg mL^{-1}) was added drop-wise using a Pasteur pipette to an equal volume water or PBS stirred at 500 r.p.m. Residual acetone was allowed to evaporate by stirring the suspension at room temperature overnight.

3.2.2   Solvent flow method

Two syringe pumps were used to enable precise flow control of aqueous and organic phase. One syringe contained the polymer dissolved in acetone (10 mg mL^{-1}) the other contained the aqueous phase (e.g. water or PBS). The syringes were connected with polyether ether ketone (PEEK) tubing (i.d. 0.02") to a T-connector where mixing occurred. The flow rates of each solution were kept constant throughout. Nanoparticle suspensions obtained were stirred at room temperature to allow the residual acetone to evaporate.

3.2.3   Drug encapsulation

Using the syringe pump method, 5 wt% of drug molecule (Doxorubicin) was dissolved in acetone with the polymer under investigation. Once residual acetone had evaporated (achieved when overall volume had reached that of the aqueous content), residual free drug was removed by gel filtration (PD-10 column).

To determine the extent of encapsulation, a sample of NPs (500 µL) was freeze-dried prior to dissolving in DCM. The absorbance was measured on Varian Cary UV-visible spectrophotometer and the resulting mass of drug was quantified from a standard curve.

3.3   Results and discussion - Nanoparticle assembly: how to enhance size reproducibility

3.3.1   Solvent drop NP formation

The first method used to assemble the thermoresponsive nanoparticles was the solvent drop method, Figure 27, a common and widely used technique for nanoparticle assembly. A selected amount of polymer (10 mg/mL) was

dissolved in acetone and the solution added in a dropwise manner to water or PBS stirred at a constant rate (500 r.p.m). The ratio of aqueous to organic phase remained constant at 1:1 v/v. Upon complete addition of the polymer solution, the resultant mixture was left to stir at room temperature to allow the acetone to evaporate.
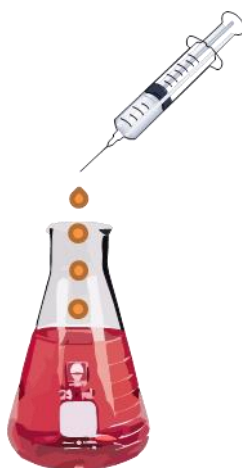
Figure 27 Schematic of solvent drop method for NP assembly. Polymer in acetone solution is added to a stirred aqueous solution using a syringe or dropping funnel. The resulting suspension is stirred at constant rate until acetone has completely evaporated.

Initially, **P1 − P5** were used to probe the efficiency of this method and to evaluate its capability to reproducibly generate NPs within a certain size range. The dynamic light scattering (DLS) data for NPs **P4a + P5a** indicates the presence of two size populations of NPs for each polymer, one at 25-30 nm and the other at ~150 nm, Figure 28. This data is representative of data generated for other polymer NP's of **P1 − P3.** The data shown is the result of numerous iterations of both stir speed and rate of solvent addition.
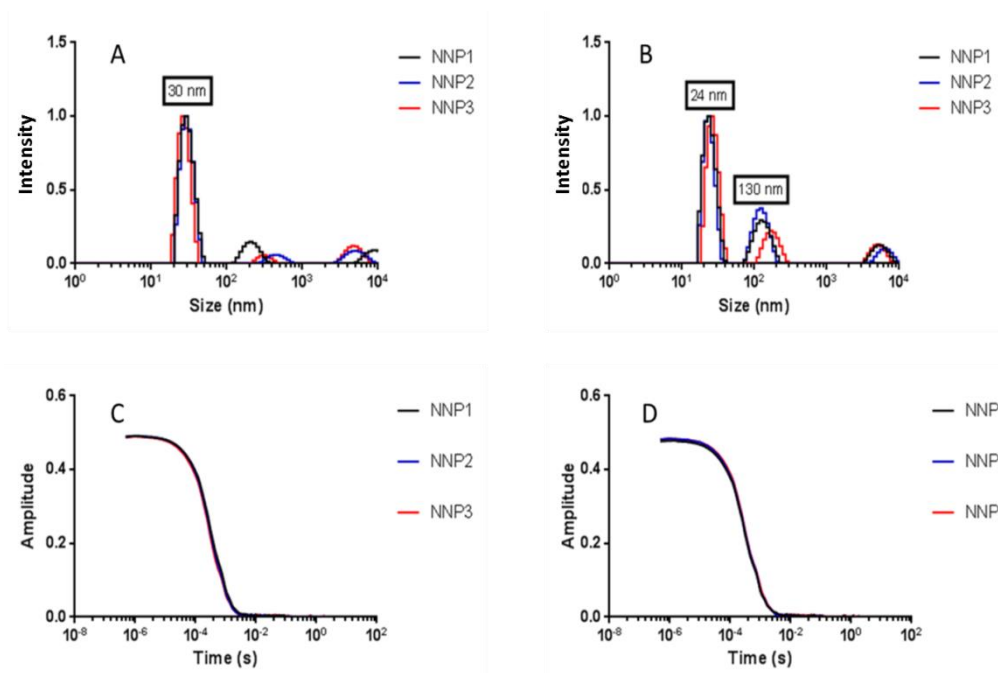
Figure 28 DLS data of 65:35 PLGA core P4 + P5 polymer nanoparticles,sizes are radii and all in nm. A) P4 intensity DLS. B) P5 intensity DLS. C) + D) Correlation curves for 3 batches of NPs the overlap of each curve shows the similarity between each batch.

The morphology of the NPs generated using the method above was assessed by transmission electron microscopy (TEM). The results of TEM imaging for NPs of **P1 – P4** (65:35 and 75:25) are shown in Figure 29.
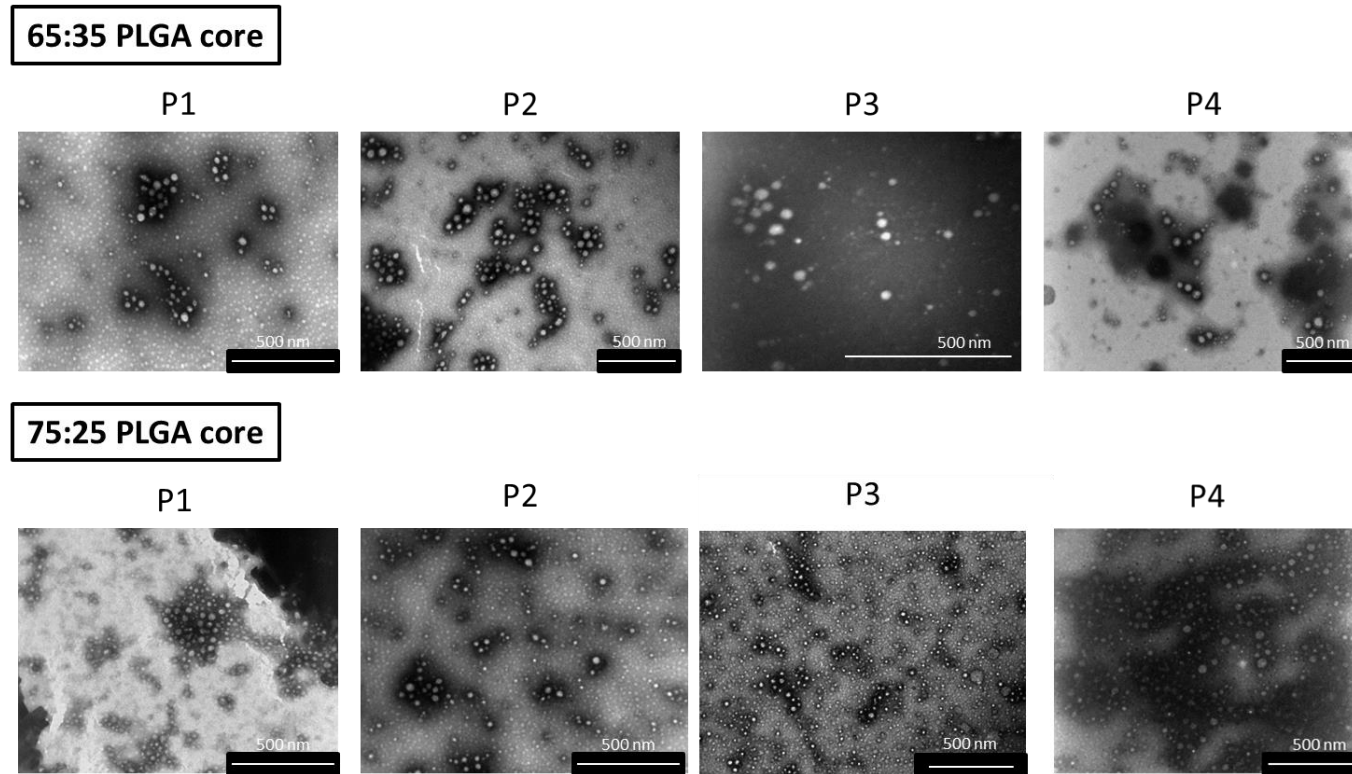
Figure 29 TEM images of thermoresponsive NPs. Samples prepared by diluting a sample of the NP suspension with a phosphotungstic acid (3 % w/v) stain. All scale bars are 500 nm.

In each image there is an observable variation in NP sizes where one size range formed the majority of the population distribution in each instance; this data agreed with the representative DLS data above. Furthermore, the TEM imaging confirms the morphology of the resulting NPs to be spherical. To compare the sizes of the NPs with those measured by DLS image analysis software was used on the TEM images. As an example, the NPs of **P4** were found to range from 17 – 50 nm in diameter, Figure 30. These sizes are within the limits determined by DLS measurements for the smaller population (25 – 30 nm). There was a noted absence of the larger population within the TEM images. There are two possible reasons for this; firstly, the drying process associated with TEM sample preparation resulted in the loss of water from the corona of the NPs, thus polymer shrinking occurred and smaller particle sizes were observed. Secondly, the imaged sample may not have been typical of the system as a whole, only containing a few NPs of larger size and so the population distribution was not accurately represented.

An alternative explanation for the limited number of larger NPs seen in TEM imaging may relate back to the initial DLS analysis. Intensity measurements by DLS are proportional to d^6 (where d is the diameter of the NP), therefore although the DLS analysis is suggestive of a population of NPs with a larger diameter, there are likely few of these NPs present in the sample. The NP sizes observed are broadly in agreement with those observed for similar polymer types, PLA-*b*-PEG.[145]
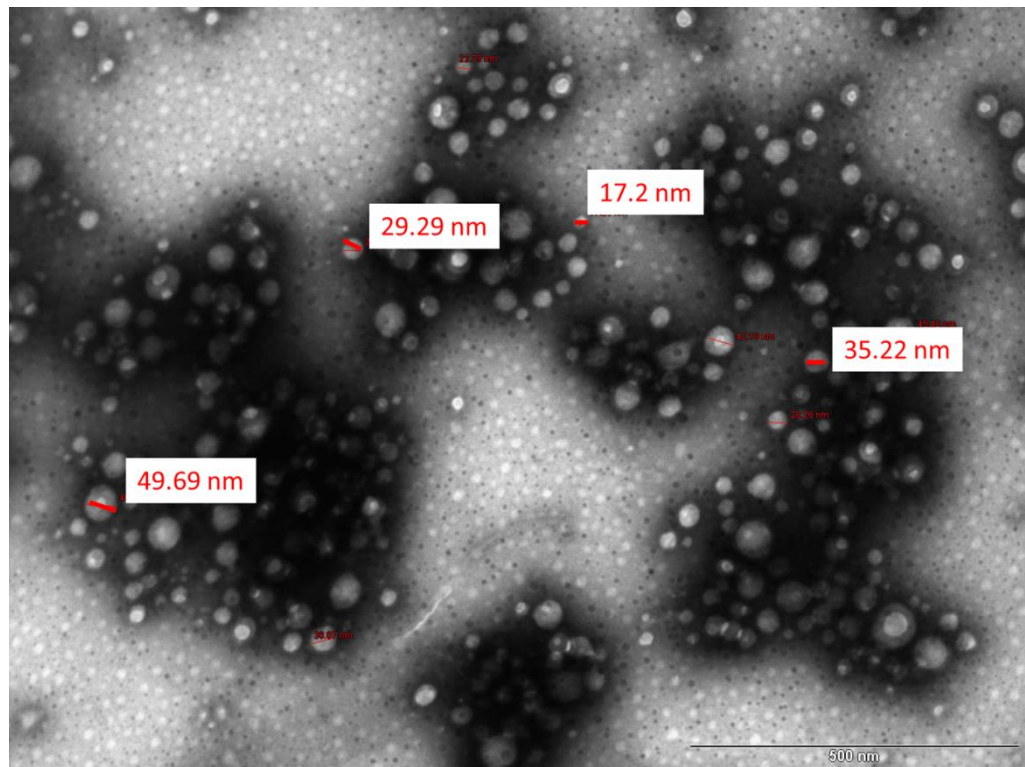
Figure 30 TEM image of P4 NP with a selection of sizes measured using TEM imaging software. Scale bar 500 nm

Additional testing was carried out in cell culture media for a prolonged period of exposure to test whether proteins would be adsorbed to the surface and affect the NP size.

3.3.2 Stability and thermoresponsive properties of NPs in cell culture media

As the NPs assembled using PLA-*b*-((DEGMA)-*stat*-(OEGMA)) were intended for testing within cell systems, it was important to determine whether the cell culture medium would alter the transition temperature (T_t) or stability of the NPs. The NPs were suspended in RPMI media containing 10 % foetal calf serum and PBS as a comparison. The NPs were tested at 4 mg/mL and 0.4 mg/mL to ensure dilution also had no effect on the T_t. **P12** and **P13** were

chosen for this study as these were rhodamine tagged for the intended cell studies.
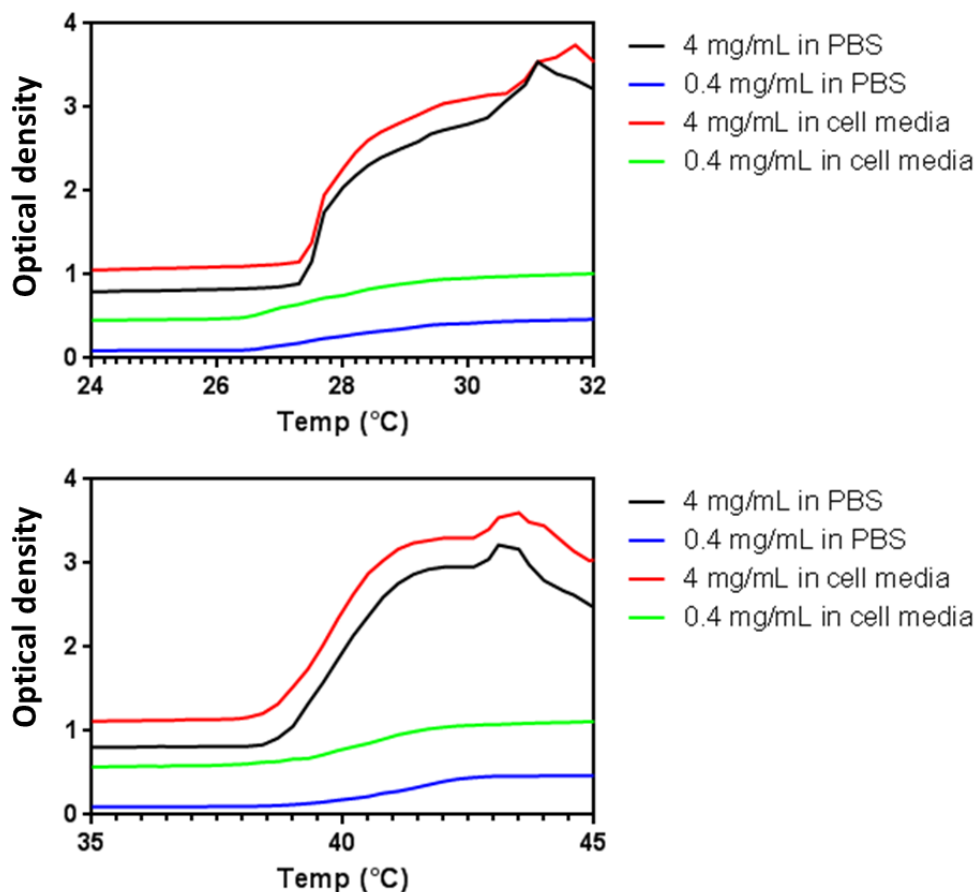
Figure 31 T_t data for P12 NPs (top) and P13 NPs (bottom). For both types of NPs T_t was determined using UV-vis spectrophotometry reading the abs at 550 nm every 30 seconds. Cuvettes were heated at 0.3 °C/min.

The addition of cell media and protein from the foetal calf serum was found to have no effect on the overall T_t of the NPs of both **P12** and **P13**, Figure 31. This result is suggestive that the proteins are not interacting with the thermoresponsive corona of the NPs. Upon dilution of the NPs, the T_t also remained the same in both environments with only a slower overall 'clouding' of the suspension noted; this was shown by the gradient of the curve for 0.4 mg/mL being less than that of the 4 mg/mL NPs. The cause of the more

gradual gradient and lower optical density is due only to the lower concentration of NPs present. With a less concentrated suspension of NPs the change in recorded optical density (due to light scattering) will be less than the higher concentration suspension. As the polymer chains collapse upon reaching their lower critical solution temperature the hydrogen bonds are broken between the water and the polymer. This in turn makes the NPs become hydrophobic and will become attractive to other hydrophobic NPs which bring about the overall colloidal instability of the bulk suspension. The less NPs present results in a longer time period for the bulk suspension to aggregate and the less aggregates present means less scattering, thus less change in optical density.

In addition to ensuring the presence of proteins had no effect on T_t, the NPs were suspended in cell culture media with serum proteins for 6 hours to ensure there was no change to the dimensions of the particles, thus stability of particles. The samples were analysed using DLS measurements, Figure 32.
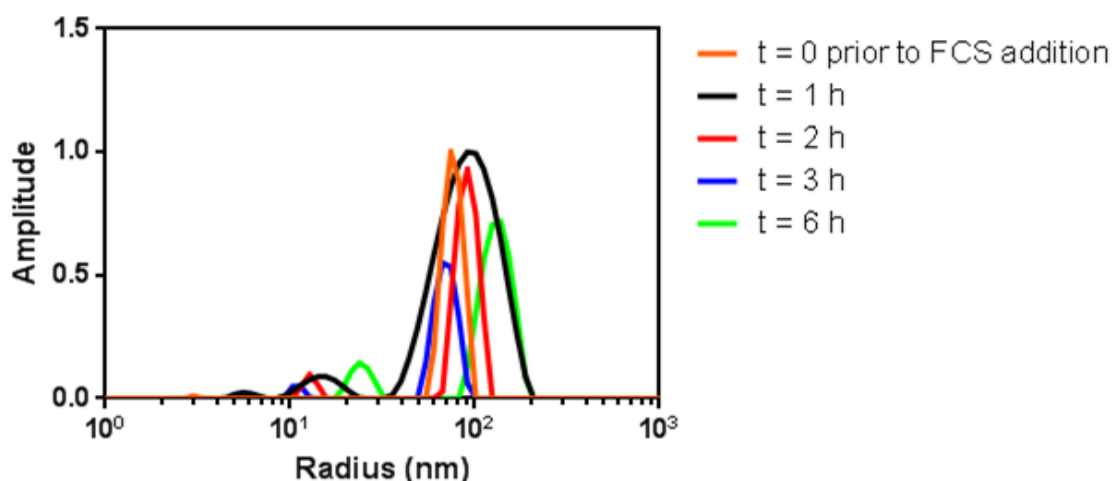
Figure 32 NP stability in RPMI containing 10% FCS at 37 °C for 6 h. NPs were incubated in a water bath containing a shaker moving the samples at 100 r.p.m. A 100 μL sample was removed and diluted with 900 μL distilled water for analysis by DLS. Data shown is from N=7 replicate readings.

The DLS intensity measurements showed only a slight increase in size of NPs at the 6 h time point of the study in the presence of serum proteins, the size of the NPs remained between 100-150 nm. There was also no observable precipitation of NPs during the 6 h incubation period. This is important as it indicates there is likely no substantial protein adsorption to the surface of the NPs which would inhibit their use for cell targeting and possible long term circulation within the body. Although it has been shown previously that PLA-PEG NPs do show some sign of adsorbing plasma proteins (especially adsorbed albumin, fibrinogen (α, β and γ), IgG γ, Ig light chains, apos A-IV, E, A-I and C-III) to the surface when mixed with human blood plasma depending on length of PEG chains.[146] It was also found that when comparing with PLGA and polycaprolactone core NPs the proteins adsorbed depended on the hydrophobicity of the core. This would need to be tested in the future to ensure the long circulation capacity of these NPs with PEGMA corona.

NP size is an important consideration from a pharmacokinetics view point. To be effective as a drug delivery device the NPs need to get to the area of action in a sufficient quantity to be effective. To reach the diseased area numerous barriers that exist in the human body to protect from foreign bodies need to be overcome. As the method of delivery of these NPs would be intravenous injection some of these initial barriers, such as breakdown in the gut and crossing gastrointestinal tract, would be avoided. The largest barrier to prolonged circulation of the NPs is the reticuloendothelial system (RES) and hepatic clearance. Shielding NPs from proteins within the body ensures the minimisation of opsonisation and thus phagocytic recognition and clearance by the RES;[147-149] the attachment of PEG to the surface was found to substantially reduce the quantity of apolipoproteins present on the surface compared to pure PLA NPs (~80 % reduction).[146] It has been shown that NPs can be cleared within seconds of intravenous delivery of the formulation due to the high concentration of phagocytic cells in the liver and spleen;[5,150] therefore with the PEGMA corona acting as a shield similar to the shielding effects of PEG, the NPs would be expected to have an extended circulating time to ensure higher uptake *via* EPR effect. NPs with a hydrodynamic diameter larger than 200 nm, whether shielded or not, are rapidly cleared by the bloodstream.[151] This means that even a PEGylated 200 nm diameter NP would be cleared much faster by the renal system than a 60-100 nm NP. In addition the size of NPs also affects the biodistribution as NPs < 150 nm produced an increased uptake in the bone marrow of rabbits; NPs that were 250 nm were mostly sequestered in the liver and spleen.[152] If the NP

formulation is to be effective the particle size and distribution need to be consistent from batch to batch.. Additionally, the NP size controls the rate at which the drug would be released *in vivo*, either retarding release or facilitating a burst release profile.

The NPs assembled using the solvent drop method were between 60 - 150 nm and the TEM also showed a wide dispersity within each NP sample. Controlling this size is important to ensure the NPs behave in the same manner once delivered to the patient, i.e. clearance level and targeting to tumour site.

An alternative controlled solvent flow method was investigated in an attempt to reduce the size variability observed for the solvent drop method.

3.3.3   Solvent flow NP assembly

NP formulation using a solvent flow set-up affords a more controlled method, utilising syringe pumps and a small mixing device, to deliver the aqueous and organic phase in desired ratios and at a constant rate. Advantages of this technique include the opportunity to remove the potential for human error during the addition of the polymer solution; additionally it ensures the mixing occurs in a controlled manner *via* the T-junction, Figure 33, facilitating the reproducible formulation of NPs ensuring they assemble with a consistent size distribution.
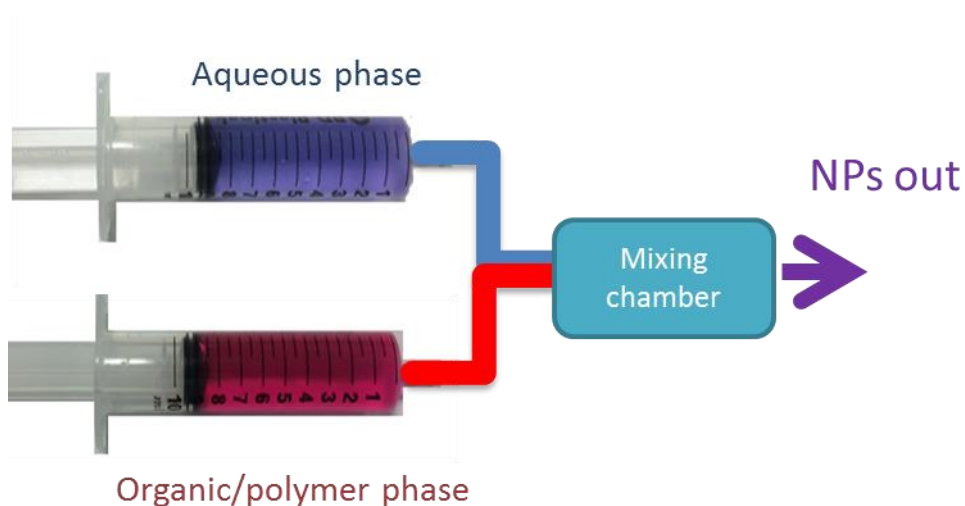
Figure 33 Schematic representation of syringe pump method for NP assembly. Mixing chamber is the T-junction.

P6 was used as a representative of the PLA-*b*-p(DEGMA-*stat*-OEGMA) library to assess the syringe pump method for enhanced reproducibility over the previously described solvent drop method. The concentration of the polymer was kept constant between methods (10 mg/mL), with a final aqueous volume of 5 mL. The flow rates for both organic and water phases was 1 mL/min.
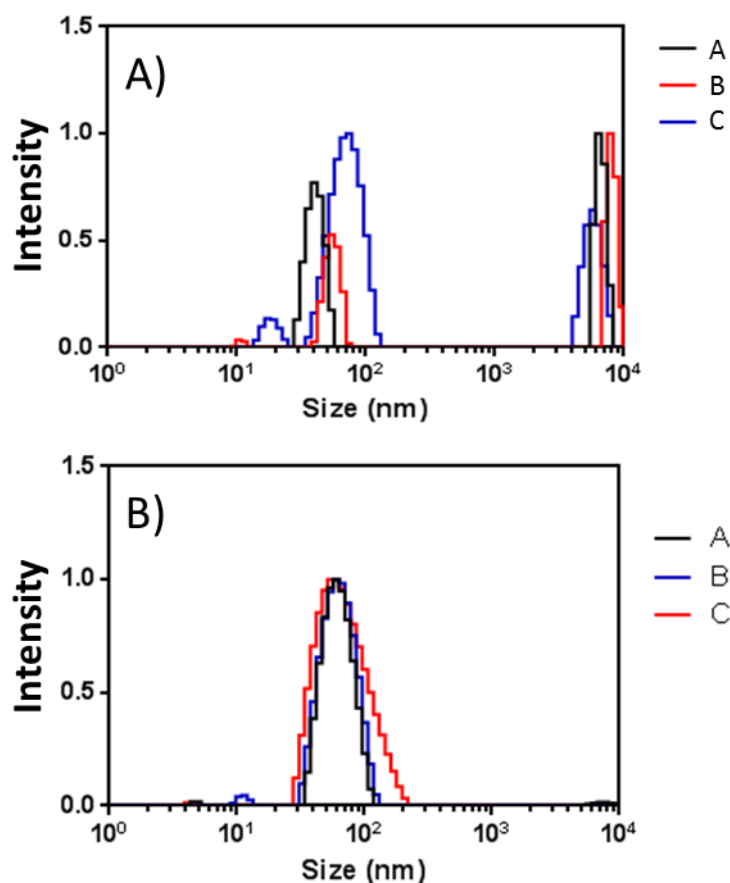
Figure 34 DLS data for comparison between solvent drop and solvent flow method. A) DLS intensity measurement of 3 replicate NPs formed from solvent drop method (10 mg/mL polymer concentration, 2.5 mL acetone, 5 mL PBS, stir speed 500 r.p.m). B) DLS intensity measurement of 3 replicate NPs formed from syringe pump method (1 mL/min flow rate, 10 mg/mL polymer concentration, 2.5 mL acetone, 5 mL PBS (2.5 mL for flow then diluted with further 2.5 mL). A, B and C are 3 replicate intensity measurements.

DLS data validated the syringe pump method as a superior method for producing NPs with a consistent size distribution (Figure 34B) when compared to the solvent drop method. The solvent drop method showed an observable size difference between all 3 replicates. The difference most likely occurred as the addition of solvent to water to instigate the NP assembly is not a controlled process. Slight variations in the rate of addition and size of droplet can cause differences in how the polymers will begin to interact with the water and thus NPs assembled were not consistent in size. During the solvent flow method, each stream, solvent and aqueous, were mixed together in a

consistent manner within a small area in the T-junction. The flow of solvent ensured that the polymer in the organic phase is mixed rapidly with the aqueous phase, resulting in the consistent nature of the NP assembly across batches, as observed in the overlap of each DLS intensity measurement of NP assembly repeats.

To further investigate the solvent flow method of NP assembly, different flow rates were chosen to determine whether this would impact upon the size of NPs assembled. Flow rates were chosen from 0.1 mL/min to 1 mL/min and each NP sample was analysed by DLS, .
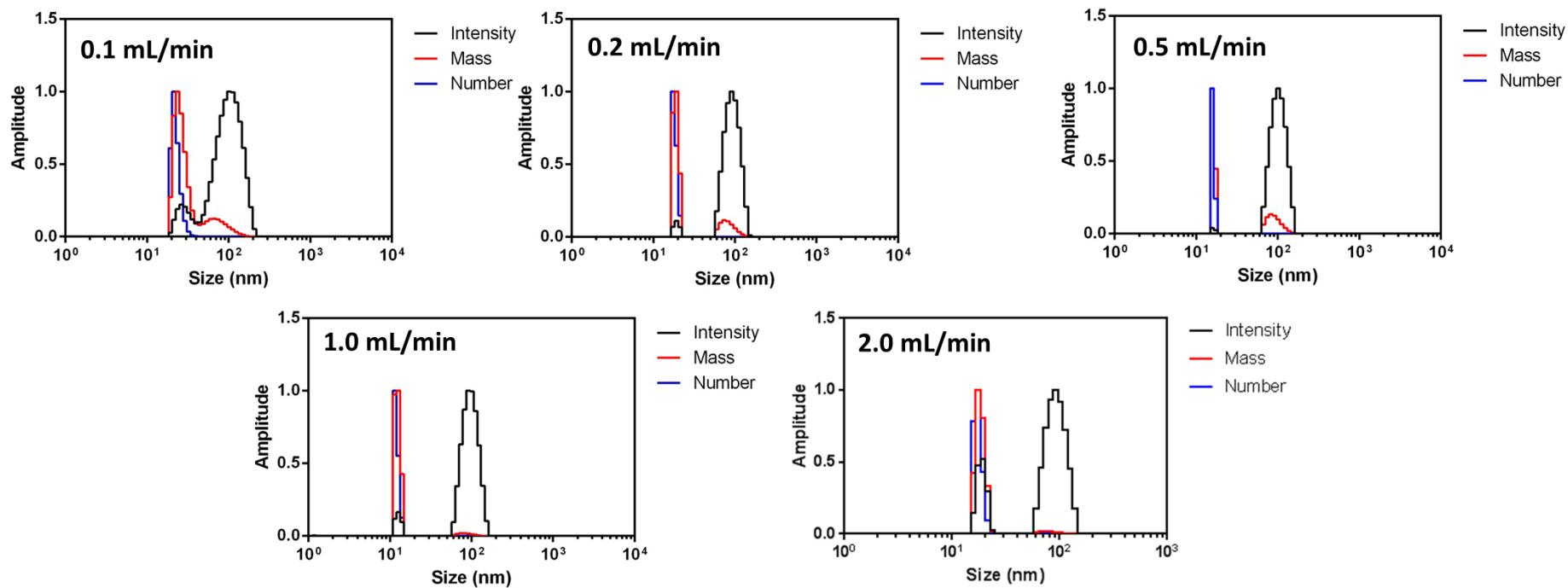
Figure 35 DLS data for NPs assembled under various flow conditions. Flow rate of both syringes remained equal. (Intensity: intensity average distribution, Mass: mass average distribution and number: number average distribution of NPs as measured by DLS.) Data representative of 3 replicate samples.

It was found that when the flow rate was ≥ 0.2 mL/min the size of the NPs produced remained consistent. It was only when the flow rate was reduced to 0.1 mL/min that the NPs formed were of a larger average size and the range of NP sizes were more diverse. The least disperse sample was that observed for particles assembled between 0.2 - 1 mL/min. There was slight broadening of the DLS intensity peak representative of 100 nm however the NP populations observed was representative of the lower flow rates tested.

Further to investigating the effect the flow rate had on the NP size reproducibility, the ratio of solvent to buffer was also explored. **P6** was used as above to further the proof of concept of this method. For this study the NP concentration, 10 mg/mL was kept constant. The rate of addition of the buffer was changed so the overall solvent to buffer ratios was as follows: 1:1, 1:2, 1:3, 1:4 and 1:5. Once the acetone had evaporated a sample of equal concentration was removed from each test for analysis by DLS. When the flow rates of each stream remain equal the NPs formed are of a reproducible size as shown previously in Figure 33. When the flow rate of the buffer stream is increased, thus increasing the buffer:acetone, the batch-to-batch reproducibility of the NP size decreases; this is shown in Figure 36 by the DLS intensity no longer overlapping when the ratio is 1:2-1:5. As the ratio is pushed to the extremes of 1:4 and 1:5 a dual size population begins to emerge. It was concluded from this optimisation of the solvent flow method of NP assembly that if the flow rate is equal for both streams and the flow

rate was > 0.2 mL/min NPs of a reproducible size and distribution were assembled.
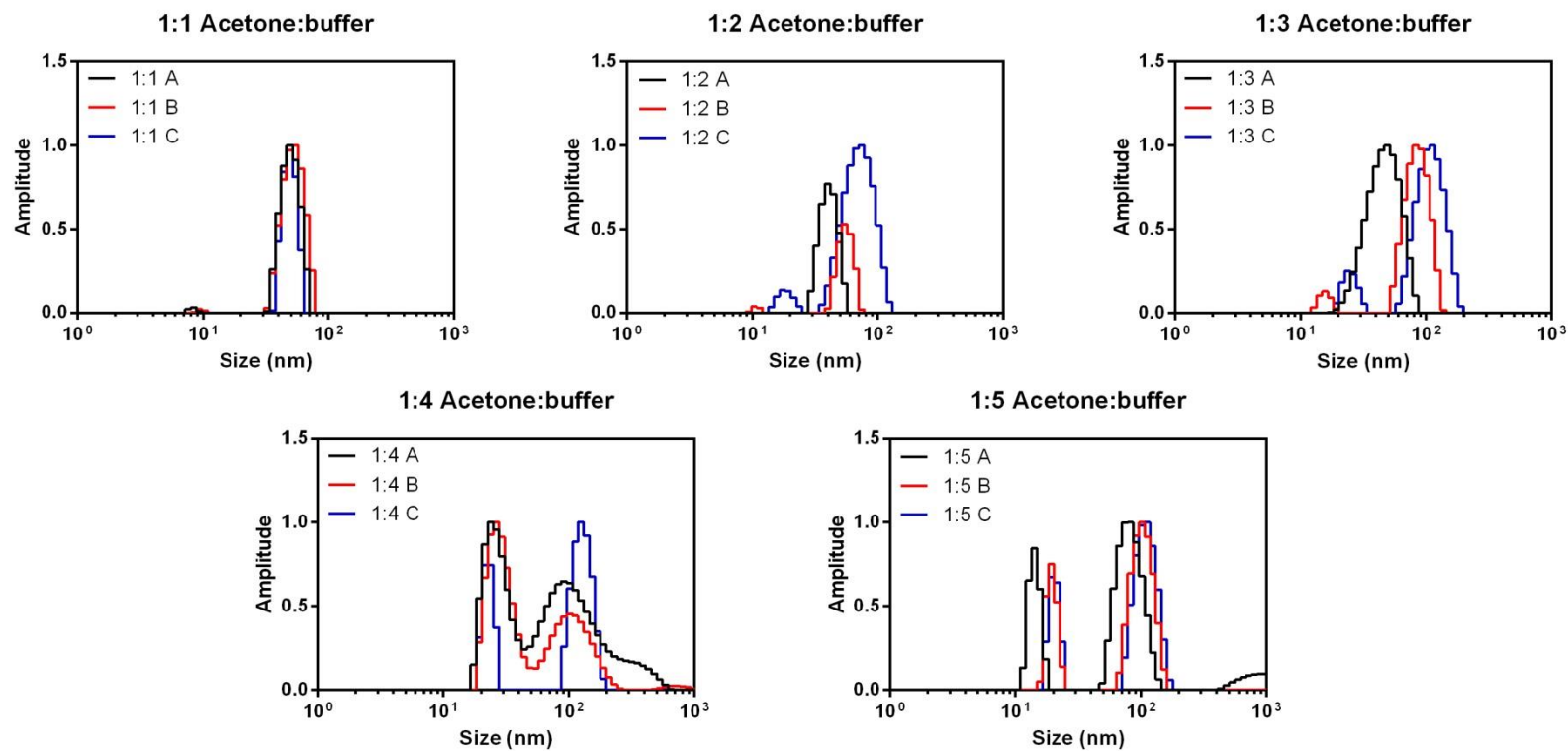
Figure 36 DLS intensity measurements of NPs formed from P6 by varying acetone:PBS buffer as proof of concept. When the flow rates of both acetone and PBS buffer were equal reproducible sized NPs were observed. When the ratio of buffer was increased the size of NPs were no longer reproducible. 2 distinct populations were noted for 1:4 and 1:5 ratios.

Overall these data for the solvent flow method of NP assembly were in agreement with those shown by Karnik *et al.* where homogeneous NP suspensions of PLGA-*b*-PEG were achieved using a similar method within a pre-formed chip.[143] When microfluidics are used the major advantage over the 'bulk' drop method is the consistency in size of NPs produced. However there remains a notable disadvantage and that is the rate of NP production. A method of avoiding this problem that other groups have utilised is to use parallel assembly using multiple chips. Although when this method was implemented the maximum rate of NP production was 84 mg/h, compared to 2.5 mg/h for a single chip.[144] This does mean that it still takes 18 minutes to assemble only 25 mg of NPs, which for a scalable and industrial process would be limiting as an inexpensive and high through-put method.[153] With a polymer concentration of 10 mg/mL and flow rate of 1 mL/min the solvent flow method described above is capable of producing 600 mg/h. By using simple and cost-effective apparatus and without the need for prior assembly of a micromixer chip, this method can be considered universally accessible.

Each type of NP assembled above using both techniques had a mean hydrodynamic diameter of < 200 nm. This is important for the passive targeting of NPs *via* the enhanced permeation and retention (EPR) effect. It has been summarised that NPs should be sub-300 nm to be possible to permeate through the leaky vasculature around tumour sites.[6,154] As these NPs should be capable of passive targeting *via* the EPR effect, due to their size

and shape, the ability of the NPs to carry a drug payload for delivery was investigated.

3.3.4   Capacity of nanoparticles for drug encapsulation

The polymers described in Chapter 1 were shown to be capable of consistently assembling into NPs with a size of < 200 nm. The assembly method was tested to ensure it produced NPs which could efficiently act as drug carriers. This was to ensure that prior to any further *in-vitro* testing there was confirmation of drug encapsulation and therefore validation that the carrier was capable as acting as a drug delivery vehicle.

Doxorubicin (dox) was chosen as a model hydrophobic drug due its hydrophobicity in its free base form (16 µg/mL at 25 °C)[155] and thus problematic for oral and intravenous formulation at higher concentrations. Dox is used regularly as a test of encapsulation as it is an active drug molecule,[38,156,157] used in the treatment of cancers,[158] and allows for easier quantification of drug loading due to the presence of a chromophore.

As previously discussed during the formation of NPs, section 3.3.3 , the solvent flow method was validated as the superior method for NP. With the knowledge that the flow rate could be altered without a detrimental effect on the NPs, the rate was investigated for any effect on drug encapsulation.

Three flow rates were chosen, 0.5, 1.0 and 2.0 mL/min, with the concentration of polymer and doxorubicin remaining constant throughout. To ensure the dox was encapsulated as a free base 2 equivalents of triethylamine were added to the dox.HCl prior to mixing with **P12**.
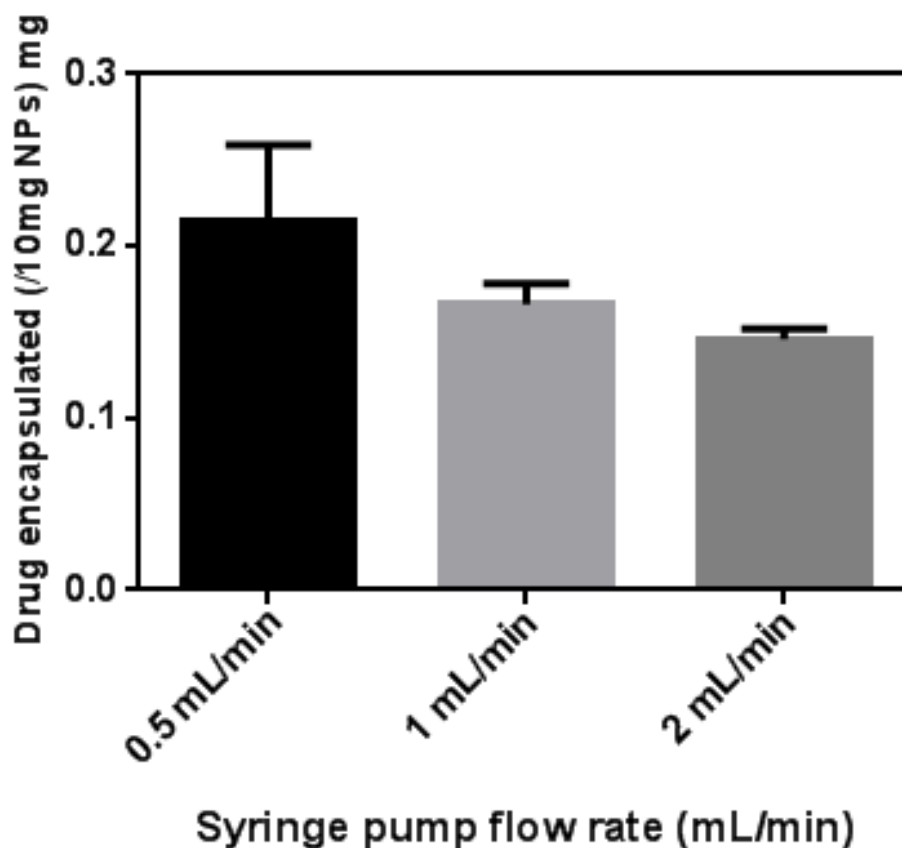
Figure 37 Doxorubicin encapsulation within NPs assembled using the solvent flow method. There were minimal differences noted between the three flow rates chosen with no significant difference using Sidak's multiple comparison test. Data shown is from 3 independent repeats.

The mass of drug encapsulated across the range of flow rates was 0.15-0.21 mg/10 mg of NPs, Figure 37. For each of the repeats the quantity of drug encapsulated was found to be very consistent and the higher the flow rate of the syringe pump the more consistent the encapsulation achieved. The flow rate of mixing was determined not to have a significant effect on the amount of drug encapsulated, though the efficiency of the encapsulation appeared to drop when the flow rate was increased, however the efficiency did not drop below 29 %.

Table 11 Mass of drug encapsulated and encapsulation efficiencies by varying flow rate for NP assembly.

Flow rate (mL/min)	Mass of drug encapsulated (mg/10 mg NPs)	Encapsulation efficiency (%)
0.5	0.214 ± 0.036	42.9 ± 7.2
1	0.166 ± 0.010	33.2 ± 1.9
2	0.146 ± 0.005	29.2 ± 1.0

The amount of dox encapsulated within each particle was quantified and correlated with that reported by other groups (e.g. 0.32 mg/10 mg NPs for PEG-*b*-p(4-vinylbenzylphoshonate,[159] 0.18-0.22 mg/10 mg NPs for PEG-*b*-(PLA-*co*-p(β-amino esters) [160] and 0.3-0.5 mg/10mg for PNIPAM-*b*-PLA NPs[161]) and although it has to be noted that whilst the polymers used were different to those previously reported, they all were of the micellar NP type. This data confirmed the PLA-*b*-((DEGMA)-*stat*-(OEGMA)) NPs were capable drug carriers in line with the drug carrying capacities of similar types of core-shell NPs. It is worth noting at this point that these are still low amounts of drug being encapsulated. The standard dose of doxorubicin is 40 – 60 mg/m^2 every 21 – 28 days, for an equal dose 187 – 280 mg of these NPs would be required. This high dose of NPs could themselves then cause toxicity problems and the need for high amounts of polymer to be removed from the body. The advantage of using these types of NPs would be the targeting capabilities and accumulation *via* the EPR effect and addition of targeting ligand. The targeting

would cause NPs to accumulate and the tumour site and therefore dose their drug payload site specifically unlike the systemic release of free drug in standard chemotherapies. Due to this, a much lower dose would be required to provide effective treatment and thus lower quantities of NPs.

The data to this point has shown that with the flow method of NP assembly the PLA-*b*-((DEGMA)-*stat*-(OEGMA)) polymers are capable of forming NPs reproducibly and within the size range desired for targeting *via* the EPR effect, sub-300 nm, in addition to being able to encapsulate a model hydrophobic drug.

3.4   Conclusions

Nanoparticles assembled using the solvent flow method offered enhanced reproducibility in size than those assembled by the solvent drop method across all the polymers tested. It was determined that the flow rate had a negligible effect on the size of NPs produced, this was most likely due to the stabilisation effect of the PEGMA chains forming the shell of the NPs. The NPs were capable of encapsulating a hydrophobic drug, doxorubicin, within levels observed by others with a maximum encapsulation efficiency noted of 43 % at a flow rate of 0.5 mL/min. The NPs produced were proven to be capable of being further tested *in-vitro* without detriment to the NPs and this is shown in Chapter 4.

4   Tuning the aggregation temperature of thermoresponsive nanoparticles

4.1   Introduction

Thermoresponsive nanoparticles are of interest for a range of applications, including sensing, diagnostics, adaptive optics and therapeutics.[34,48,49,162,163] The most widely studied nanoparticles of this type have been those intended for drug delivery, as the thermal triggering of a response in a carrier vehicle potentially allows exogenous control of particle location or drug release at a specific site.[164-168] The thermoresponsive behaviour of these nanoparticles is usually bestowed by a surface corona of polymer chains which undergo a phase transition at a specified temperature in solution/suspension. The polymers themselves can be attached to a pre-formed nanoparticle, or can be self-assembling block co-polymers in which the inner block is solvophobic. In both cases the outer block or corona polymers exhibit changes in their solvation properties according to a change in temperature.

The thermoresponsive polymers forming the corona are characterised by their Lower or Upper Critical Solution Temperature (LCST[169] or UCST[170]) behaviour. For the LCST polymers, which have been most widely investigated for thermoresponsive nanoparticles, there is a critical temperature above which the polymer is only partially miscible in its solvent. Below the LCST, the polymer and the solvent are in the same phase, stabilized for example by hydrogen bonds between the solvent and polymeric chain. Above the LCST, the entropy-driven phase separation, results in collapse of the polymer chain.[5] In the case of nanoparticles with a corona of polymers displaying an

LCST in water, the result of the polymer phase change is a decrease in surface solvation and an enhancement in apparent particle hydrophobicity. In pure aqueous suspensions, the LCST change of surface-displayed polymers results in a loss in colloidal stability, which then leads to particle precipitation or aggregation, dependent on concentration.[162] In more complex environments, for example in biological fluids or in tissue, the phase changes and increase in surface hydrophobicity can result in differential protein adsorption or cell membrane interaction.[171] These variations in bio-interfacial behaviour[172] have been the most widely explored, as nanoparticles with these properties have been shown to exhibit controllable cell attachment and endocytosis.[168,173]

As a result, there have been many efforts to tune nanoparticle-surface interactions by varying the temperatures at which phase changes occur. However, while there have been many papers showing that the LCST (and UCST) of linear polymers in solution can be controlled very precisely by co-monomer content, molar mass and end-group content,[61,174-177] the control of nanoparticle thermoresponsive properties has been more elusive.[162,178] In part, this is because many studies have had a strong application focus, particularly in drug delivery, where interpretations of data are often confounded by alterations in polymer LCST by electrolytes[133] and biopolymers, which in turn lead to highly variable protein adsorption or cell membrane association dependent on the specific environment.[179] There are also the well-known issues in characterising polymers grown from the surface

of nanoparticles, or estimating polymer surface coverage when the polymers are grafted to pre-formed nanoparticles.

The focus in this chapter was the exploration of routes by which precise and reliable thermoresponsive behaviour might be introduced into polymer nanoparticles, ultimately to develop predictable and constant release systems for drug delivery. It was also an intention to develop simple formulation rules, through which temperature response could be 'dialled in' to nanoparticles in a manner analogous to that in linear responsive co-polymers. The experiments in this chapter were thus designed to show how mixtures of different thermoresponsive polymers, based on oligo(ethyleneglycol) methacrylate monomers, and their resulting nanoparticles could be mixed to yield a range of temperature responses. This work was based on the hypothesis that aggregation temperature of nanoparticles can be controlled through 2 ways: a) mixing of pre-formed co-polymers of poly(lactic acid) (PLA)-*block*-poly(oligo(ethyleneglycol)methacrylate) (p(OEGMA))–*co*-poly(diethyleneglycomethacrylate) (pDEGMA) with varying LCST prior to nanoparticle formation through nanoprecipitation, and b) mixing of pre-formed nanoparticles from constituent PLA-*b*-p-OEGMA-*stat*-DEGMAs of varying critical aggregation temperature, Figure 38. Copolymer and nanoparticle mixtures were evaluated at different constituent ratios, and the results of dynamic light scattering and turbidimetry experiments are shown to characterise size and transition temperatures of the resulting nanoparticles.
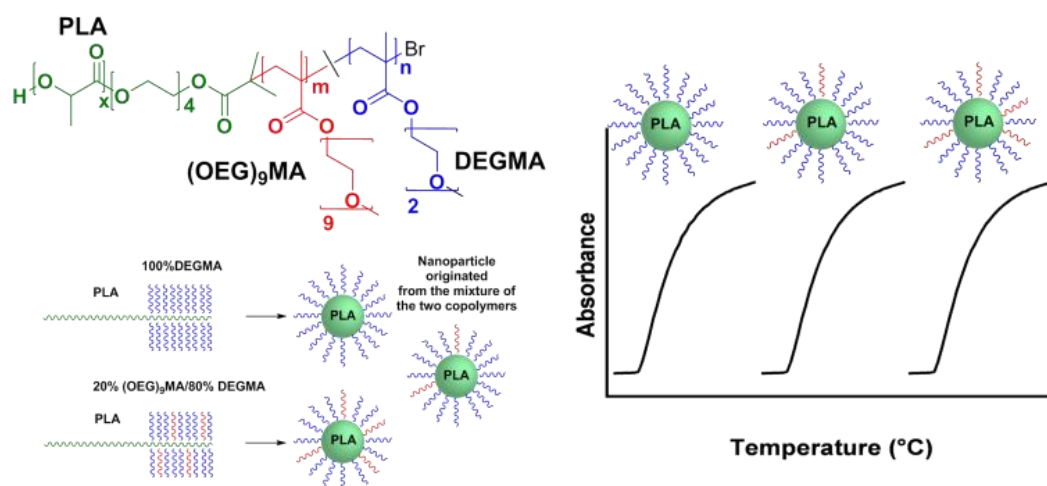
Figure 38 Structure of polymers and cartoon representation of different PLA-p(OEGMA) copolymers used to form thermoresponsive nanoparticles. Polymers with different ratios of OEGMA and DEGMA were mixed prior to nanoparticle formation or pre-formed nanoparticles with different aggregation temperatures were mixed. The resulting nanoparticles displayed variable aggregation temperatures dependent on the relative concentrations of the copolymers in the blends.

4.2　Methods

4.2.1　Synthesis of polymers

The synthesis of polymers was carried out as discussed within chapter 1.

Studies were carried out using **P6-P11** as they were shown to produce

nanoparticles (NPs) of a reproducible size and each had a different transition

temperature (T_t) when assembled into NPs. -

4.2.2　Characterisation of polymers - NMR

^{1}H NMR spectra were recorded at 20 °C on a Bruker instrument operating at

400 MHz. Chemical shifts (δ) are referenced to CDCl$_3$ (δ 7.26 ppm). The data

were processed using MestReNova (v. 6.0.2) software. To determine degree

of polymerisation (DP) of PLA macroinitiator the C<u>H</u> proton peak for lactide (δ

5.3-5.1 ppm) was integrated in relation to protons on the terminal methyl of

bromoisobutyryl bromide group (δ 1.96 ppm, 6H). The DP of copolymers were

measured from DP of PLA (δ 5.3-5.1 ppm, set to 1H) then integrating the

protons on the terminal PEGMA methyl (δ 3.46-3.36 ppm, yH), y * (PLA DP) = copolymer DP.

4.2.3 Gel permeation chromatography (GPC)

GPC was performed on a Polymer Laboratories GPC 50 system equipped with a refractive index detector. Separations were achieved with a pair of PLgel Mixed-D (5 µm bead, 7.8 × 300 mm) columns with a matching guard (7.8 × 50 mm) and chloroform as eluent at a flow rate of 1 mL min-1. Calibration was performed using narrow polystyrene standards (Polymer Labs) in the molecular weight range 0.13-210 kDa. Molecular weights and dispersity values were calculated using Cirrus GPC 3.0 software.

4.2.4 Nanoparticles preparation

The copolymers were dissolved in acetone at a concentration of 5 mg/mL and the solutions then mixed together at different ratios. Each blend was prepared using a double syringe pump. One syringe was used to introduce the polymeric solution; the other one to introduce an equal volume of water. The two solutions were loaded at the same time and mixed together in a T-junction, using the same flow rate of 1 mL/min and loading the same volume for both syringes. Copolymers precipitated as a nanoparticle suspension at the interface between water and acetone. The final suspension was then left to stir at room temperature to allow the acetone to evaporate.

4.2.5 Transition temperature determination by cloud point analysis

The transition temperature (T_t) of the nanoparticles was determined by measuring the change in optical density of light using UV-vis spectrophotometry at 550 nm. This allowed for the increase in scattered light

upon sample aggregation to be measured (cloud point). Cloud point evaluations were performed using a Beckman Coulter DU-800 UV/Vis Spectrophotometer f working at concentrations ranging from 1 mg/mL. Samples were heated at a rate of 0.5 ˚C/min. Measurements were taken at 0.5˚C intervals. The absorbance/optical density was converted to % transmittance (% transmittance = 10^(2-absorbance). Transmittance data were plotted versus temperature and T_t taken to be the point at which there was a 50% drop in the normalised transmittance (normalised to 100%).

4.2.6   DLS measurements

Dynamic light scattering was performed using a Viscotek Model 802 instrument. Samples were taken from nanoparticle suspensions in ultrapure water (1:20 dilution), typically at 0.25 mg/mL and 25 °C measurements. Analyses were repeated 3 times for each sample, and a minimum of 7 measurements was performed for each analysis.

4.3   Results and discussion

4.3.1   Thermoresponsive copolymer synthesis

The prerequisite for the study was the preparation of co-polymers with a hydrophobic block to provide a driving force for self-assembly in aqueous media and a thermoresponsive segment to provide temperature-switchable behaviour. The characterisation data for **P6-P11** are outlined in Chapter 1 and summarised in Table 12. When these polymers were assembled into single component NPs the T_t observed was between 28 – 78 °C.

Table 12 Reaction and mass information for PLA-*b*-((DEGMA)-*stat*-(OEGMA)) polymers

Polymer	PLA M_n (kDa)	Total $M_{n,GPC}$ (kDa)	$Đ_{GPC}$	M_n (kDa)$_{NMR}$	OEG$_9$MA, theoretical (mol%)	OEG$_9$MA content (mol%)$_{NMR}$	NP T_t (°C)
P6	14.7	37.3	1.32	34.8	0	0	28
P7	14.7	50.2	1.29	38.7	5	6	35
P8	14.7	52.1	1.26	37.4	10	8	42
P9	14.7	41.7	1.38	39.7	20	17	50
P10	13.1	36.6	1.45	28.7	35	30	64
P11	13.1	47.5	1.46	30.5	50	44	78

GPC: CHCl$_3$ mobile phase flow rate: 1 mL/min. Oven temp: 30 °C Samples dissolved in CHCl$_3$ prior to analysis. NMR: Bruker 400 Ultrashield at 400MHz and 25 °C.

P6: y = 278, m = 77, n = 0
P7: y = 278, m = 85, n = 5
P8: y = 278, m = 73, n = 7
P9: y = 278, m = 69, n = 14
P10: y = 313, m = 55, n = 24
P11: y = 313, m = 41, n = 32

Scheme 7 Synthetisof PLA-*b*-P((DEGMA)-*stat*-(OEGMA)) polymers used in this study

The synthesised polymers were then formulated into kinetically-trapped core-shell nanoparticles by two different methods. In the first method, solutions of individual block co-polymers in a good solvent for both blocks were added into water, thus producing single component nanoparticles. In the second method, solutions of two block co-polymers with different DEGMA:OEGMA ratios were added to water, producing blended polymer nanoparticles. Subsequently, the thermal transition temperatures (T_t) were measured for the single component NPs, the blended polymer NPs, and mixtures thereof.

4.3.2   Single component polymer nanoparticles (NPs)

The measured solution cloud points (T_t) of the block co-polymers in this study ranged from 28-78 °C with a linear increase in T_t with OEGMA content (Figure 39).
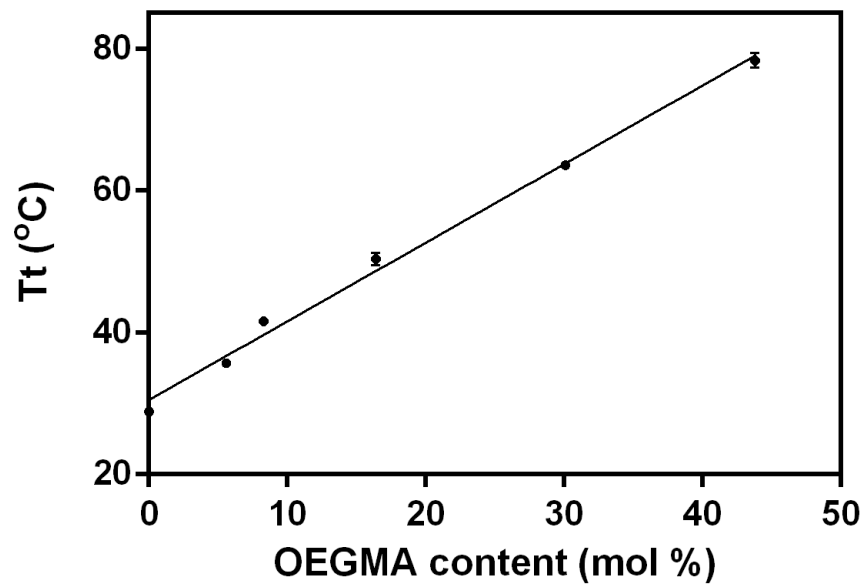
Figure 39 Positive linear relationship of OEGMA content of single component NPs against T_t. The error bars represent standard deviation of 3 replicate tests.

These values were in accord with those reported previously for similar block co-polymers of poly(poly(propyleneglycolmethacrylate)-*co*-OEGMA-*b*-PLGA.[49,180] and also for statistical poly(DEGMA-co-OEGMA) thermoresponsive polymers.[60,133,181] It has been previously shown that the transition temperatures of POEGMA-based polymers are not dependent on the solution molar mass,[60] and thus it is unlikely that the changes in particle transition temperature observed were a function of variations in molar mass in the constituent polymers.

Copolymer blends were then investigated to determine what effect this had on the overall aggregation of the NP suspensions assembled..

4.3.3 Nanoparticles formed by simultaneous co-precipitation of polymers with different individual cloud points

In order to investigate possible control of cloud point by nanoparticle composition, mixtures of two PLA-*b*-P(DEGMA-*stat*-OEGMA) polymers each with different T_t were nano-precipitated from acetone into water to obtain the blended NPs. The ratios of the individual polymers in the formulated nanoparticles were systematically varied from 0, 25, 50, 75 and 100 weight percent such that any relative enrichment of one co-polymer over another in the surface corona might be detected.

Table 13 NP formulations for blends of P6+P7 and P6+P9.

NP formulation	P6 (wt%)	P7 (wt%)	P9 (wt%)	T_t (°C)
NP$_{6-7}$1	100	0		28
NP$_{6-7}$2	75	25		30
NP$_{6-7}$3	50	50		33
NP$_{6-7}$4	25	75		35
NP$_{6-7}$5	0	100		38
NP$_{6-9}$1	100		0	28
NP$_{6-9}$2	75		25	40
NP$_{6-9}$3	50		50	48
NP$_{6-9}$4	25		75	50
NP$_{6-9}$5	0		100	52

The initial formulation series was based on one 'standard' polymer, **P6**, and then varying amounts of co-polymer with a higher OEGMA content (**P7** and **P9**

and thus higher individual T_t), in the blend, Table 13. The compositions and the overall Tt values of the resulting copolymers are reported in Figure 40. When **P6** was mixed with increasing quantities of **P7** the T_t of the resulting NPs increased as the quantity of **P7** increased. By comparison with the normalised transmittance curves, as well as the first differential of these curves, a distinct transition could be seen for each of the NP mixes analysed. In contrast when these data were compared with the blends of **P6** with **P9** (0 mol% and 17 mol% OEGMA respectively) the change in T_t noted was not as well defined as that for the previous mixtures.NP_{6-9}3-5 all showed T_t at around 50 °C with only small differences between each. For this mixture the polymer with the higher T_t (**P9**) seemed to dominate the appearance of the cloud point and thus the measured T_t. It must also be noted that the overall turbidity measured for NP_{6-9}3-5 was higher than that for the NP formed solely from **P6**. When the T_t was plotted versus the OEGMA content for the blended polymer NPs of **P6+P7** the relationship was very close to linear, as observed for non-blended polymer NPs, Figure 41.
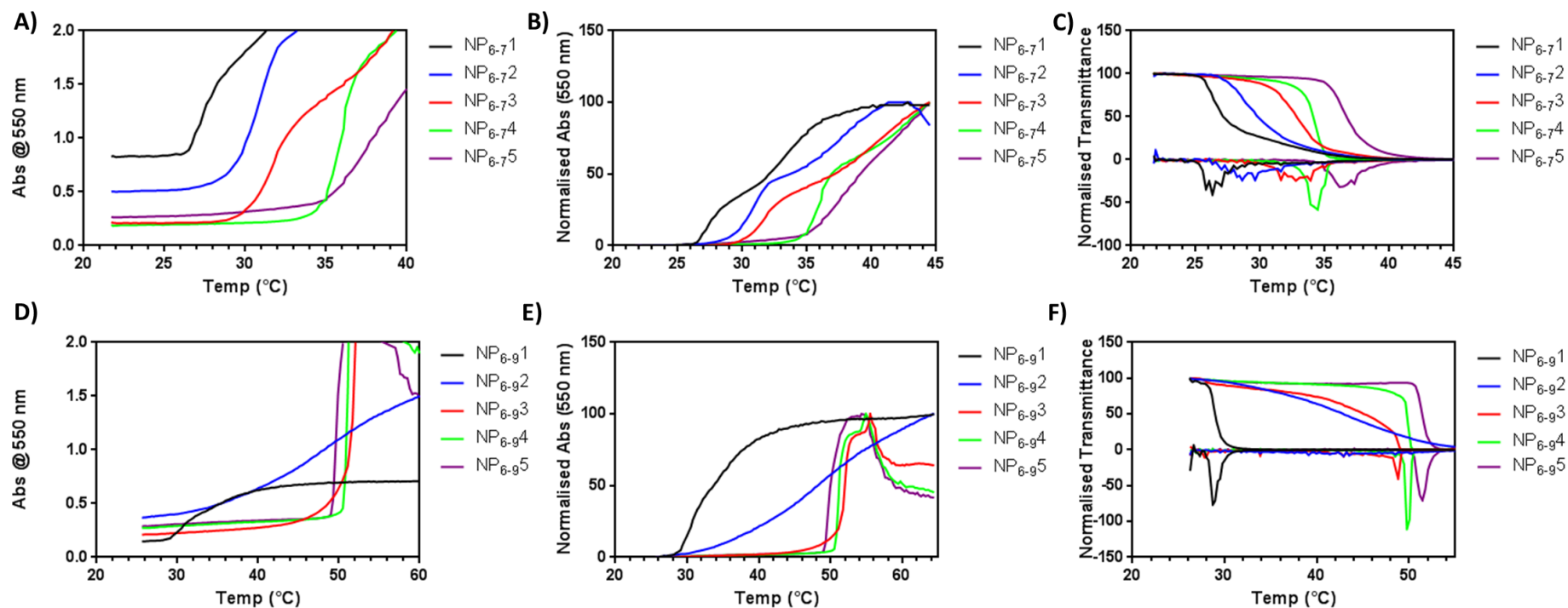
Figure 40 Optical density and transmittance data for the NPs formed from mixtures of P6 and P7/9. A) optical density data for P6 mixed with P7. B) Normalisation of the Abs data from A. C) Normalised transmittance data of data from A plus the 1st differential of these curves to show the inflection temperature (cloud point). D)-F) as for A)-C) but with the P6+P9 mixtures. NP suspensions (1 mg/mL) were heated at a rate of 0.5 °C/min and measured every 0.5 °C.
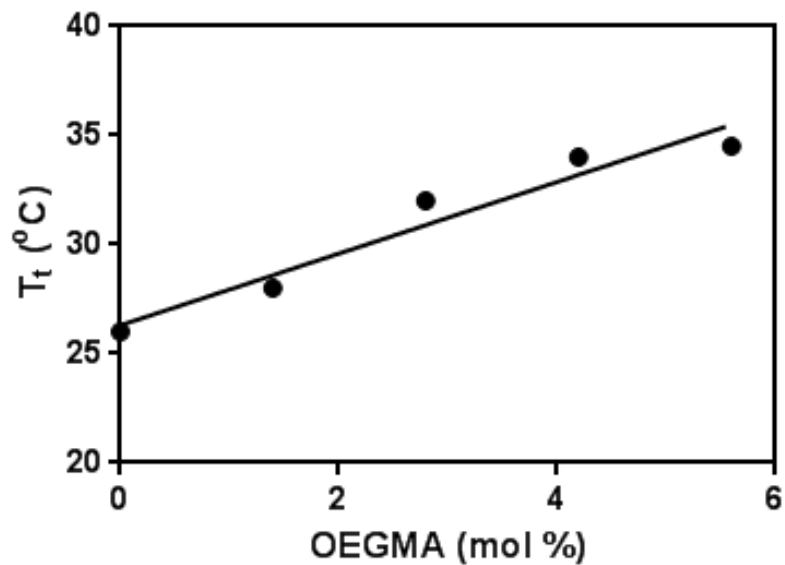
Figure 41 Positive linear relationship of the T_t from blend NPs of P6+P7 against OEGMA content.

From these data it was initially hypothesised that for there to be cooperativity between the two polymers being mixed the OEGMA content between them should be similar. The cooperativity mentioned here relates to the binary mix of polymers within the blend having an influence on one another due to the presence of only one cloud point within the polymer blend NPs and not the presence of two transitions of the individual polymers within the blend.[182] In experiments to test these individual hypotheses, first blends of NPs in which the constituent individual co-polymers displayed similar T_t values as well as both containing DEGMA and OEGMA were mixed. To determine if this was the case mixtures of **P7** with **P8** and **P8** with **P9** were assembled into NPs in the same manner as before and their T_t was measured for each, Table 14. For both these mixes there was some form of cooperativity noted in that the T_t of each blend was altered depending on the ratio of the constituent polymers.

Table 14 NP formulations for blends of P7+P8 and P8+P9.

NP formulation	P7 (wt%)	P8 (wt%)	P9 (wt%)	T_t (°C)
NP$_{7-8}$1	100	0		37
NP$_{7-8}$2	75	25		39
NP$_{7-8}$3	50	50		40
NP$_{7-8}$4	25	75		41
NP$_{7-8}$5	0	100		42
NP$_{8-9}$1		100	0	43
NP$_{8-9}$2		75	25	48
NP$_{8-9}$3		50	50	50
NP$_{8-9}$4		25	75	51
NP$_{8-9}$5		0	100	49
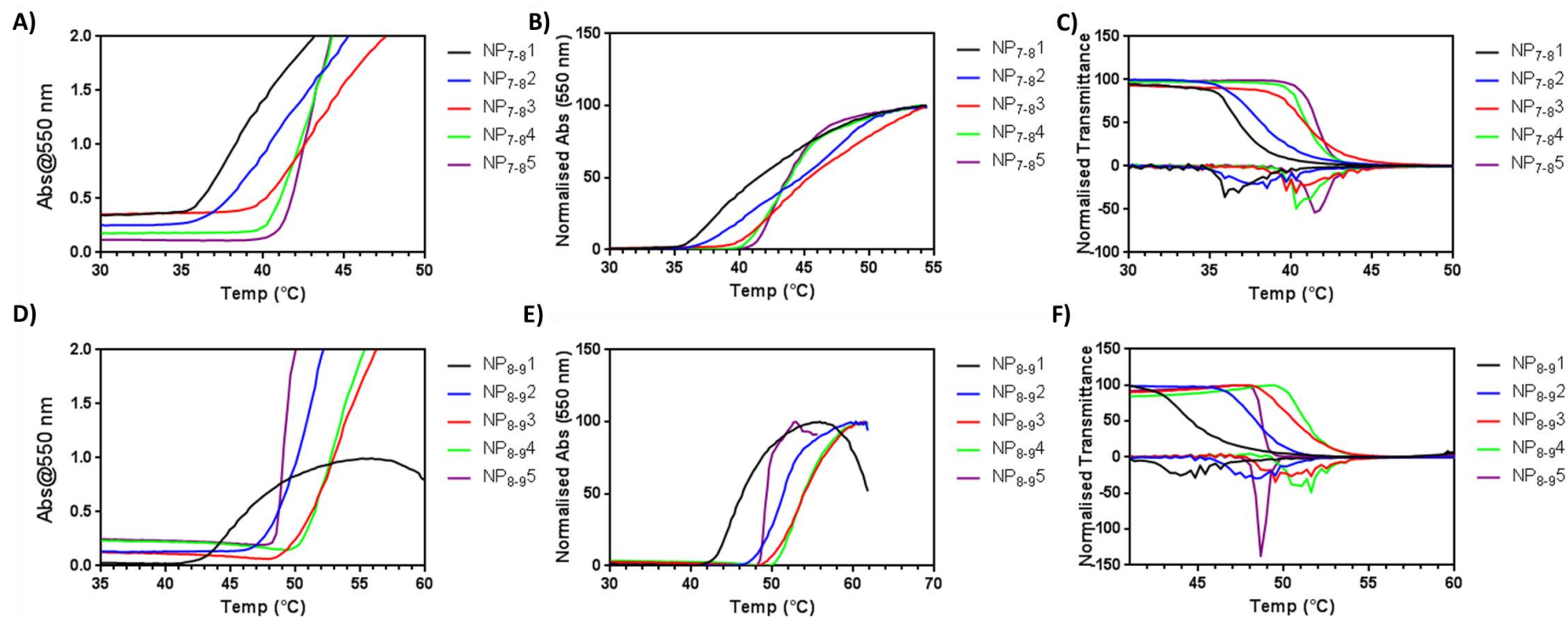
Figure 42 Optical density and transmittance data for the NPs formed from mixtures of P7+P8 and P8+P9. A) optical density data for P7 mixed with P8. B) Normalisation of the Abs data from A. C) Normalised transmittance data of data from A plus the 1st differential of these curves to show the inflection temperature (cloud point). D)-F) as for A)-C) but with the P8+P9 mixtures. NP suspensions (1 mg/mL) were heated at a rate of 0.5 °C/min and measured every 0.5 °C.

As apparent from Figure 42, while there were clear increases in T_t for the blended nanoparticles with increase in OEGMA content, the relationships were not linear. Further investigation was carried out using the higher T_t polymers (**P9-P11**) to ascertain whether linearity in T_t could be achieved for these polymers, Table 15.

Table 15 NP formulations for blends of P9+P10 and P10+P11.

NP formulation	P9 (wt%)	P10 (wt%)	P11 (wt%)	T_t (°C)
NP$_{9\text{-}10}$1	100	0		52
NP$_{9\text{-}10}$2	75	25		58
NP$_{9\text{-}10}$3	50	50		62
NP$_{9\text{-}10}$	25	75		64
NP$_{9\text{-}10}$5	0	100		65
NP$_{10\text{-}11}$1		100	0	64
NP$_{10\text{-}11}$2		75	25	67
NP$_{10\text{-}11}$3		50	50	70
NP$_{10\text{-}11}$4		25	75	72
NP$_{10\text{-}11}$5		0	100	77
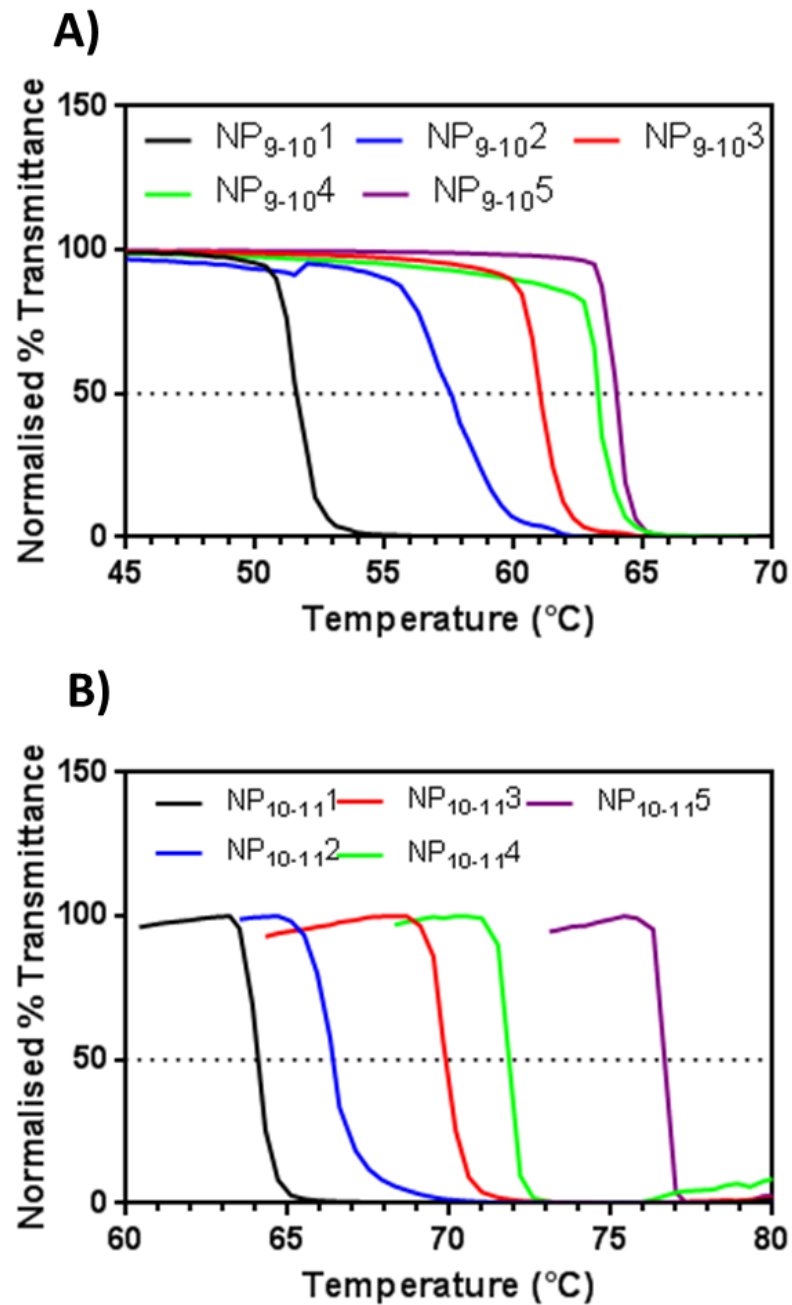
Figure 43 Normalised transmittance data for the NP blends of A) P9+P10 and B) P10+P11. A sharp transition was observed for each NP type across all the blends. NP suspensions (1 mg/mL) were heated at a rate of 0.5 °C/min and measured every 0.5 °C.

As shown in Figure 43 there was complete cooperativity between each polymer within the blended polymer NPs as each NP showed one distinct T_t. As there was only one transition observed it can be concluded that each polymer is well mixed with the other within each set of NPs. The T_ts noted for

NP_{10-11} blends was 64 °C through to 77 °C and the onset of T_t for each blended NPs was found to increase by 3-4 °C upon moving through the series of NP formulations (NP_{10-11}1-5). When the T_t from both these sets of blended NPs was plotted versus the OEGMA content a linear relationship could again be observed, Figure 44.
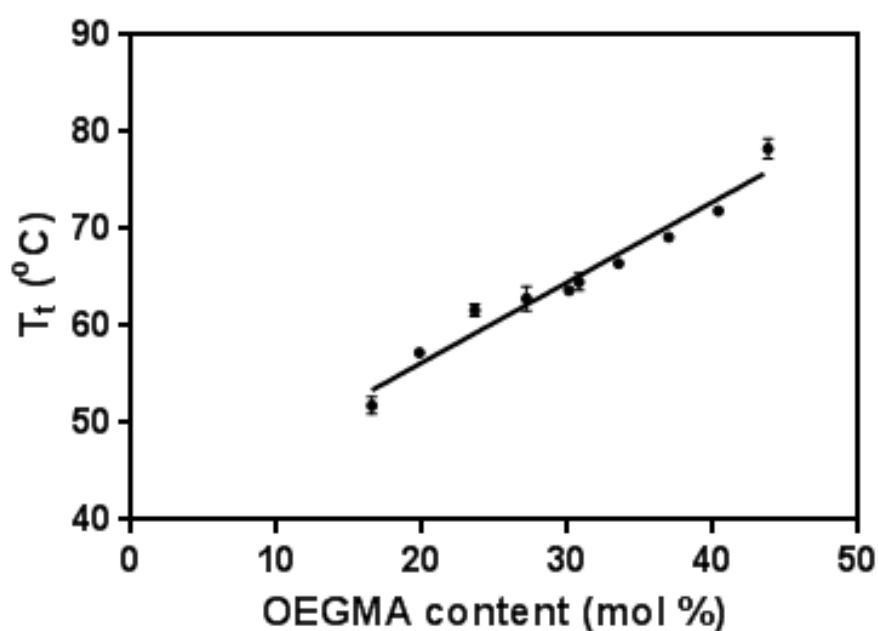
Figure 44 Positive linear relationship of OEGMA content from NP blends NP_{9-10} and NP_{10-11}.

For characterisation, a sample of the NPs was removed and freeze-dried from water prior to dissolution in chloroform to enable NMR analysis of the polymer composition. As shown in Table 16 the polymer composition of the blended NPs agreed well with the theoretical composition based on the mixing ratios of the two polymers (**P10+P11**).

Table 16 Polymer composition within the blended NP formulations NP$_{10-11}$ as determined by ^{1}H NMR.

NP blend	P10 (wt%)	P11 (wt%)	% OEGMA$_{theo}$	%OEGMA$_{NMR}$
NP$_{10-11}$1	100	0	30.1	31.5
NP$_{10-11}$2	75	25	33.5	33.9
NP$_{10-11}$3	50	50	36.9	38.0
NP$_{10-11}$4	25	75	40.4	41.9
NP$_{10-11}$5	0	100	43.8	45.4

The linear correlation observed between OEGMA percentage and the cloud T_t partially refutes the data observed by previous studies. Paris *et al.* demonstrated some cooperativity between different polymer chains influencing T_t upon mixing PEGMA polymers in aqueous solution although the P(OEG$_{8-9}$MA)-P(glycidyl methacrylate) produced two distinct transitions above equimolar mixes and one transition below.[183] They hypothesised this was due to the first polymer transition hindering the observation of the two transitions at lower ratios; when the concentration of the polymer with lower LCST dominated, the less abundant copolymer collapsed on the aggregates of the other copolymer, so that in this second collapse, an increase of the optical density was not observed.

To date the mixing of polymer blends and assembling into mixed polymer NPs has not been shown. The constraining of two polymers into NPs may elucidate why only one transition is observed independently of the molar ratio of mixing. If there was a large enough difference in molar mass between

the two polymers the lower molar mass polymer will be unlikely to influence the overall aggregation of the NP suspension as the higher molar mass polymer will either retain hydrophilic state (if it is the higher T_t polymer) or will collapse to from large hydrophobic regions (if it is the lower T_t polymer) to stimulate aggregation of the suspension which the lower molar mass polymer will be unable to inhibit. Steric hindrance is also likely to play its part within the phenomenon as the higher the degree of steric hindrance around each polymer on the corona of NPs (in the coiled state) the less likely each polymer chain is going to be able to undergo the coil-to-globule transition independently of the neighbouring polymers. If these polymers were to behaving independently of one another and no cooperative behaviour then there would be two T_t points observed, however this is clearly not the case as one transition is observed in all cases.

The data in this chapter does agree to an extent with Ieong *et al.* who showed that there was some cooperativity in the T_t tuning process when PEGMA polymers with a small change in independent T_t were blended (ΔT_t 7 °C).[177] However they determined this not to be true cooperativity due to the shift in T_t of each blend being insufficient to what should have been observed based on the blending ratios.

Conjugating PEGMA to gold nanoparticles however has also been shown to have some tuning ability but Gibson *et al* determined this was due to the size of the particles. [182] They showed an inverse relationship between particle size and LCST with the larger Au NPs demonstrating lower T_t. To ensure particle

size did not influence our findings each formulation was measured to ensure

consistent size of NPs. As an example the DLS sizing of the NP_{10-11} blends are

shown in Figure 45.
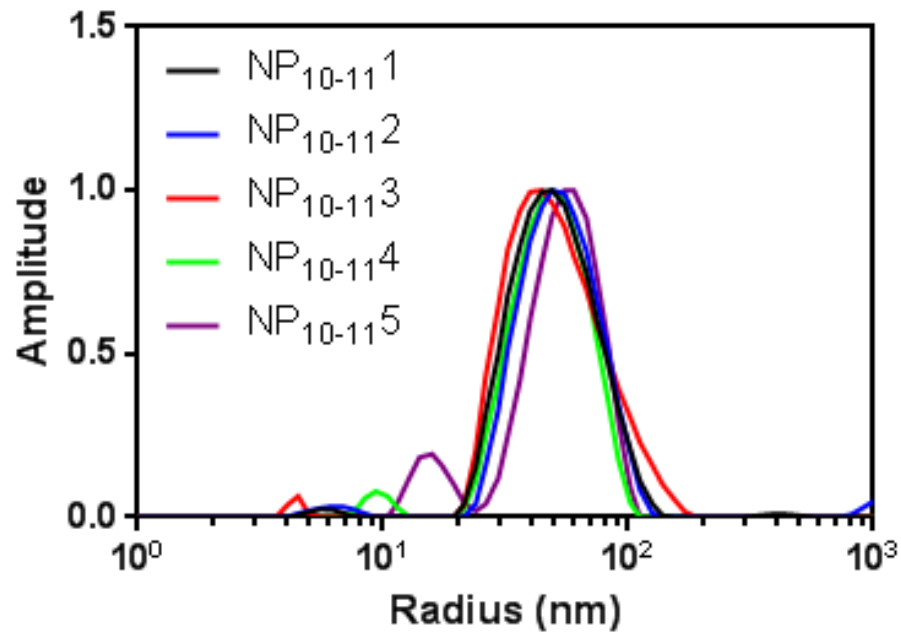
Figure 45 Size measurements of each NP_{10-11}1-5 obtained by DLS (NP_{10-11}1-5 formed from mixing P10+P11, Table 15). The measurements show the consistent size of each NP formulation used for T_t analysis. The size shown is from at least 7 measurements of each sample

The NPs assembled were very consistent in size as shown by the DLS intensity

measurements all overlapping for each blend. Therefore it is likely that it is

the ratio of polymer blends used, and hence the DEGMA:OEGMA content,

that tunes the T_t in both blended and non-blended polymer NPs.

In order to ascertain whether the effect was due to the polymers being

constrained within blended NPs or not, mixtures of single component NPs

were analysed.

4.3.4 Comparison with preformed nanoparticle blends

Previous studies showed that tuning can be obtained through mixing preformed nanoparticles, instead of mixing polymers before nanoparticles formation.[177] Therefore it was decided to evaluate the blending of NPs and compare with the data obtained for the polymer blend NPs. **P6, P7** and **P8** were chosen as they had previously shown T_t tuning ability when mixed. Preformed NPs were mixed in the same ratios as before for polymer blend NPs (i.e. 75:25, 50:50 and 25:75 vol%), Table 17.

Table 17 Formulation of the NP blends of NP$_{6-7}$ and NP$_{7-8}$.

NP blend formulation	NP$_{6-7}$1 (vol%)	NP$_{6-7}$5 (vol%)	NP$_{7-8}$1 (vol%)	NP$_{7-8}$5 (vol%)	T_t (°C)
MNP$_{6-7}$2	75	25			29
MNP$_{6-7}$3	50	50			30
MNP$_{6-7}$4	25	75	-		33
MNP$_{7-8}$2	-		75	25	41
MNP$_{7-8}$3			50	50	43
MNP$_{7-8}$4			25	75	45

The results obtained for these NP mixtures are shown in Figure 46. Similar changes in the optical density and transmittance data was observed as for the polymer blend NPs; as the ratio of NPs with higher T_t increased compared with the lower T_t NPs the recorded T_t increased also. In all the NP blends 1 transition was noted which shows that the NP mixture was behaving as one and not as two separate entities showing their individual T_t. However the

optical density and transmittance curves do show a more gradual onset of the cloud point. It can be hypothesised that as the lower T_t NPs begin to lose colloidal stability upon reaching their T_t the NPs within the suspension of a higher T_t stabilises the suspension for a time until the suspension reaches full aggregation.
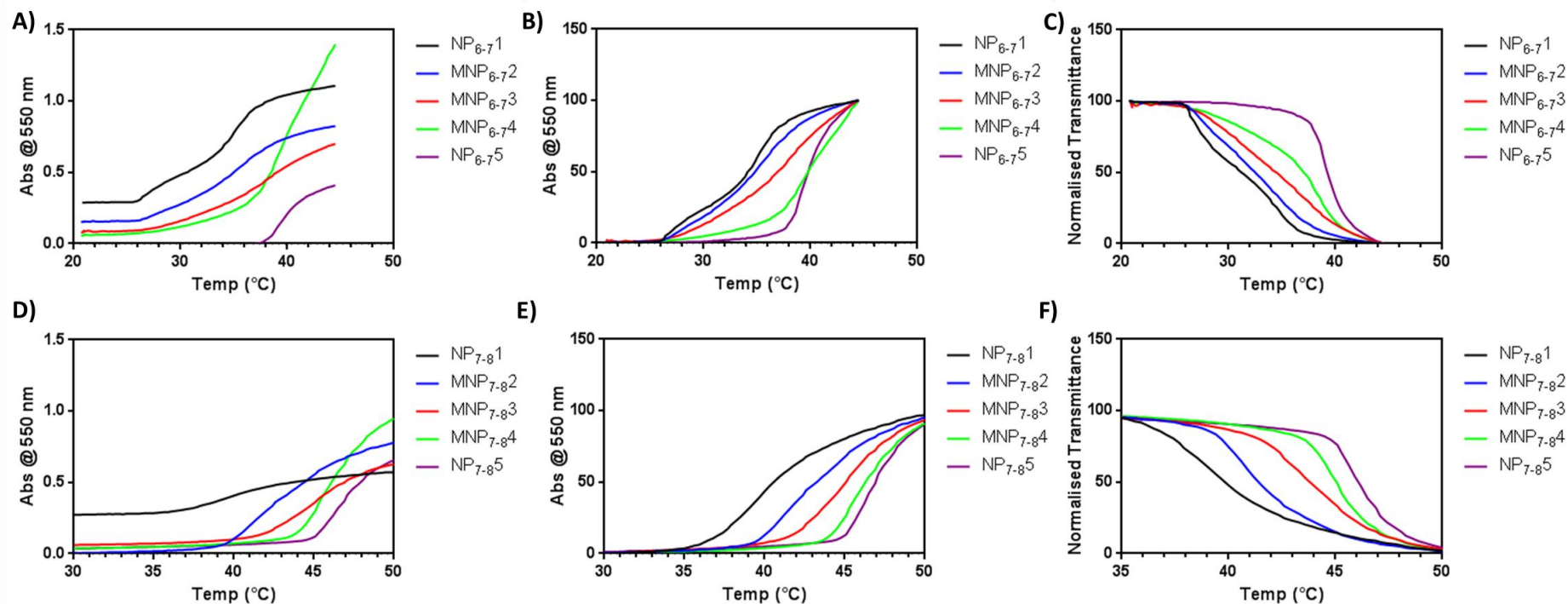
Figure 46 Optical density and transmittance data for the NP blends formed from NP mixtures of $NP_{6-7}+NP_{7-8}$. A) optical density data for NP_{6-7} mixtures. B) Normalisation of the Abs data from A. C) Normalised transmittance data of data from A. D)-F) as for A)-C) but with the NP_{7-8} mixtures. NP suspensions (1 mg/mL) were heated at a rate of 0.5 °C/min and measured every 0.5 °C.

4.4   Conclusions

Here it has been demonstrated that the transition temperature of PLA-*b*-P((DEGMA)-*stat*-(OEGMA)) nanoparticles can be tuned by altering the ratio of DEGMA:OEGMA within the thermoresponsive corona of the NPs similar to that of P((DEGMA)-*stat*-(OEGMA)). However the T_t was found to be slightly higher than for the PEGMA polymer alone. For the first time it was shown that there was a cooperative process involved in tuning the T_t of blended polymer NPs. The constrained nature of the mixed polymers within the NPs allows for improved control over the T_t tuning than PEGMA polymer blends. A similar outcome was noted when preformed NPs were blended in the same ratios as for the polymer blend NPs although with a more gradual onset of full aggregation.

5   Assessing the targeting capabilities of the thermoresponsive nanoparticle system *in vitro*

5.1   Introduction

The *in vitro* testing of formulations is one of the most important steps in the development of any successful cancer cell targeting nanoparticle (NP) system. Not only should the formulation itself not be toxic to cells, due to the possibility of the NPs coming into contact with healthy cells, but, it is also crucial to develop ways of targeting these new therapies to tumour cells specifically, safely, and efficiently, not only to enhance anti-tumour efficacy but also to reduce uptake into healthy tissues.

The discovery of the enhanced permeation and retention (EPR) effect nearly three decades ago by Maeda and Matsumura revolutionised the way scientists thought about the field of drug delivery.[184] The key mechanism for the EPR effect in solid tumours, when applied to macromolecules, more recently has been found to be retention. Low-molecular weight compounds were shown to be returned to the circulatory system *via* diffusion, whereas macromolecules above 40 kDa were retained within the interstitial space.[185] Exploitation of the EPR effect offers the opportunity for macromolecule and particle combinations to act as an alternative to the conventional small molecule chemotherapeutic drugs, which generally have poor pharmacokinetic and bioavailability profiles. The first PEG-protein conjugate (Adagen) entered the market in 1990, this was followed three years later in 1995 by the first anti-cancer liposomal formulation (Doxil and Abelcet) being approved and the first protein-based nanoparticle delivery system (Abraxane)

gained approval in 2005.[186] More recently the first thermoresponsive particle
treatment for cancer therapy has entered phase III trials.[106] The treatment,
ThermoDox®, is a heat-sensitive liposome which is used to encapsulate
doxorubicin and deliver it in a burst effect when the temperature is raised to
a specific temperature. At this temperature the liposome rapidly changes its
structure which allows the doxorubicin to escape, Figure 47.[187] ThermoDox®
has shown efficacy in primary liver cancer (hepatocellular carcinoma, or HCC)
in phase III trials and is currently being evaluated in phase II trials for patients
with recurring breast cancer.
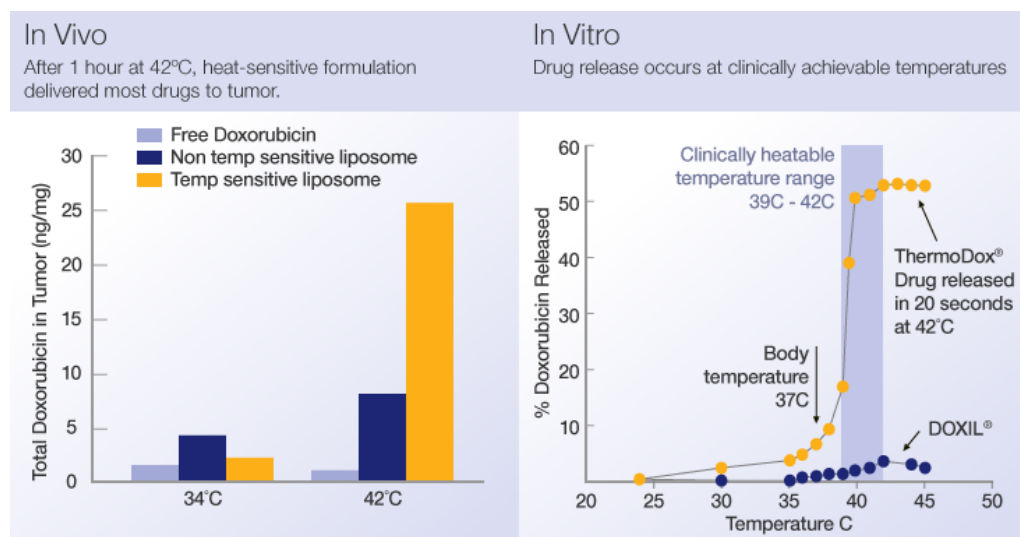
**Figure 47 Comparison of the *in vitro* and *in vivo* data from the development of
ThermoDox®. The treatment was shown to rapidly deliver doxorubicin to the tumour *in
vivo* upon raising the temperature beyond the point of liposomal stability. Figure
reproduced from Celsion website.[187]**

The development of delivery systems which are capable of targeting tumour
tissues by two methods, i.e. EPR effect and stimulus/targeting ligand,
increases the likelihood of higher uptake and thus better pharmacokinetics
with fewer side effects from off target drug release.

The design of the targeted nanoparticle system in this study was based on the correct size to passively target tumour sites *via* the EPR effect and targeting the folate receptor on tumour cells. The targeting of the folate receptor (FR+) has often been referred to as a Trojan horse approach as molecules conjugated to folate are transported stealthily into FR+ cells. Folic acid shows a very high affinity ($K_D \sim 10^{-10}$ M) for the cell surface orientated receptor.[94,95] As the folate rapidly binds with its receptor, internalisation occurs *via* an endocytic process.[13] The folate receptor is overexpressed on many cancer cells (e.g. ovarian, lung, breast, endometrial, renal and colon)[188] which makes it a very useful target for drug delivery.

With the advantages of using folic acid, e.g. low molecular weight, stability to solvents, lack of immunogenicity and high affinity for its receptor, it is of no surprise that there have been many studies on using this ligand to target nanoparticles to tumour sites.[189-193] A similar approach was taken for the NP system under study in this work; the folate was attached to a PEG chain which acted as a spacer between the targeting ligand and the PLA core. This was due to previous studies showing that by attaching the folate to a PEG linker prevents occlusion of the folate if it was attached directly to the core of any particle.[194,195] The advantage of the NP system studied here is that the folate ligand would only be 'visible' to the receptor upon heating the NP beyond the LCST of the thermoresponsive corona of the NP, Figure 48.
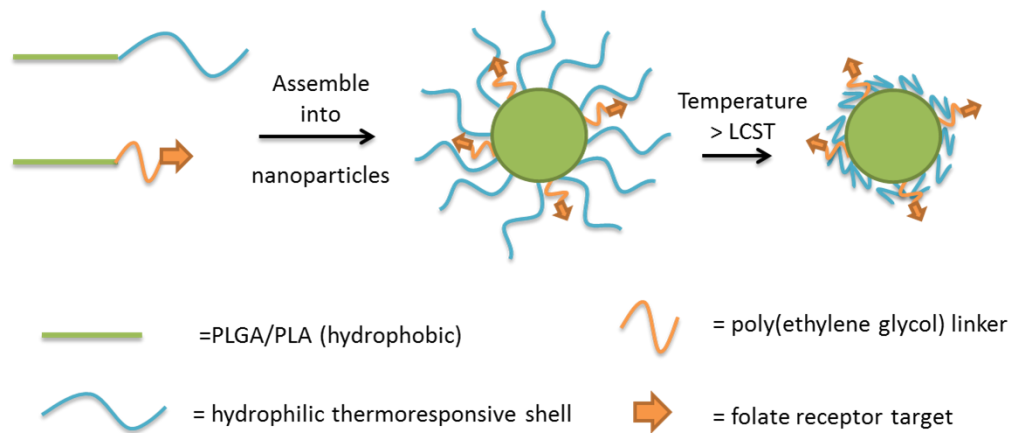
Figure 48 Design of the NP system under study

As the folate receptor is only able to target its receptor upon heating the off-site targeting is reduced. Although the presence of the receptor in healthy cells is low[196] any reduction in off-site targeting would be a huge advantage for cancer therapy and patient health.

Within this chapter the testing of the NP system aims to show whether raising the temperature of the cell environment above NP T_t stimulates uptake. Also, whether the addition of folate targeting can enhance the NP uptake and if so does the length of PEG spacer affect the ability of the folate to target its receptor.

5.2   Methods

5.2.1   Cell culture

HCT116 (colon cancer, folate receptor negative) and MCF-7 (breast cancer, folate receptor positive) cell lines were chosen for the study of the drug delivery nanoparticles.

Both cell lines were cultured in RPMI medium and the medium was replaced every two – three days as needed (10 mL). The cells were split once 80% confluency had been reached.

5.2.1.1 Cell passaging

5 mL of sterile EDTA was added per flask to wash the cells prior to adding 5 mL of trypsin and incubating for 5 minutes (until cells had detached) at 37 °C and 5% CO_2. Once the cells were detached 5 mL of RPMI media was added and the cell suspension was centrifuged at 1500 rpm for 5 minutes The resulting cell pellet was resuspended in 5-10 mL RPMI media and 10 µL of the suspension was used for cell counting. The splitting ratio for both cell lines was 1:5.

The cells were cultured in folate negative RPMI medium for at least two passages prior to being used for any studies.

5.2.1.2 Cell counting

The 10 µL of cell suspension was diluted with 10 µL trypan blue solution and cells were counted using a haemocytometer. To determine the number of cells the following equation was used:

$$cell\ number\ (mL^{-1}) = (average\ cell\ count)x\ 2\ x\ 10,000$$

5.2.2 Cytotoxicity assays

5.2.2.1 Lactate Dehydrogenase assay

Flat bottomed 96 well plates were seeded with $1x10^4$ cells/well for 24 h in folate free RPMI media at 37 °C and 5% CO_2. After 24 h the media was

removed and replaced with NP dilutions (200 µL of concentrations from 1 – 10 mg/mL) in folate free RPMI including two lanes with no NPs added for spontaneous and maximum LDH release measurements. The plates were incubated at 37 °C under a 5% CO_2 atmosphere for 24 h. After 24 h LDH lysis buffer was added (10 µL) to lane of maximum LDH release and incubated for 45 min. 50 µL of the solution from each well was removed and added to new 96 well plate, to this 50 µL of LDH assay buffer was added (Pierce™ ThermoScientific LDH assay kit) incubated for 30 min. The absorbance of each well was analysed using a visible light plate reader at 490 nm and 680 nm (background).

$$\% \; cytotoxicity = \frac{NP \; treated \; LDH \; release - spontaneous \; LDH \; release}{maximum \; LDH \; release - spontaneous \; LDH \; release} \; x \; 100$$

5.2.2.2 Resazurin assay (alamar blue)

Black 96 well plates were seeded with $1x10^4$ cells/well for 24 h in folate free RPMI media at 37 °C and 5% CO_2. After 24 h the media was removed and replaced with NP dilutions (200 µL initial concentrations from 0.1 – 10 mg/mL) in folate free RPMI including a lane for '100% cell death' (DMSO treated) and '100% cell live' (media only) controls. The plates were incubated at 37 °C and under 5% CO_2 atmosphere for 24 h. To each well 50 µL 44 µM resazurin in phenol-red free HBSS was added and incubated at 37 °C and 5% CO_2 for 90 minutes. Fluorescence (λ_{ex}= 530nm; λ_{em}= 590nm) determined and % metabolic activity determined by normalising between 100 % death lane (0 % metabolism) and 100 % live lane (100 % metabolism).

5.2.3   Time dependent uptake

6 well plates were seeded with 2.5×10^5 cells/ well for 24 h. The media was removed and replaced with 100 µg/mL rhodamine labelled nanoparticle suspensions in folate free RPMI media. In each plate R5%, FAR5%, R12% and FAR12% were added. For each time point a plate was removed from incubator and the NP suspension was removed, the cells washed with cold NaN_3 (5 mM) then warm trypsin was added to remove cells from the well-plate surfaces for analysis. The harvested cells were washed twice with PBS before being fixed with 4% PFA in PBS. For each time point a separate plate was used and processed in the same manner as each other.

5.2.4   Temperature dependent uptake

6 well plates were seeded with 2.5×10^5 cells/ well for 24 h. The media was removed and replaced with 100 µg/mL rhodamine labelled nanoparticle suspensions in folate free RPMI media. To control the temperature two incubators were used, set at 22 °C and 37 °C, both under a 5% CO_2 atmosphere. Each plate was placed in the respective incubator dependent on the temperature of choice for the experiment for 3 h.

 The wells were then washed quickly with cold 5 mM sodium azide to inhibit any exocytosis then 500 µL trypsin was added to detach the cells which were recovered by centrifugation (3,500 r.p.m. for 3 minutes), washed with cold PBS twice and fixed with 4% paraformaldehyde ready for flow cytometry measurements.

5.2.5 Folate dependent uptake

24 well plates were seeded with 1.5×10^5 cells/well for 24 h in folate free RPMI media. After 24 h the media was removed and replaced with media containing varied concentrations of free folic acid (0, 100, 200, 500, 750 and 1000 µM in 500 µL) for 2 h. This media was then replaced with media containing the same concentration of free folic acid + 100 µg/mL of rhodamine labelled nanoparticles (500 µL). The plates were incubated at 37 °C and under a 5% CO_2 atmosphere for 3 h. The wells were then washed quickly with cold 5 mM sodium azide to inhibit any exocytosis then 500 µL trypsin was added to detach the cells which were recovered by centrifugation (3,500 r.p.m. for 3 minutes), washed with cold PBS twice and fixed with 4% paraformaldehyde ready for flow cytometry measurements.

The above protocol was repeated for fluorescent microscopy studies in a 96-well plate (seeded at 1×10^4 cells/well for 24 h). However the cells were not trypsinised and Hoechst 33342 was added prior to fixing to stain the DNA of the cells.

For confocal microscopy 8 chamber borosilicate glass slides were seeded with 5×10^4 cells/chamber for 24 h. Two wells were incubated with folate free media with a further two incubated with media containing 500 µM folic acid for 2 h. The media was then replaced with media (500 µL) containing 100 µg/mL rhodamine labelled NPs for 3 h. The cell nuclei were then labelled with Hoechst 33342 after removing NP suspensions. The cells were washed with PBS and fixed with 4% paraformaldehyde. Wells were imaged using a 40X dry

objective and the image plane was set to image through the middle of the cell by focusing on the nuclei.

5.3   Results and discussion

To determine the effectiveness of the nanoparticle system *in-vitro* 3 key areas were investigated:

1. The effects of NPs on cell metabolism and membrane integrity

2. Temperature dependent uptake of the NPs

3. Folate dependent uptake of the NPs
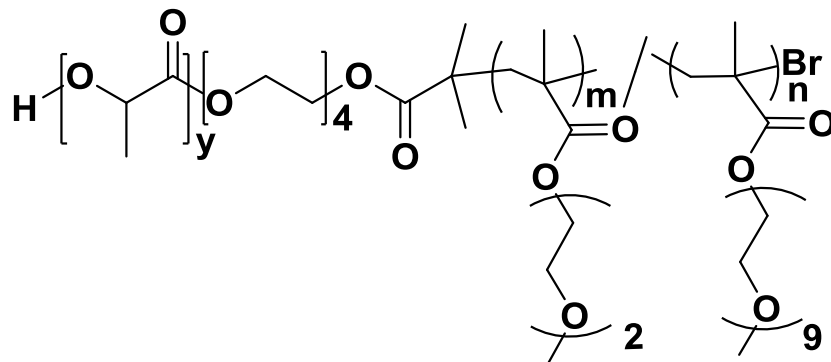
P12 (thermoresponsive)
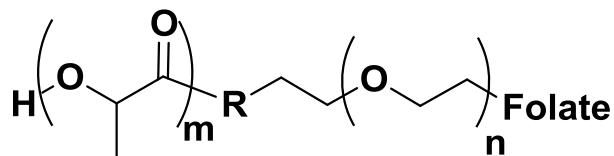
PLA-PEG-folate general structure (targeting)

Figure 49 Structure of P12 and the general structure for PLA-PEG-folate polymers used in Chapter 5

Table 18 Nanoparticle formulations investigated throughout Chapter 4

NP formulation	PLA-PEG$_x$-folate (mg)	PLA-PEG$_x$ (mg)	Thermoresponsive polymer (**P12**) (mg)
R5% (PEG$_{450}$ linker)		5	45
FAR5% (PEG$_{450}$ linker)	5		45
3kR5% (PEG$_{3k}$ linker)		5	45
FA3kR5% (PEG$_{3k}$ linker)	5		45
10kR5% (PEG$_{10k}$ linker)		5	45
FA10kR5% (PEG$_{10k}$ linker)	5		45

5.4 Effects of nanoparticles on cell metabolism and membrane integrity

Two assay types were used to determine the toxicity of the NPs. Firstly, resazurin assay was used which is an assay for measuring the metabolic activity of the cells after exposure.

Resazurin is converted to a fluorescent molecule (resorufin) in metabolically active cells, Figure 50. By measuring the fluorescence of the wells and

comparing this against wells containing cells which have not been exposed to NPs the metabolism of the exposed cells can be calculated.
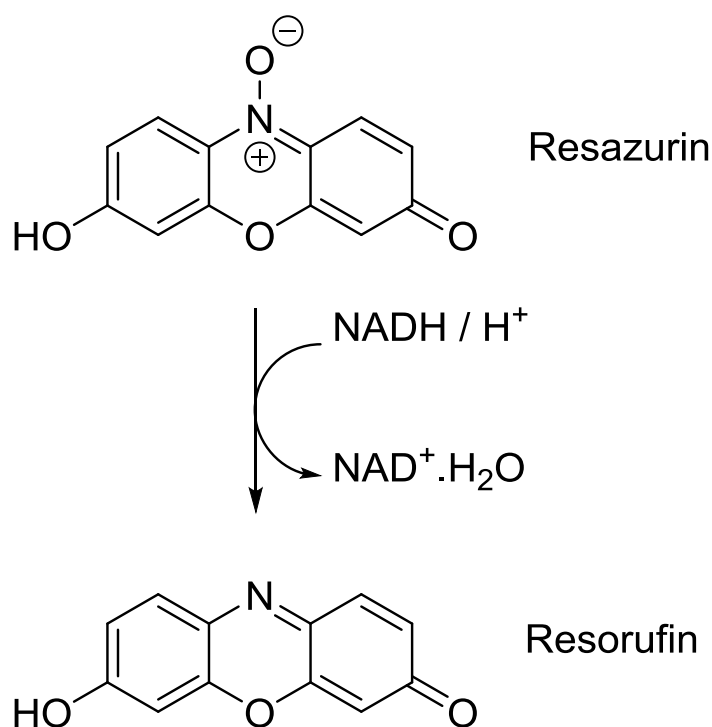
Figure 50 Metabolism of resazurin to resorufin in healthy cells

For the metabolic activity testing NPs with T_t above and below 37 °C were analysed. This was to determine whether the NPs with their polymer shell in their chain-extended (more hydrophilic) or chain-collapsed (more hydrophobic) state had any effect on the cells metabolic activity. The NPs were incubated for 24 h at 37 °C with concentration of NPs 0.1 – 10 mg/mL.

Cells exposed to NPs with a T_t below 37 °C (thus in colloidally unstable hydrophobic state) showed a lower cell metabolism than those exposed to NPs with T_t > 37 °C, Figure 51. The metabolic activity differences between each cell line were negligible, with the metabolic activity being > 50 % for each formulation < 5 mg/mL.
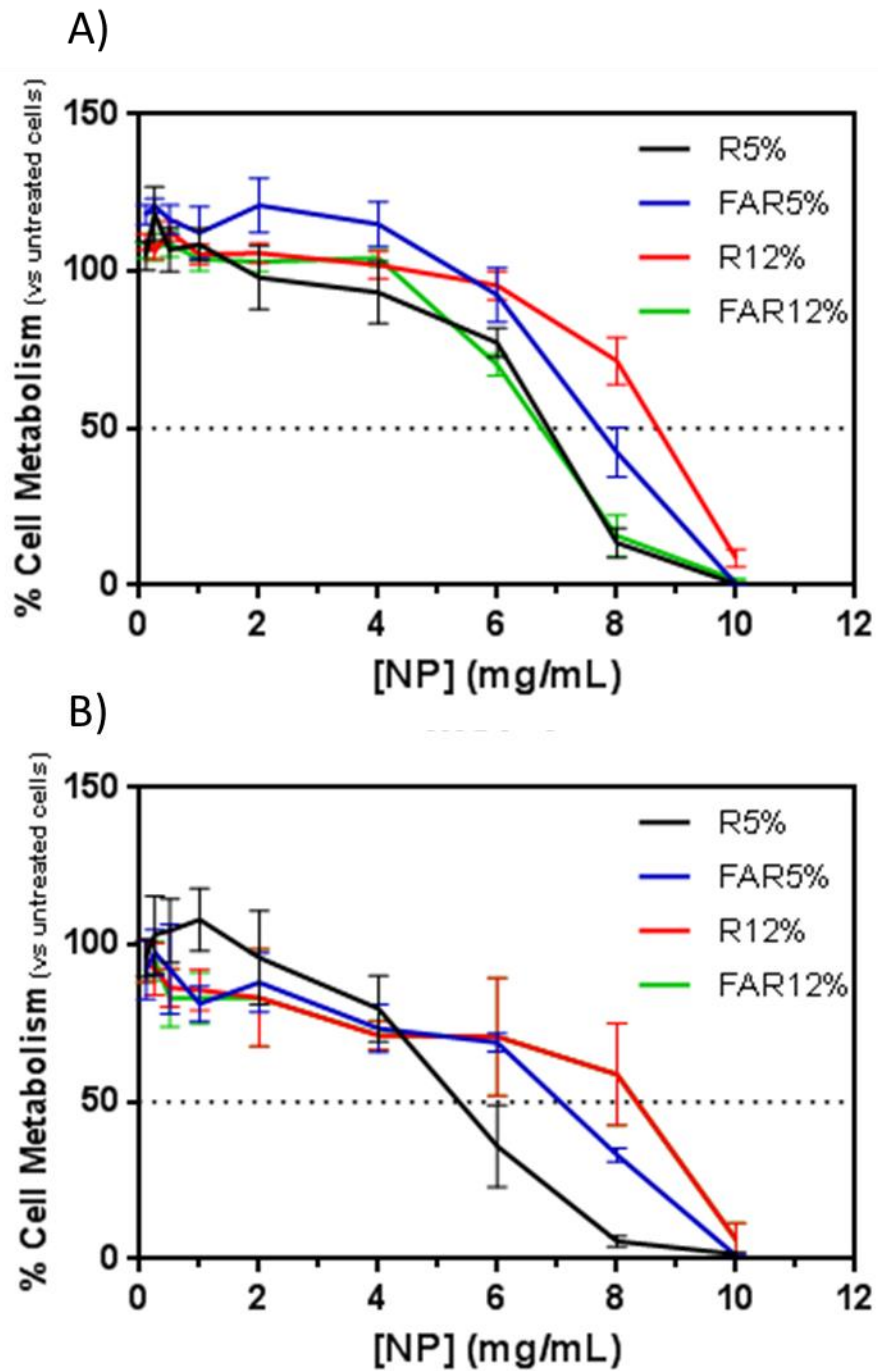
Figure 51 Resazurin assay showing percent cell metabolism for HCT116 (A) and MCF-7 (B) cell lines exposed to varied range of NP concentrations, metabolism calculated against healthy unexposed cells. Cells were exposed for 24 h at 37 °C prior to analysing. Results shown are for N=4. NPs are shown to not have an adverse effect on cell metabolism in either cell line below 5 mg/mL.

In order to investigate further the effects on cells of the NPs (< 5 mg/mL) a Lactate Dehydrogenase (LDH) assay was performed. This assay differs from the resazurin assay in that it is used to measure how "leaky" the cell membranes are. The permeability of cell membranes increases as they become necrotic, therefore the quantity of LDH released from the cell will increase with the permeability of the membrane. The quantity of LDH present can be analysed colorimetrically, Figure 52.
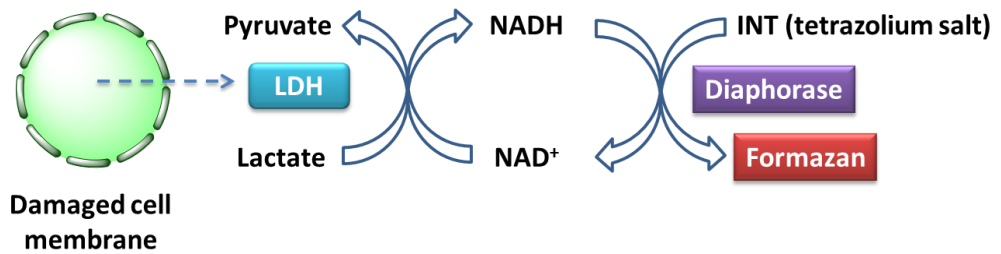
Figure 52 Schematic of the determination of LDH content by the colorimteric analysis of formazan product

The NPs were tested from 1 – 10 mg/mL again for 24 h replicating the resazurin assay conditions.
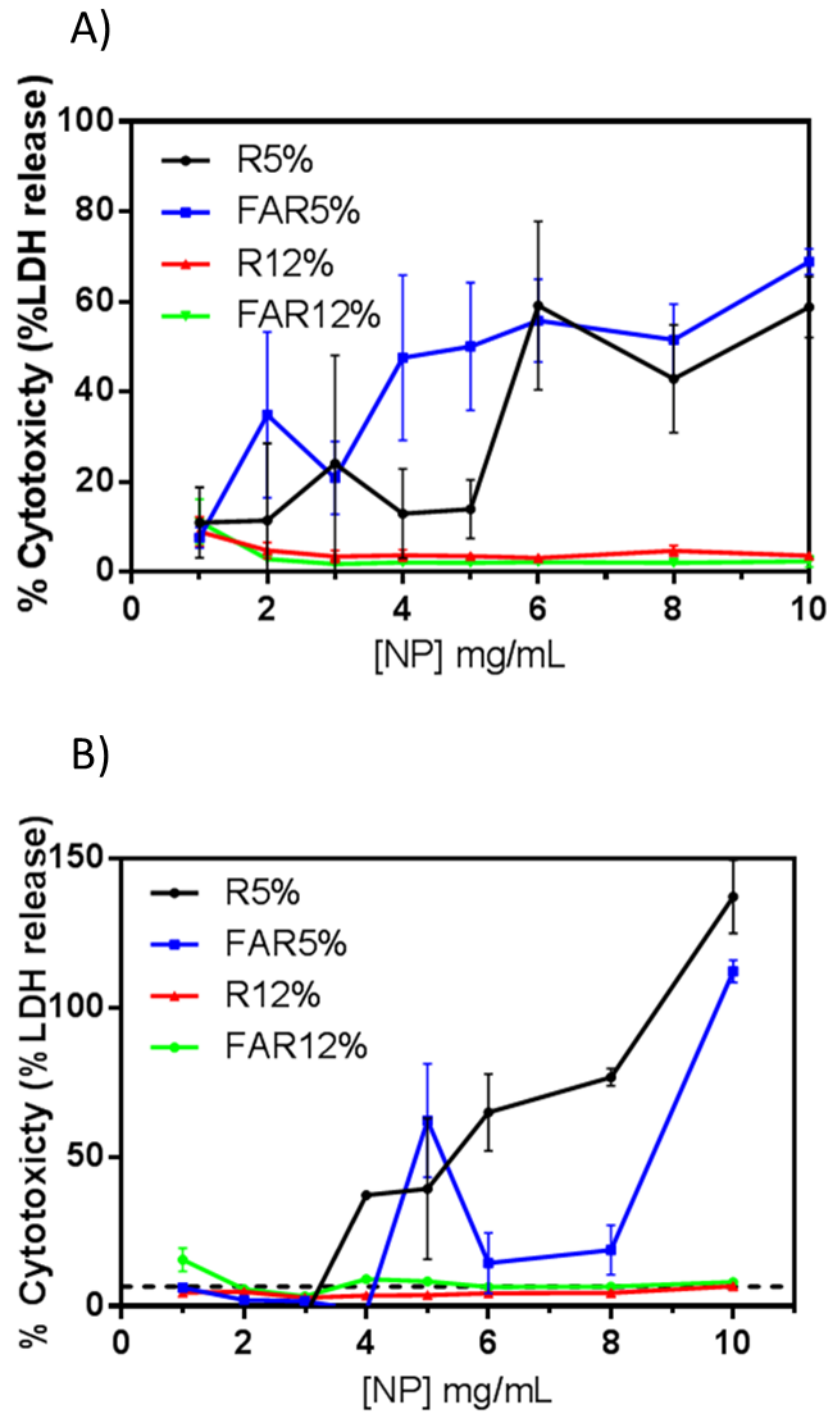
Figure 53 LDH assay showing percent LDH release for HCT116 (A) and MCF-7 (B) cell lines exposed to varied range of NP concentrations. LDH release calculated against healthy unexposed cells and 100% LDH release (cells treated with trigene). Cells were exposed for 24 h at 37 °C prior to analysing. Results shown are for N=4. NPs are shown to not have an adverse effect on LDH release in either cell line below 4 mg/mL.

For both R5% and FAR5% the %LDH release was found to increase when the

concentration of NPs was raised above 4 mg/mL, Figure 53. The R12% and

FAR12% NPs showed a different trend however with no % LDH release noted above the spontaneous control for all concentrations of NPs. This may be due to the NPs not causing any detrimental effect on the cell membrane as the NPs are in their non-collapsed hydrated state therefore not interacting with the cell membrane. The 5% NPs, with a T_t of 32 °C, were in their collapsed non-hydrated state and thus would be interacting with cell membranes due to the hydrophobicity of both. This interaction at high concentrations of NPs is likely to be the reason for the leakage of LDH observed. An alternate reason for the lack of LDH release observed for the 12% NPs could be due to small quantities of copper present from the polymerisation process. It has been suggested in literature that copper can cause inactivation of LDH,[197] this would have to be tested further to fully comprehend the reason behind the lack of LDH release.

These two assays showed that both types of NPs regardless of their T_t induced limited adverse effects on the cells when the concentration was kept below 5 mg/mL.

As the NPs were shown to be well-tolerated by the selected cells at lower concentrations the next stage was to determine the rate of uptake of the NPs.

5.5   Time Dependent Uptake

For rate of uptake studies, the cells were dosed with identical concentrations of NPs (100 µg/mL) and at each time point (between 20 and 180 minutes) cells were harvested for analysis by the addition of trypsin to the well. One well was chosen per time point and the uptake was measured over 3 h.

Each set of NPs showed increased uptake over time in the HCT116 cell line, with R5% NPs uptake reached a maximum after 90 minutes, the remaining NPs were all showing increasing uptake up to the final time-point at 3 h, Figure 54. Both types of thermoresponsive NPs were taken up regardless of whether they were expected to be in their hydrophilic/hydrophobic state: this will be further investigated in section 5.6
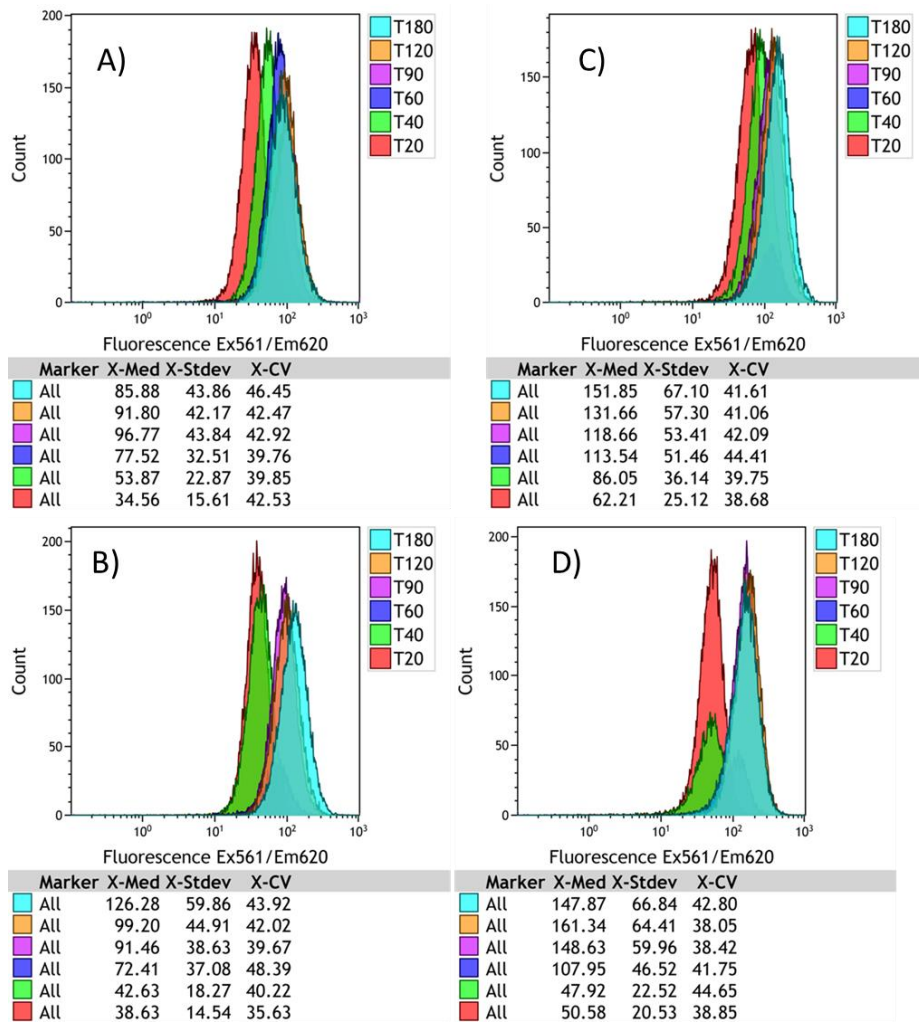
Figure 54 Time dependent uptake of NPs in HCT116 cell line from 20 – 180 minutes, NPs were added at T0 100 µg/mL. Cells were harvested for flow cytometry using trypsin and fixed with 4% PFA in PBS. A) R5%. B) FAR5%. C) R12%. D) FAR12%. Results representative of 3 independent experiments.

The MCF-7 cell-line showed similar results to the HCT116 cell line in that the uptake of both R12% and FAR12% NPs increased up to the 3 h timepoint, Figure 55. The R5% NPs uptake however appeared to reach a maximum after 60 minutes compared to the 90 minutes as described above.
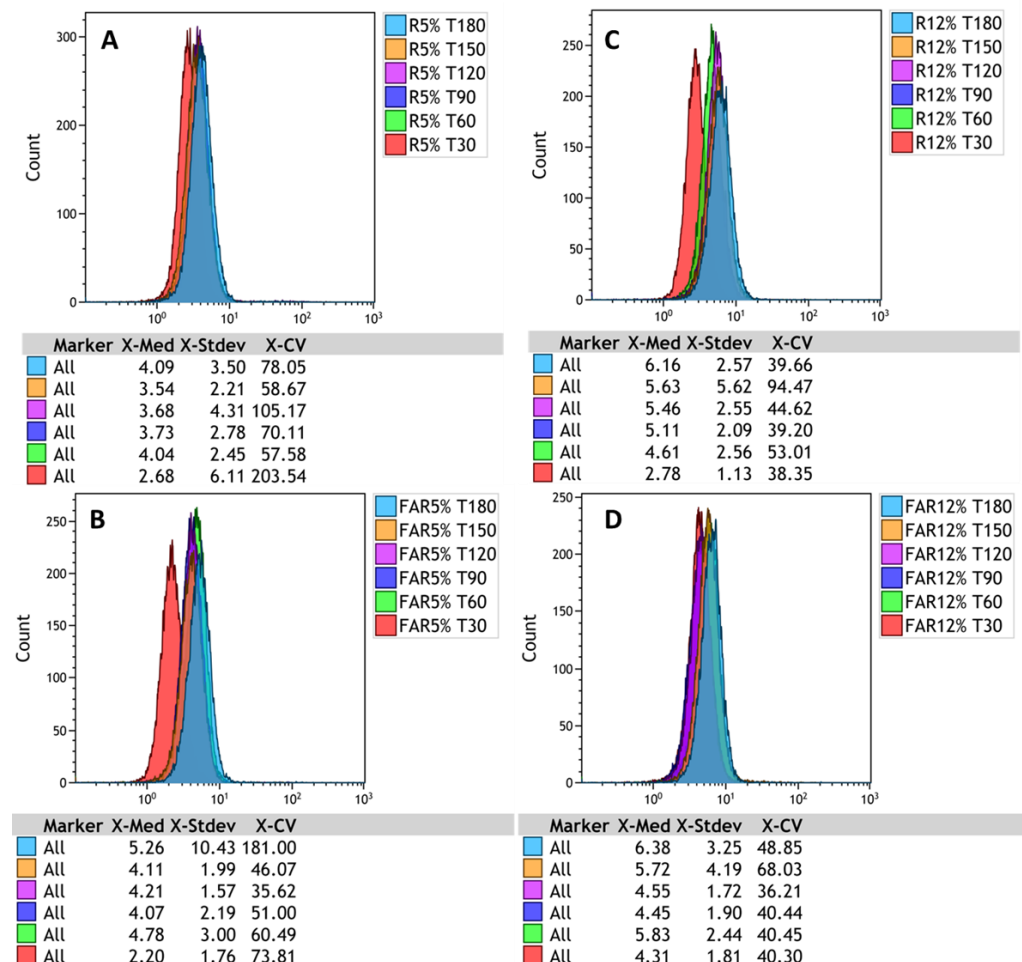
Figure 55 Time dependent uptake of NPs in MCF-7 cell line from 30 – 180 minutes, NPs were added at T0 100 µg/mL.Cells were harvested for flow cytometry using trypsin and fixed with 4% PFA in PBS. A) R5%. B) FAR5%. C) R12%. D) FAR12%.

A further study was carried out to determine how long the NPs remained in the cells once the NP suspension was removed from the cells. The premise for this study was to determine whether the NPs were being exocytosed or had the opportunity to remain in the cell for a prolonged period of time.

NPs were added to the cells (MCF-7 and HCT116) for 3 h then the NP suspension was removed using a pipette. For time point 0 the cells were harvested as soon as NPs were removed however for each additional time point the chosen well was washed twice with warm HBSS and replaced with warm HBSS. At each time point the contents of a well were trypsinised and fixed with 4% PFA in PBS.
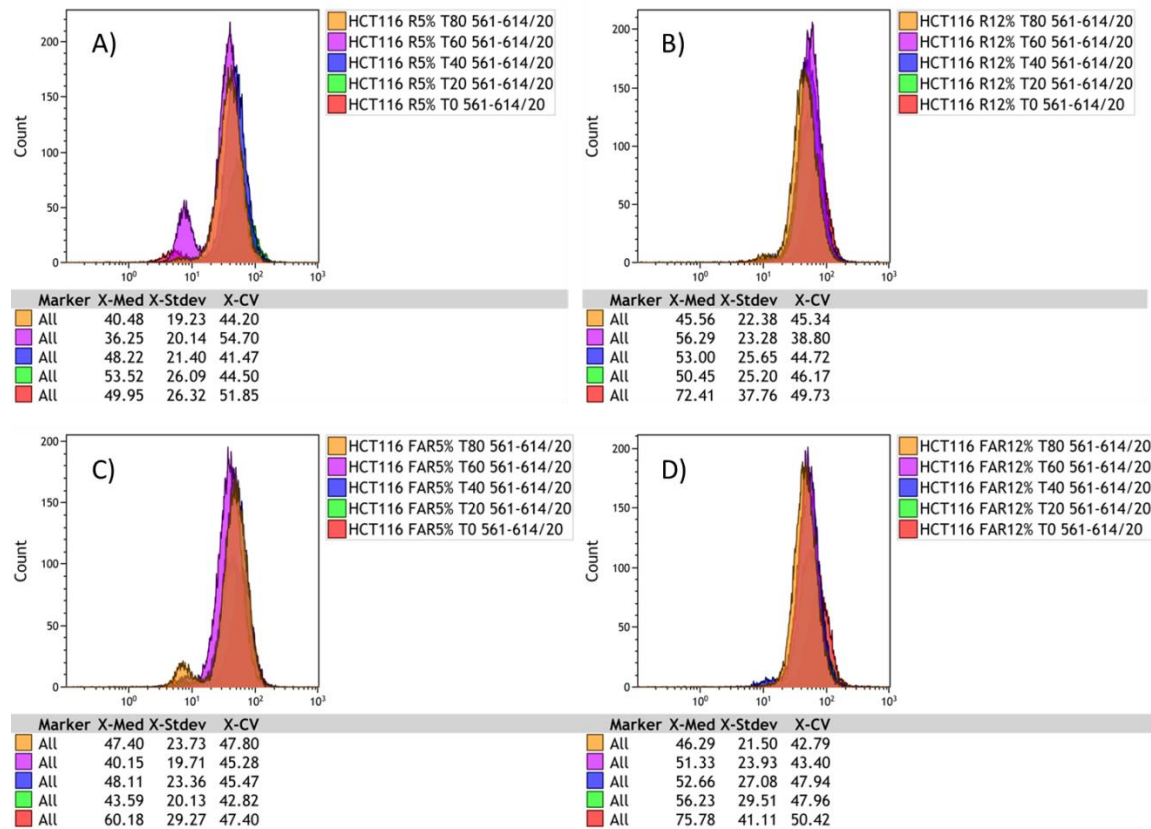
Figure 56 HCT116 flow cytometry data for the residency time of NPs within cells after removal of NP suspension. A) R5%. B) FAR5%. C)R12%. D) FAR12%. For each NP formulation the level of NPs in the cells did drop over time however there were at least 50% of the NPs remaining 80 minutes after exposure, by fluorescence. At least 15,000 events were recorded for each sample.
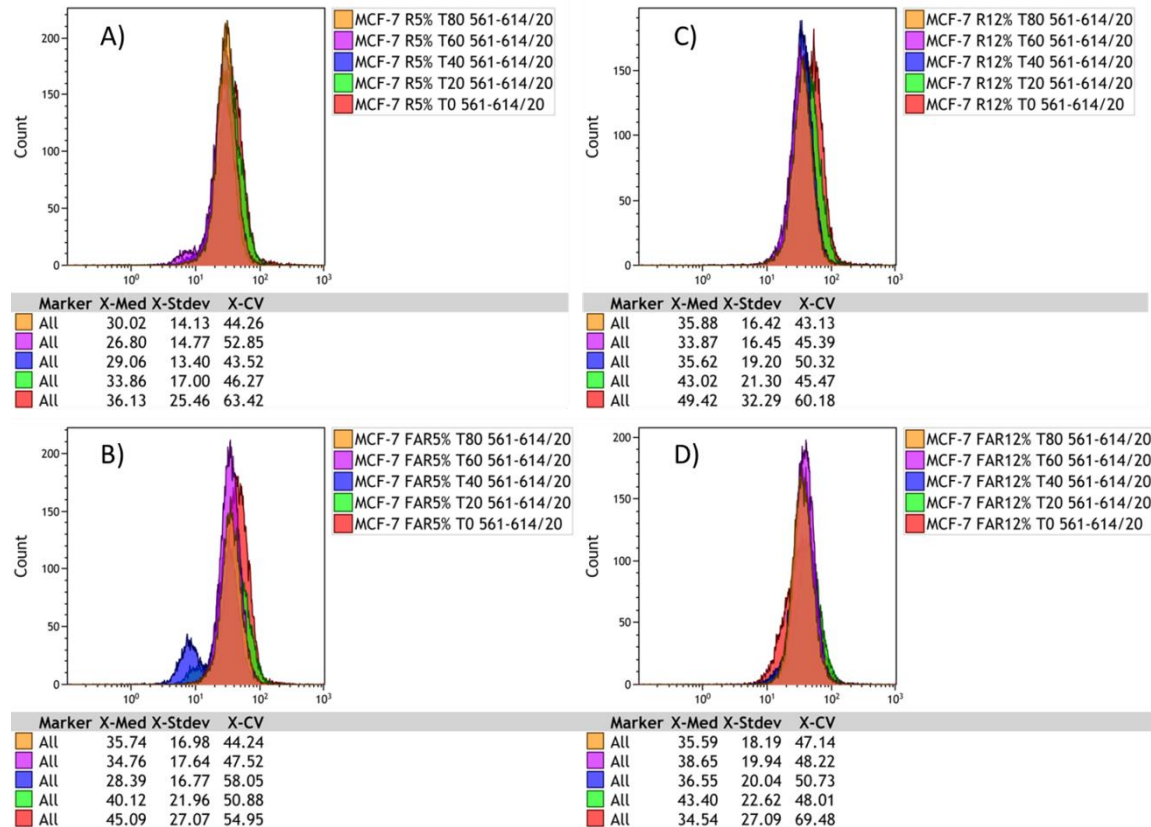
Figure 57 MCF-7 flow cytometry data for the residency time of NPs within cells after removal of NP suspension. A) R5%. B) FAR5%. C)R12%. D) FAR12%. For each NP formulation the level of NPs in the cells decreased over time however there were at least 50% of the NPs remaining 80 minutes after exposure, as demonstrated by quantitation of fluorescence. At least 15,000 events were recorded for each sample.

As expected the fluorescence decreased with each time point up to 80 minutes after exposure, Figure 56 and Figure 57. Upon further analysis of the data there was between 51 – 81% of the initial quantity NPs taken up remaining after 80 minutes, however there was no observable trend between type of NP being exocytosed and amount remaining within the cells, Table 19.

Table 19 Quantity of NPs remaining within cells 80 minutes after exposure

NP type	HCT116	MCF-7
R5%	73%	55%
FAR5%	81%	63%
R12%	60%	51%
FAR12%	52%	67%

It has been shown previously that shape and size of NPs is important on their exocytosis processes;[198,199] however the NPs studied above for time dependent uptake were all of a similar size and spherical in morphology. Panyam *et al*. noted that PLGA NPs of ~97 nm were exocytosed much slower than small molecule marker (Lucifer yellow) with approximately 65 % of the initial quantity of NPs exocytosed after 30 minutes.[199] When these results are compared with those of poly(methyl methacrylate)-*block*-poly(polyethylene glycol methyl ether methacrylate) NPs similar results were obtained however these NPs were only ~25 nm in diameter.[200]

This data when compared with that shown for the NPs under study here it can be concluded that the NP exocytosis is relatively slow (when compared with

small molecules) and that this is positive for the use as a drug delivery vehicle. The longer the NPs remained in the cells the more likely sufficient drug would be released to kill the cell. It also allowed for the knowledge that there would be very little exocytosis occurring during processing of the cells between washing and fixing for flow cytometry and microscopy measurements minimising any error in the analysis.

The initial studies of both toxicity and time dependent uptake allowed for the parameters to be distinguished for further examination of the NP system.

5.6   Thermoresponsive Dependent Uptake

The nanoparticles formulated for these assays were expected to show temperature-dependent uptake based on prior assays.[48,49,173] When the temperature is raised beyond the T_t and the water molecules bonded to the polymers keeping the NPs in solution begins to dissociate from the DEGMA and OEGMA units in the polymer backbone the NPs should show a higher uptake. This is due to the NPs increasing their hydrophobicity which would make them more susceptible to non-specific endocytosis due to both the interactions with the hydrophobic cell membrane and protein adsorption. To test this hypothesis NPs were incubated with cells both above and below their T_t for 3 h and analysed for uptake using flow cytometry.

The R5% thermoresponsive polymer was used for all further testing as the T_t of NPs assembled from this polymer was ~ 32 °C, thus by incubating at room

temperature (22 °C) and 37 °C (usual incubator temperature) the NP uptake could be assessed above and below the T_t. All testing was carried out within an incubator at chosen temperature with a 5% CO_2 atmosphere.

Firstly, the colon cancer cell line, HCT116, was incubated with NPs (100 µg/mL, far below the toxic limit) for 3 h at each temperature. The NPs used contained either the PEG_{450} or PEG_{3k} linker i.e. (FA)R5% and (FA)3kR5%.

The uptake of the NPs was found to increase (by almost double) for each type of NPs (R5% and 3kR5%) when the incubation temperature was raised from 22 °C to 37 °C, Figure 58. This increase implied that the higher uptake was due to the NPs transitioning to their colloidally unstable hydrophobic phase or that with the increased temperature the cells were more stable and enough energy present to increase NP endocytosis. In order to determine whether this was inherent only to the HCT116 cell line the experiment was repeated with the breast cancer cell line MCF-7, which over-expresses the folate receptor.[190,201,202]
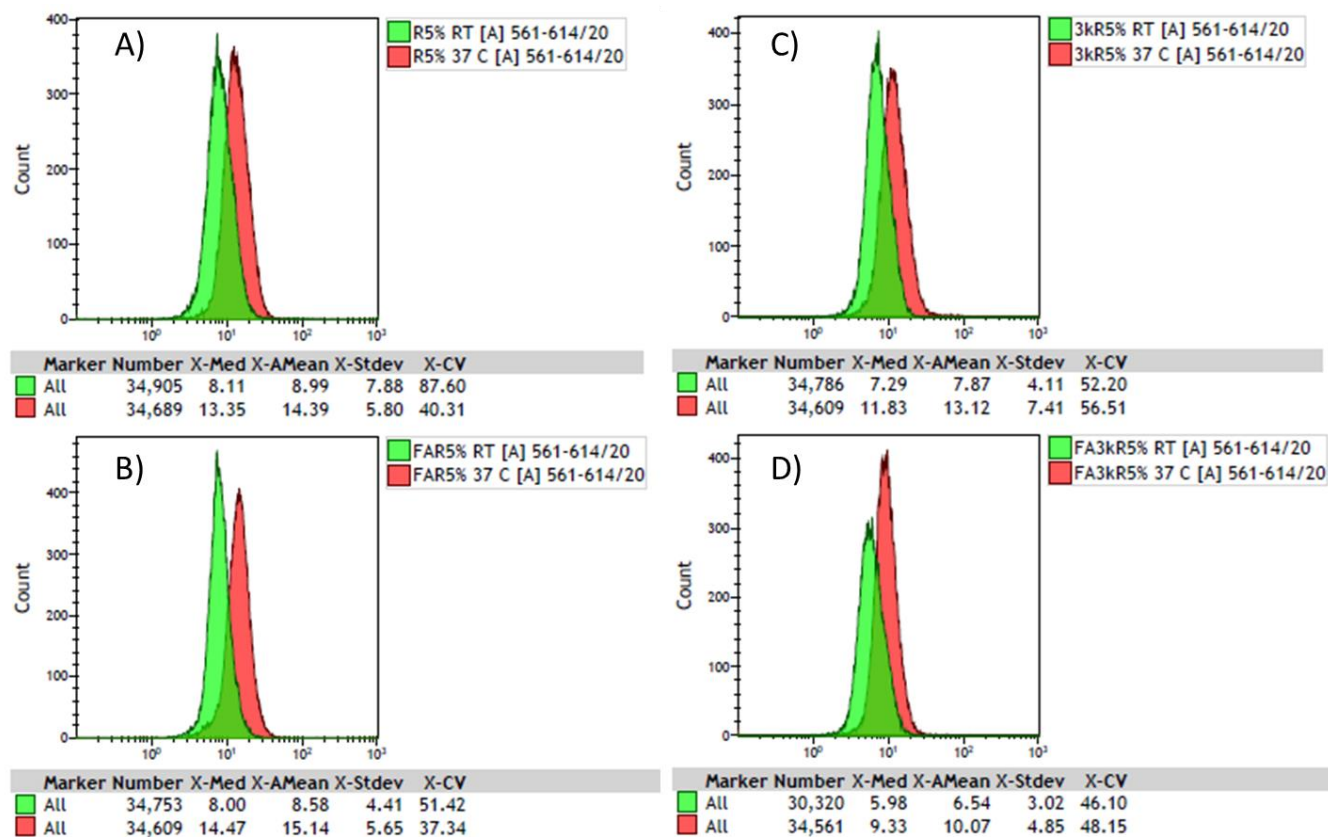
Figure 58 Flow cytometry measurements of HCT116 cells incubated with NPs at 22 °C (RT - green) or 37 °C (red). A) R5%. B) FAR5%. C) 3kR5%. D) FA3kR5%. For each type of NP (A-D) the median fluorescence (uptake) almost doubled when the incubation temperature was raised from 22 °C – 37 °C. At least 30,000 cells were analysed and the results above are representative of at least two repeats.

Similar results regarding NP uptake were observed for the MCF-7 cell line, Figure 59. For each formulation the uptake had again doubled upon increasing the temperature beyond the NPs T_t. There may however be another cause for the difference in rate of uptake; that could be due to the cells being out with their normal incubation conditions, at room temperature, and therefore less energy available to be used for the endocytosis of NPs. In order to determine whether this could be the cause of the uptake differential the uptake experiment was repeated with dextran, known to be a marker for uptake and macropinocytosis.[203,204] Two types of dextran were used which had a molecular weight of 4 kDa and 40 kDa respectively. Each type of dextran was tagged with FITC to ensure the uptake could be monitored by flow cytometry
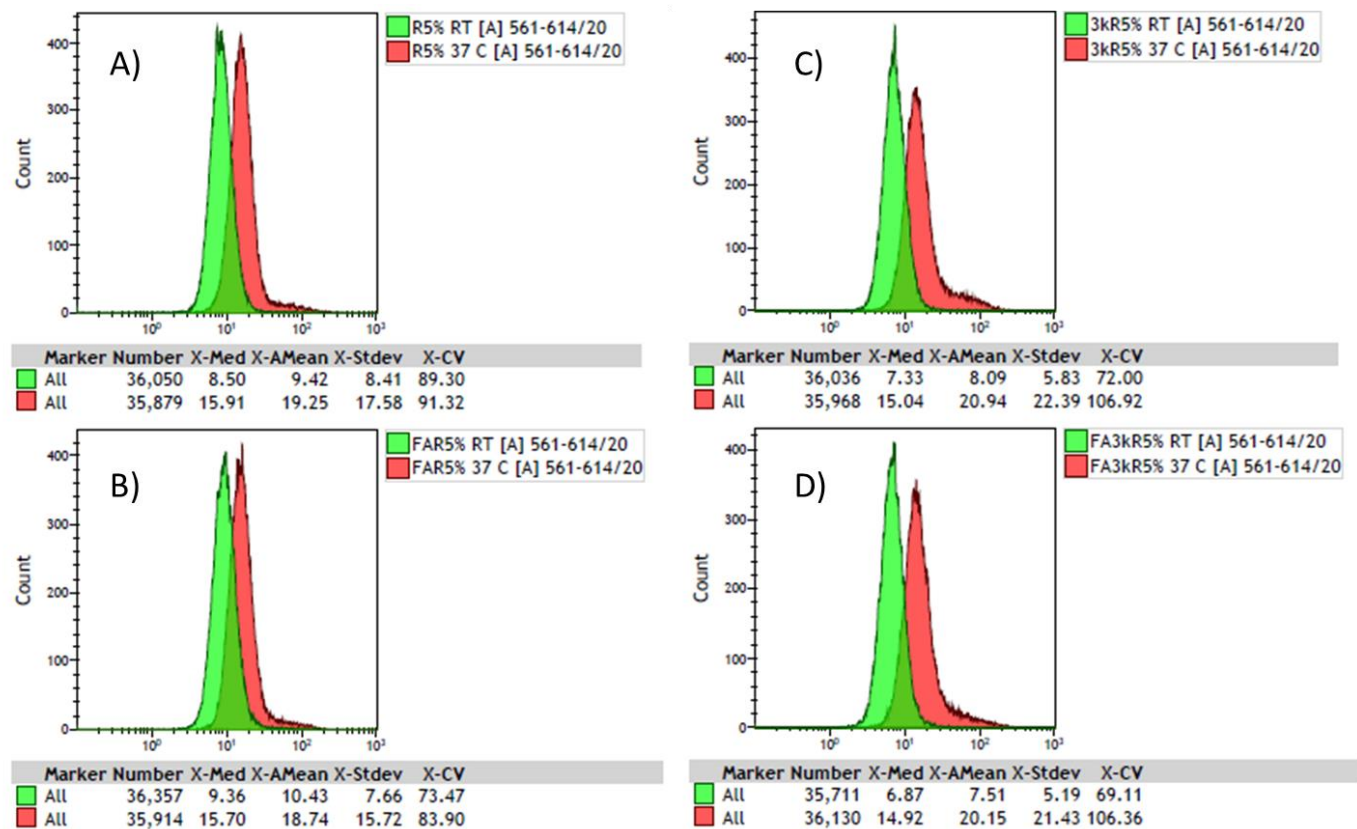
Figure 59 Flow cytometry measurements of MCF-7 cells incubated with NPs at 22 °C (RT - green) or 37 °C (red). A) R5%. B) FAR5%. C) 3kR5%. D) FA3kR5%. For each type of NP (A-D) the median fluorescence (uptake) almost doubled when the incubation temperature was raised from 22 °C − 37 °C. At least 35,000 cells were analysed and the results above are representative of at least two repeats.
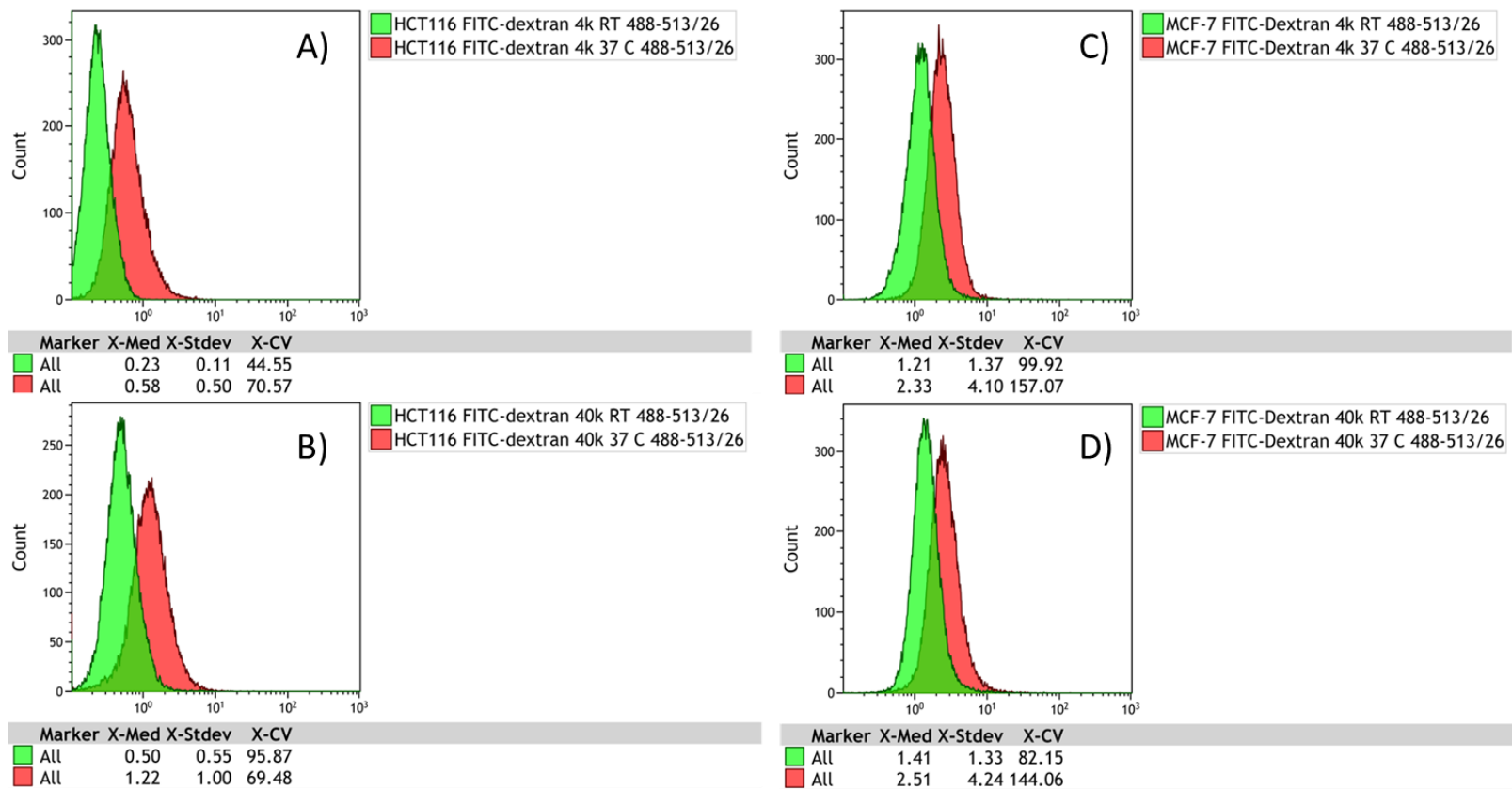
Figure 60 Flow Cytometry data showing the difference in uptake of FITC-dextran at room temperature and 37 °C. A) FITC-dextran 4k HCT116. B) FITC-dextran 40k HCT116. C) FITC-dextran 4k MCF-7. D) FITC-dextran 40k MCF-7. For both types of dextran and both cell lines the uptake was shown to double when the temperature was raised from RT to 37 °C.

The uptake of both types of FITC-dextran resembled that of the thermoresponsive NPs, Figure 60. When the cells were incubated at 37 °C the uptake was twice that of the dextran incubated with cells at 22 °C. The uptake was independent of the cell line used. This result would mean that there is likely no thermoresponsive dependent uptake of these NPs. However, it is possible that the uptake pathways of NPs and dextran are different thus this would require further study.

To ascertain whether there were NPs which were beginning to aggregate earlier than previous thought and hence becoming hydrophobic at temperatures around 22 °C, which may explain why the NPs are being taken up at both temperatures, R5% NPs were analysed further by DLS. A 100 μg/mL suspension was tested at increasing temperatures from 20 – 32 °C and the radius and counts were recorded.
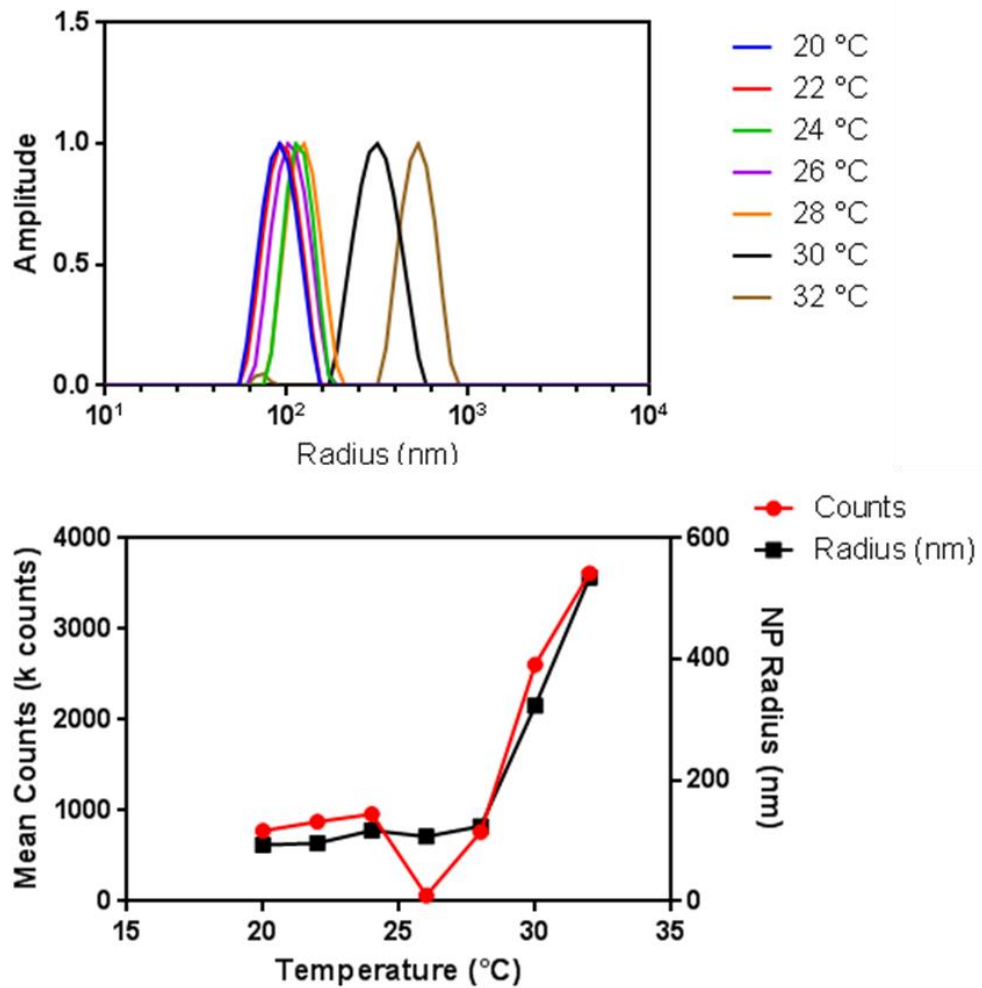
Figure 61 DLS of R5% NPs showing the increase in both size and counts at 29- 30°C.

The DLS data showed that there was no increase in the apparent size (and thus aggregation state) of the particles until the temperature reached 30 °C, Figure 61. Therefore it is not possible that the particles were in their collapsed, colloidally unstable state at the lower 22 °C temperature chosen for the uptake study. It can therefore be concluded that the NPs were being taken up in a manner independent of the chain conformations of the outer polymer shell.

Similar studies have been carried out regarding the thermoresponsive uptake of NPs to varying degrees of success. Li *et al*. used poly(N-

isopropylacrylamide-co-N,N-dimethylacrylamide-b-lactide) (PID$_{118}$-b-PLA$_{59}$) NPs which had a T$_t$ of 39 °C. Uptake measurements were carried out in a N-87 stomach cancer cell line at both 37 °C and 40 °C.[205] The author concluded that there was a difference in uptake of 4x between the 37 °C and 40 °C measurements. However by studying the flow cytometry data the largest point of fluorescence appears to be at 9 h and the uptake has doubled not quadrupled. There is also considerable uptake of the NPs below the T$_t$ identified for these types of NPs, similar to the data shown in this chapter.

The microscopy images clearly showed uptake of NPs at both temperatures, therefore although there is a temperature enhanced uptake the NPs still accumulate below their T$_t$. This group hypothesised that the NPs below T$_t$ were being taken up by endocytosis however when the NPs became hydrophobic, above the T$_t$, the NPs bound with the cell membrane hence the enhanced uptake.

Barhoumi *et al*. investigated gold NPs coated with a pNIPAAm-*co*-polyacrylamide using a peptide targeting agent (hidden below the T$_t$) to determine cell binding.[206] The NPs were found to bind to the human umbilical vein endothelial cells (HUVECs) below their T$_t$, however it should be noted that above the Au NPs T$_t$ there almost a 3-fold increase in cell interaction (24.3 ± 9.3 µg/kg below T$_t$ and 71.4 µg/kg above the T$_t$).

Further to these studies a report in literature showed chitosan-*g*-poly(*N*-vinylcaprolactam) NPs (TRC-NPs) being used as a delivery vehicle of curcumin to cancer cells.[207] The TRC-NPs were found to have a T$_t$ of 38 °C however the

cell uptake experiments analysed by flow cytometry were carried out at 37 °C. As the NPs were in their hydrophilic state it would be expected that the NPs would not show uptake. This was not the case, uptake was observed in both cell lines tested, mouse fibroblast (L929) and prostate cancer cell line (PC3), at temperature below the T_t of the NPs. The NPs were incubated for 24 h in the presence of the cells before being analysed by flow cytometry. Although there was a higher uptake of NPs in the PC3 cell line than the L929 cell line both showed a higher uptake than for the control cells. Another point of note in the flow cytometry data is that for the highest concentration of NPs studied, 1 mg/mL, the uptake was less than that of the two lower concentrations, 0.2 and 0.6 mg/mL.

Although not a thermoresponsive triggered uptake, Nakamura *et al*. investigated the uptake of zinc protoporphyrin NPs with various coronas. They observed that even NPs with a hydrophilic PEG corona showed uptake in human chronic myeloid leukaemia cells (K562).[208] The presence of the NPs within the cells at 37 °C and not 4 °C showed that the NPs were taken up in an energy dependent process. The authors concluded that the PEG-ZnPP was taken into cells *via* endocytic pathway and subjected to hydrolytic cleavage by either protease or esterase inside of, or in the vicinity of, the cells. The results of this investigation also agree with the findings of the work in this chapter which shows NP uptake in both the hydrophilic and hydrophobic form.

Each of these four studies has shown either cell uptake or interaction with the cell membrane of NPs below their T_t / hydrophilic state. Comparing this data

with that shown for the PLA-*b*-P(DEGMA-*stat*-OEGMA) NPs above it can be concluded that depending upon a temperature switch alone to trigger NP uptake is not a consistently reliable method for targeted drug delivery to cancer cells.

As it was determined the uptake of NPs was due to an energy dependent process and that the thermoresponsive nature of the NPs did not lead to an enhanced uptake the use of folate was investigated as a method of targeting and increasing the uptake.

5.7   Folate Dependent Uptake

As there was no observable difference in the uptake of NPs, whether they were incubated above or below their transition temperature, the use of folate as a targeting agent was investigated. The interest of these NPs would be their "hide-and-reveal" capabilities; this involved the folate tag being obscured by the extended PEGMA corona of the NP. Once the T_t is reached the PEGMA corona was expected to collapse, thus revealing the folate tag to target the folate receptor over expressed on some cancerous cells.

To test the possibilities of the "hide-and-reveal" moiety the three lengths of PEG linker between the PLA core and folate tag were investigated when mixed with the **P12**. By using the different lengths of linker, which should theoretically then be further from the core when the longer PEG chain is used, the required length of linker could be determined.

Each of the PLA-PEG$_x$-folate polymers were mixed with the **P12** in a 1:9 ratio w/w and tested for their uptake capabilities with both HCT116 and MCF-7 cells. Free folic acid was added in varying concentrations to determine whether there was inhibition of uptake when present.[168,209,210]

For these experiments, free folic acid (FA) was incubated for 2 h with the cells prior to the addition of the folate-NPs. This incubation period was used to allow free FA to equilibrate the cells in the wells to the presence FA. The subsequent addition of free FA alongside the folate-NPs serves to maintain a constant free FA concentration in solution ensuring the cell environment was unchanged during addition of NPs. The concentration of NPs applied to the cells was kept constant, 100 µg/mL, for each experiment and incubation time was 3 h as for previous uptake experiments. After 3 h the cells were harvested using trypsin and fixed with 4% PFA in PBS prior to analysing with flow cytometry.

When the NPs were incubated with the HCT116 FR-ve cell line there was no observable difference in uptake between the folate tagged and untagged NPs, as shown in Figure 62. This result was expected, as with no folate receptor expressed on this cell line, the presence of folate on the NPs should not enhance the uptake, as there would be no receptor mediated endocytosis.
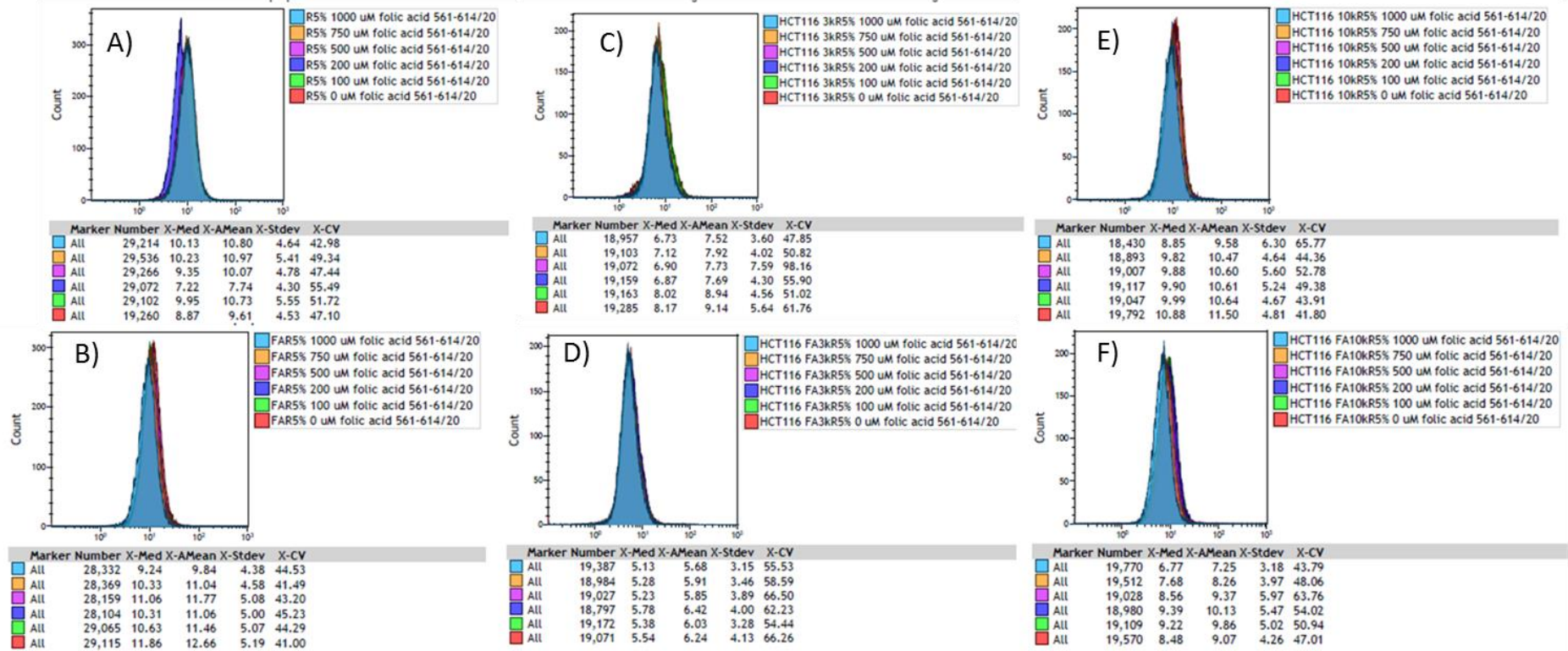
Figure 62 HCT116 folate dependent uptake flow cytometry data. A) R5%. B)FAR5%. C) 3kR5%. D) FA3kR5%. E) 10kR5%. F) FA10kR5%. The uptake was similar for all NP types with added folate having no impact on the uptake. Data representative of a minimum of 18,000 events.
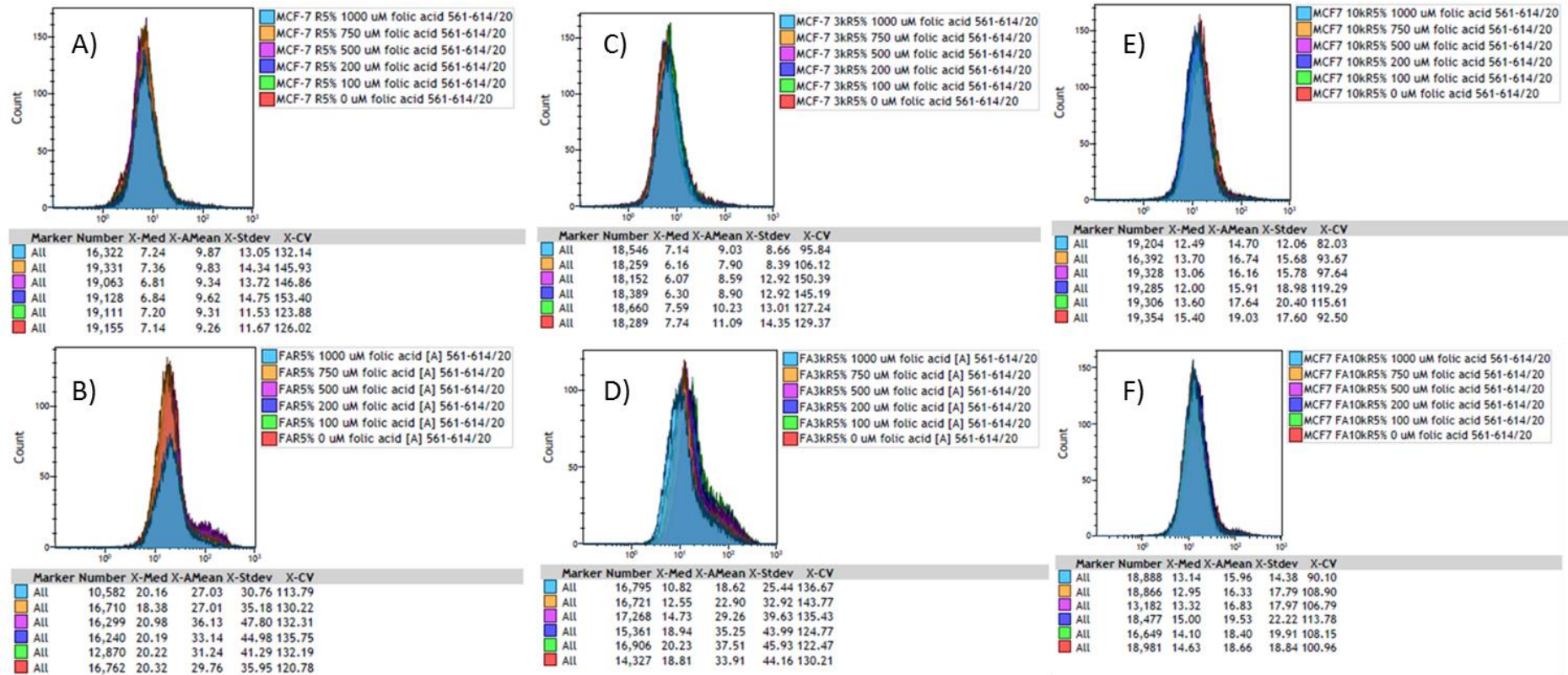
Figure 63 MCF-7 folate dependent uptake flow cytometry data. A) R5%. B)FAR5%. C) 3kR5%. D) FA3kR5%. E) 10kR5%. F) FA10kR5%. For FAR5% and FA3kR5% there was a 100% increase in uptake compared to the untagged versions of the same NPs, there was no difference for the 10k variety. When there was a large amount of free folic acid added (750-1000 μM) the uptake of FA3kR5% was inhibited. There was no effect on the uptake of FAR5% and FA10kR5%. Data representative of a minimum of 10,500 events.

The MCF-7 cell line (FR +ve) when incubated with each type of NP showed differences depending on the NP being studied. The two shorter length PEG linker NPs, FAR5% (intensity of ~ 20 compared with intensity of ~ 7 for R5% NPs) and FA3kR5% (intensity of ~ 20 compared with intensity of ~ 7 for 3kR5%), had more than double the uptake of their non-folate tagged counterparts, Figure 63. The FA10kNPs had no difference in uptake with the folate tag compared to the untagged (average fluorescence of 12 - 15 for both). As the quantity of free folic acid was added to compete with the NPs for uptake by folate receptor endocytosis there was a drop in uptake for the FA3kNPs compared to the 3kNPs of around 50% (drop from 18.8 for 0 µM FA to 10.8 fluorescence for 1000 µM FA). The concentration of free folic acid had to be high, 750 – 1000 µM for there to be any inhibition in NP uptake. The addition of free folic acid appeared to have no effect on the uptake of both FAR5% and FA10kR5% NPs.

As there was a considerable increase in the uptake of both FAR5% and FA3kR5% in MCF-7 cell line compared to both their non-folate counterparts and the uptake of both in the HCT116 cell line the additional uptake was attributed to folate receptor mediated endocytosis. It was clear that all types of NPs were also being taken up by another energy dependent uptake, as there was fluorescence recorded in both cell types for all NPs.

This data would suggest that when the temperature is raised beyond the T_t of the thermoresponsive corona both the PEG$_{450}$-linked folate and PEG$_{3k}$-linked folate is capable of binding to the folate receptor on MCF-7 cells; with no

difference in fluorescence between 10kR5% and FA10kR5% this would suggest the folate is not capable of binding to receptor to enhance the uptake. A possible cause of this is that the folate bound to the end of the PEG chain was embedded within the hydrophobic core of the NP. It has been shown that when PLGA-PEG$_{5k}$-folate was used as a targeted self-assembled NP only ~20% of the folate was present on the surface of the NP, the remainder was hypothesised to be within the core due to interactions with the PLGA.[142]

To elucidate further the NP uptake differential, when the folate targeting ligand is used, the uptake was visualised using confocal microscopy. 8 well chamber slides were seeded with cells for 24 h and the uptake experiment was repeated as for the flow cytometry analysed samples. The folate and non-folate versions of R5% and 3kR5% were chosen for imaging as they had shown an uptake differential unlike the 10kR5% NPs. Each well of cells was fixed with paraformaldehyde, after incubation and washing steps with PBS, prior to imaging. For the confocal microscopy the image plane was set to cut through the centre of the cell by focussing on the cell nucleus. For the purposes of the imaging the cell nuclei were stained with Hoechst 33342. Within each well that was imaged there was observable uptake across both cell lines, shown by the green in Figure 64 (MCF-7) and Figure 65 (HCT116) plus zoomed confocal in Figure 66. There was substantial aggregation present around the cells incubated with 3kR5% and FA3kR5% for both cell types. This is not surprising considering the assays were carried out above the T_t of the

NPs. As shown previously, as the temperature is raised above the T_t the NPs will begin to aggregate. For both of these NPs the aggregates adhered to the hydrophobic glass slide as well as the cell membranes. Even though there was considerable aggregation present the NPs were still taken up by the cells. There was no obvious localisation of the NPs within the cells and all types were spread homogeneously throughout the interior. However this could not be fully confirmed without the use of colocalisation imaging.
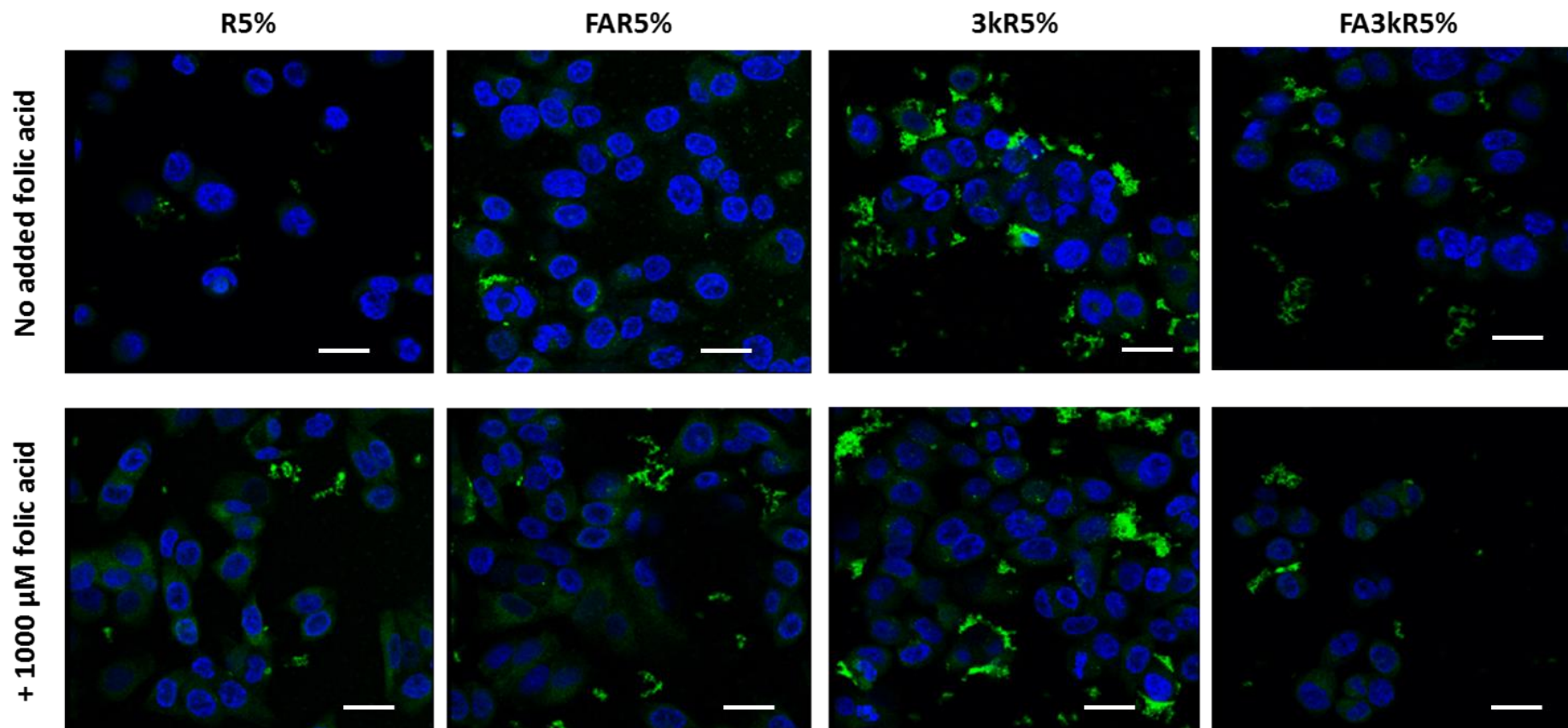
Figure 64 Confocal microscopy images of NP uptake (green) with MCF-7 cells. NPs were incubated with cells for 3 h with or without the presence of free folic acid. Nuclear staining: Hoechst 33342 (blue). There was uptake observed for all types of NPs including when free folic acid was added. There was noticeable aggregation present in all images however this was most noticeable for the 3kR5% NPs. Scale bar 30 μm.
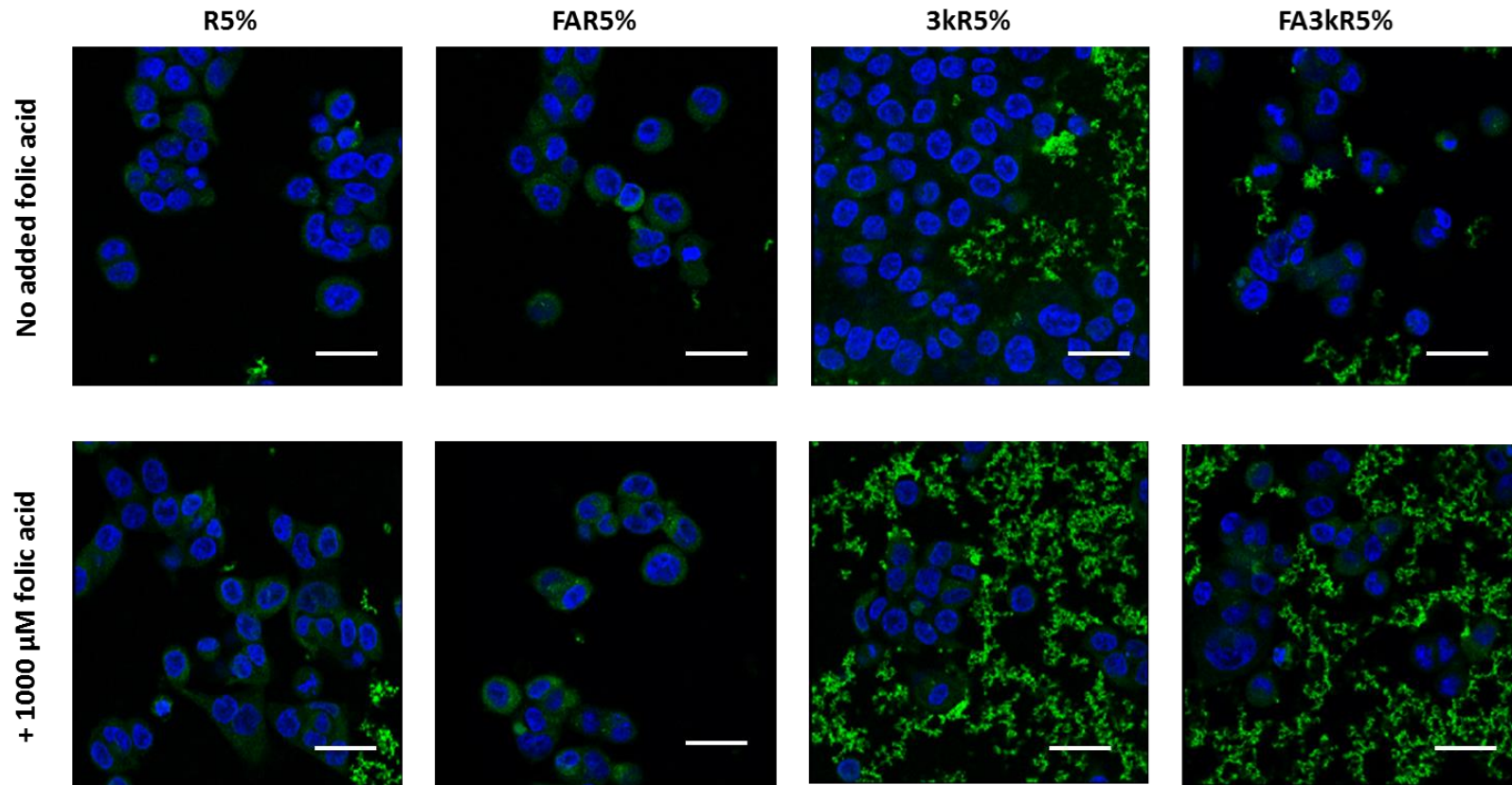
Figure 65 Confocal microscopy images of NP uptake (green) with HCT116 cells. NPs were incubated with cells for 3 h with or without the presence of free folic acid. Nuclear staining: Hoechst 33342 (blue). There was uptake observed for all types of NPs including when free folic acid was added. There was noticeable aggregation present in all images however this was most noticeable for the 3kR5% NPs. Scale bar 30 μm
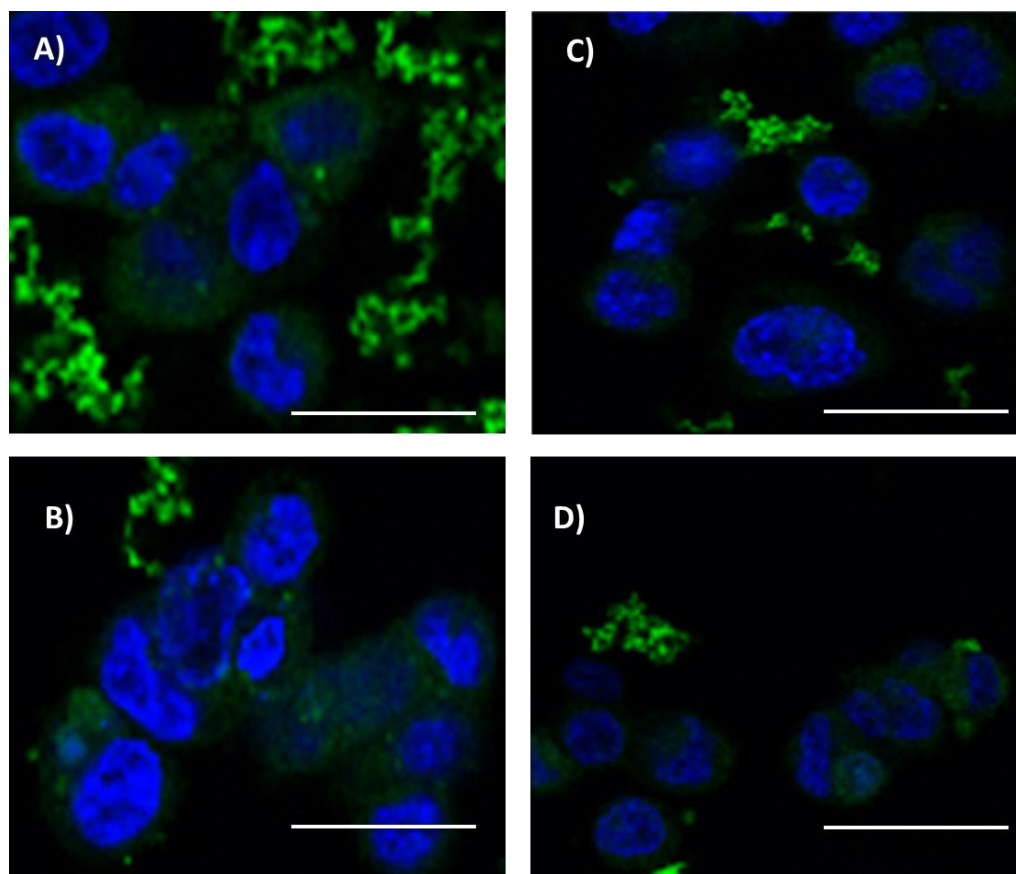
Figure 66 Zoomed confocal images of NP uptake. A) HCT116 FA3kR5% (no added FA) B) HCT116 FA3kR5% (+ 1000 µM added FA) C) MCF-7 FA3kR5% (no added FA) D) MCF-7 FA3kR5% (+ 1000 µM added FA). Sclae bar 30 µm.

The confocal images confirmed that there was NP uptake across both cell types, although the uptake differential between NPs with and without the folate tag could not be confirmed. Confocal microscopy as used here is a qualitative analytical device and not quantitative as flow cytometry is. Therefore without there being a substantial difference in the uptake, confocal microscopy can only show where the NPs are located within the cells.

Previous imaging of **P12** NPs (with no targeting ligand present) on HCT116 cells had confirmed uptake as depth profiling was carried out as shown in Figure 67. The arrows within the figure show that the NPs (green) are located within the boundaries of the membrane (red) thus proving internalisation.

The confocal images taken above were focused through the middle of the cells to ensure fluorescence noted from the NPs were those internalised within the cells.
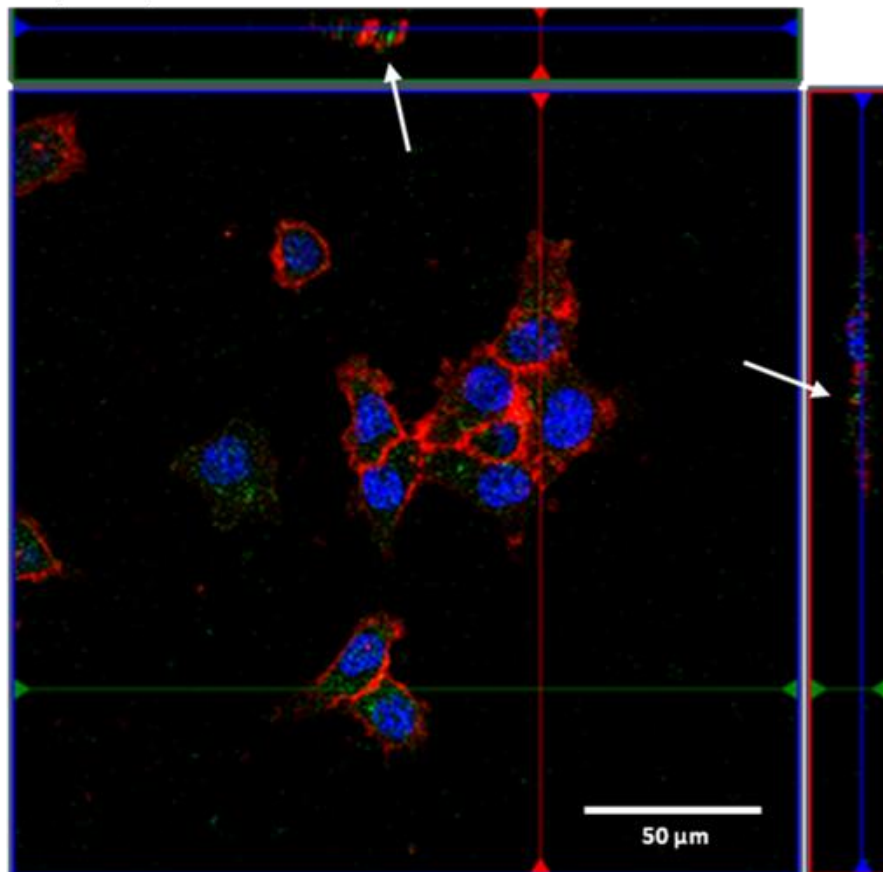
Figure 67 Orthogonal projection of a 3D image acquired of HCT116 cells treated with 250 µg/ml of P12 NPs overnight at 37°C. The arrows point at the internalization of the nanoparticles (Green) where its fluorescence can be localised within the boundaries of the red membrane. Nuclei: Blue. Scale bars represent 50 µm. Analysis performed by Luana Sasso.

What the images recorded had shown was that the NPs were being taken up and not just remaining bound to the cell membrane as is possible due to the hydrophobic interactions of NP with cell membrane.[154] With the knowledge that the NPs were definitely within the cell itself and not around it, the

differences observed in flow cytometry data can be confirmed to be differences in the NP uptake.

By taking together the confocal results with the flow cytometry data it can be concluded that when the folate targeting agent is visible to the folate receptor, NP uptake is enhanced. From the three lengths of PEG spacer chosen between the NP core and folate, NPs containing either the PEG_{450} or PEG_{3k} linked folate were suitable for targeting the folate receptor. This showed that the targeting polymer was not covered to an extent which obscured the folic acid end group upon thermoresponsive corona collapse. The NPs containing the PEG_{10k} linker showed no difference in uptake whether the folate was present or not. There are two possible reasons for this; either the folate is trapped beneath the collapsed NP corona; or the increased PEG length resulted in the hydrophobic folic acid moiety being embedded within the NP core due to hydrophobic interactions with PLA and thus not available for targeting the receptor.[142]

5.8   Conclusions

The observed uptake of thermoresponsive NPs reached their maximum uptake between 90 – 180 minutes after application of the NPs. The temperature triggered change in surface properties of the NPs did not change the extent of uptake to a significant degree compared to the inherent temperature change alone. Although this result was unexpected it was in agreement with some prior work which had shown both thermoresponsive NPs below their T_t were capable of being taken up by cells. The use of a folic

acid derivative attached via a PEG linker to the NPs when combined with the thermoresponsive polymer enhanced the uptake of the particles in MCF-7 cells. The uptake of folate targeted NPs doubled when conjugated *via* PEG_{450} and PEG_{3k} spacer compared to the non-folate targeted NPs. When a PEG_{10k} spacer was used between NP core and folate no enhancement in uptake was observed.

.

6   Summary and potential future work

The principle aim of this thesis was to develop a thermoresponsive polymer nanoparticle formulation that was capable of targeting cancer cells *in vitro*. The nanoparticle formulation was to contain a 'hide-and-reveal' motif designed to only reveal a folate targeting ligand upon heating the formulation beyond its transition temperature. The premise behind the 'hide-and-reveal' motif was to minimise off-site targeting by the folate ligand whilst maximising uptake within cancer cells which overexpress the folate receptor. The key findings of this thesis are now further discussed.

Prior to testing the combination of thermoresponsive nanoparticles and receptor targeting for enhanced uptake a polymer with a suitable transition temperature and a amphiphilic folate tagged polymer was required. The synthesis of these was discussed in Chapter 2. After problems synthesising PLGA-*b*-P(OEGMA-*stat*-PPGMA) with a sufficiently low T_t for cell testing a small library of PLA-*b*-P(DEGMA-*stat*-OEGMA) polymers were synthesised. From the library its was chosen to synthesise two PLA-*b*-P(DEGMA-*stat*-OEGMA) polymers with a DEGMA:OEGMA ratio of 95:5 and 88:12 to allow for T_t of the NPs assembled from this polymer to be above and below 37 °C. Both these types of polymers were successfully synthesised with a rhodamine tag for *in vitro* testing. In conjunction with the thermoresponsive polymer synthesis three PLA-PEG-folate polymers were synthesised with a PEG spacer of either 450 Da, 3 kDa or 10 kDa to determine whether this would have any

effect on the targeting capabilities of the NPs formed from mixtures of the PLA-PEG-folate and thermoresponsive polymer.

In Chapter 3 a method for the reproducible assembly of the PLA-*b*-P(DEGMA-*stat*-OEGMA) polymers synthesised in Chapter 1 was developed. The method was adapted from a continuous flow/microfluidic process developed within the Langer laboratory.[143] The method developed in this chapter made use of syringe pumps to provide the continuous flow and a T-junction as the mixing device thus no microfluidic chip was needed. Nanoparticles assembled using the solvent flow method offered enhanced reproducibility in size than those assembled by the solvent drop method across all the polymers tested. It was determined that the flow rate had a negligible effect on the size of NPs produced, this was most likely due to the stabilisation effect of the PEGMA chains forming the shell of the NPs. The solvent flow method offered an advantage over other nanoparticle formulation method as it was capable of assembling nanoparticles at a rate of 600 mg/h, faster than the 84 mg/h reported in literature.

In Chapter 4 possible methods of controlling the aggregation temperature of thermoresponsive nanoparticles was investigated. It was demonstrated that the transition temperature of PLA-*b*-P(DEGMA-*stat*-OEGMA) nanoparticles could be tuned by altering the ratio of DEGMA:OEGMA within the thermoresponsive corona of the NPs similar to that of P((DEGMA)-*stat*-(OEGMA)). For the first time it was shown that there was a cooperative process involved in tuning the aggregation temperature of blended polymer

NPs. The constrained nature of the mixed polymers within the NPs allows for improved control over the aggregation temperature tuning than PEGMA polymer blends.

In Chapter 5 the thermoresponsive and folate targeted nanoparticle system was tested *in vitro* using MCF-7 and HCT116 cancer cells. It was found in this chapter that although the heating of the nanoparticles past their transition temperature did not enhance the uptake, the use of folate as a targeting ligand did provide a suitable method for enhancing nanoparticle uptake. The uptake of nanoparticles was found to double when the folate tag was present compared to NPs without the tag. It was found that when the PEG_{10k} spacer was used to link the folate to the PLA core of the nanoparticle there was no enhancement in the uptake of nanoparticles.

6.1   Overall conclusion

This thesis has found that although a temperature switch did appear to show enhanced uptake of NPs it is not a simple process; there are many points to be investigated before relying on a temperature switch alone as a method of enhancing nanoparticle uptake. The findings here have shown that by blending a thermoresponsive polymer (PLA-*b*-P(DEGMA-*stat*-OEGMA) with a folate tagged amphiphilic polymer (PLA-PEG) nanoparticle uptake can be enhanced. With the 'hide-and-reveal' motif provided by this blended nanoparticle system, the temperature switch allows for the folate ligand to only be visible when within the tumour environment; thus offering an advantage over nanoparticles which have a targeting ligand always on the surface of the particle by minimising any offsite targeting and improving

pharmacokinetics. It has been shown by other groups that nanoparticles either below their transition temperature or with a hydrophilic shell do show non-specific uptake similar to the uptake of particles studied here.[34,205,207] This is a problem area which really needs further study as to the routes of uptake of these nanoparticles before any possible widespread use as a method of drug delivery.

This thesis also puts forward a new simple method for assembling polymer nanoparticles with a reproducible size and without the need for the assembly of microfluidic chips. This method would find use within the pharmaceutical industry as it is a relatively cheap method of producing nanoparticles at a higher rate than for the more conventional microfluidic chip system (600 mg/h versus 84 mg/h).

6.2   Potential future work

The following future work would support that presented within this thesis and also progress the use of these types of nanoparticles as a suitable drug delivery system for anti-cancer therapy.

- Determine whether increasing the ratio of folate tagged polymer to thermoresponsive polymer within nanoparticle system increases targeting efficiency.
- Use cells with higher folate receptor expression as the MCF-7 cell line is known to only have a low expression of the folate receptor.

- Ascertain the uptake pathway of the nanoparticles both above and below their transition temperature to determine whether the different surface properties of the particles affects their internalisation.

- Investigate whether the residency time determined in this body of work is sufficient to allow drug to be released which would be capable of causing cell death.

7   Materials and Equipment

7.1   Materials

All materials were used as delivered without any prior purification.

Sigma-Aldrich

Tetraethyleneglycol (TEG) (99%), 2-bromoisobutyryl bromide (98%), D,L-lactide, glycolide (>99%), poly(ethylene glycol) methyl ether methacrylate (OEGMA) (Average M_n ca. 188, 475 and 500), poly(propylene glycol)methacrylate (PPGMA) (Average M_n ca. 375), *N,N,N',N'',N''*-pentamethyldiethylenetriamine (PMDTA) (99%), tin (II) 2-ethylhexanoate (95%), *O*-(2-aminoethyl)-*O'*-(2-azidoethyl)nonaethylene glycol, Roswell Park Memorial Institute (RPMI) medium, 2,2'-bypridyl, DMSO-d_6 (99.9% D) and CDCl$_3$ (99.8% D).

Alfa Aesar

Copper(II) bromide (99%), copper (I) bromide (99%) and 2-butanone (99%).

Others

Amino-PEG-alkyne (Mn 3000 and 10,000 Da, Iris-Biotech GmbH)., folate free RPMI media (Gibco). Cell culture flasks and plates (Corning). 8 well chamber slides (Lab-Tek II, Thermo Scientific), PD-10 desalting columns (GE healthcare) 2-(2-(2-azidoethoxy)ethoxy) ethanol was provided by Dr. Johannes Magnusson.

Statistical analysis and graph plotting was carried out using Graphpad Prism 6 software.

7.2   Gel permeation chromatography

GPC was performed on a Polymer Laboratories GPC 50 system equipped with a refractive index detector. Separations were achieved with a pair of PLgel Mixed-D (5 µm bead, 7.8 × 300 mm) columns with a matching guard (7.8 × 50 mm) and chloroform as eluent at a flow rate of 1 mL min^{-1}. Calibration was performed using narrow polystyrene standards (Polymer Labs) in the molecular weight range 0.13-210 kDa. Molecular weights and dispersity values were calculated using Cirrus GPC 3.0 software. All samples were dissolved in chloroform prior to analysis.

7.3   High performance liquid chromatography (HPLC)

HPLC was performed on a Shimadzu HPLC (LC-20AD pump) equipped with a C18 column (Jupiter, 5 µm, 250 x 46 mm, Phenomenex), SPD-M20A UV detector and SIL-20A autosampler. Mobile phase was water (A) and acetonitrile (B). Method: 10 – 20 % B over 17 minutes, UV detection at 363 nm.

7.4   Dynamic light scattering (DLS)

DLS measurements were carried out on Viscotek Model 802 instrument with an internal laser (825-832 nm). Samples were taken from nanoparticle suspension in ultrapure water or PBS and at least 7 measurements were taken. Results were processed using OmniSize version 3.0. DLS is a non-invasive technique used to measure the size of particles within a suspension. The diffusion coefficients of the particles are measured as they undergo random Brownian motion within the suspension. The measured diffusion

coefficients can then be converted to the hydrodynamic sizes by the Stokes-Einstein equation:

$$d(H) = \frac{kT}{3\pi\eta D}$$

Where d(H) = hydrodynamic diameter, k = Boltzmann's constant, T = absolute temperature, η = viscosity and D = translational diffusion coefficient.

7.5 Cloud point determination

Samples were analysed using Beckmann Coulter UV-vis spectrophotometer at 550 nm and 750 nm. Sample concentration was kept constant for each sample and temperature ramped at 0.5 °C min^{-1} while being measured every 0.5 °C increase. Absorbance/optical density (A) could be converted to transmittance (%T) using the following formula:

$$A = 2 - log_{10} \%T$$

7.6 Nuclear magnetic resonance (NMR)

NMR spectra were obtained from a Bruker 400 Ultrashield at 400MHz and 25 °C. Each spectrum was analysed using MestReNova v6.0.2.

7.7 Mass spectrometry

High resolution mass spectra (**HRMS**) – time of flight electrospray (TOF ES +/-) were recorded on a Waters 2795 separation module micromass LCT platform. Samples were prepared in a 1:1 mixture of acetonitrile: water containing 0.1% formic acid.

7.8   Flow cytometry

Flow cytometry measurements were made on a Beckman Coulter MoFlo Astrios flow cytometer. Samples were analysed using green laser (λ_{ex} 561 nm, λ_{em} 620 nm). All analysis was carried out using Kaluza analysis software v1.3.

7.9   Transmission electron microscopy (TEM)

5 μL of dilute NP suspensions were mixed with 5 μL 3% phosphotungstic acid and placed on Formvar® coated 3 mm 75 mesh copper TEM plate for 5 minutes, any excess liquid was wicked off using filter paper. TEM images were obtained using a FEI Technai 12, Biotwin microscope.

8   References

(1)   Allen, T. M.; Cullis, P. R. *Science* **2004**, *303*, 1818.

(2)   Cho, K.; Wang, X.; Nie, S.; Chen, Z.; Shin, D. M. *Clinical Cancer Research* **2008**, *14*, 1310.

(3)   Maeda, H.; Wu, J.; Sawa, T.; Matsumura, Y.; Hori, K. *Journal of Controlled Release* **2000**, *65*, 271.

(4)   Li, S.-D.; Huang, L. *Molecular Pharmaceutics* **2008**, *5*, 496.

(5)   Moghimi, S. M.; Hunter, A. C.; Murray, J. C. *Pharmacological Reviews* **2001**, *53*, 283.

(6)   Fang, J.; Nakamura, H.; Maeda, H. *Advanced Drug Delivery Reviews* **2011**, *63*, 136.

(7)   Maeda, H.; Matsumura, Y.; Kato, H. *Journal of Biological Chemistry* **1988**, *263*, 16051.

(8)   Matsumura, Y.; Kimura, M.; Yamamoto, T.; Maeda, H. *Japanese Journal of Cancer Research* **1988**, *79*, 1327.

(9)   Leung, D. W.; Cachianes, G.; Kuang, W. J.; Goeddel, D. V.; Ferrara, N. *Science* **1989**, *246*, 1306.

(10)   http://www.nobelprize.org/nobel_prizes/medicine/laureates/1908/ehrlich-bio.html 2015.

(11)   Alexis, F.; Pridgen, E.; Molnar, L. K.; Farokhzad, O. C. *Molecular Pharmaceutics* **2008**, *5*, 505.

(12)   Byrne, J. D.; Betancourt, T.; Brannon-Peppas, L. *Advanced Drug Delivery Reviews* **2008**, *60*, 1615.

(13)   Leamon, C. P.; Low, P. S. *Proceedings of the National Academy of Sciences* **1991**, *88*, 5572.

(14)   Saeed, A. O.; Magnusson, J. P.; Moradi, E.; Soliman, M.; Wang, W.; Stolnik, S.; Thurecht, K. J.; Howdle, S. M.; Alexander, C. *Bioconjugate Chemistry* **2011**, *22*, 156.

(15)   Ji, J.; Wu, D.; Liu, L.; Chen, J.; Xu, Y. *Journal of Applied Polymer Science* **2012**, *125*, E208.

(16)   Majoros, I. J.; Myc, A.; Thomas, T.; Mehta, C. B.; Baker, J. R. *Biomacromolecules* **2006**, *7*, 572.

(17)   Prabaharan, M.; Grailer, J. J.; Pilla, S.; Steeber, D. A.; Gong, S. *Biomaterials* **2009**, *30*, 3009.

(18)   Guo, M.; Que, C.; Wang, C.; Liu, X.; Yan, H.; Liu, K. *Biomaterials* **2011**, *32*, 185.

(19)   Pan, D.; Turner, J. L.; Wooley, K. L. *Chemical Communications* **2003**, 2400.

(20)   Connor, E. E.; Mwamuka, J.; Gole, A.; Murphy, C. J.; Wyatt, M. D. *Small* **2005**, *1*, 325.

(21)   Arnida; Malugin, A.; Ghandehari, H. *Journal of Applied Toxicology* **2010**, *30*, 212.

(22)   Daniel, M.-C.; Astruc, D. *Chemical Reviews* **2003**, *104*, 293.

(23) Hostetler, M. J.; Wingate, J. E.; Zhong, C. J.; Harris, J. E.; Vachet, R. W.; Clark, M. R.; Londono, J. D.; Green, S. J.; Stokes, J. J.; Wignall, G. D.; Glish, G. L.; Porter, M. D.; Evans, N. D.; Murray, R. W. *Langmuir* **1998**, *14*, 17.

(24) Arnida; Janát-Amsbury, M. M.; Ray, A.; Peterson, C. M.; Ghandehari, H. *European Journal of Pharmaceutics and Biopharmaceutics* **2011**, *77*, 417.

(25) Huang, X.; Jain, P. K.; El-Sayed, I. H.; El-Sayed, M. A. *Nanomedicine* **2007**, *2*, 681.

(26) Dickerson, E. B.; Dreaden, E. C.; Huang, X.; El-Sayed, I. H.; Chu, H.; Pushpanketh, S.; McDonald, J. F.; El-Sayed, M. A. *Cancer Letters* **2008**, *269*, 57.

(27) Jin, H.; Yang, P.; Cai, J.; Wang, J.; Liu, M. *Applied Microbiology and Biotechnology* **2012**, *94*, 1199.

(28) Rengan, A. K.; Bukhari, A. B.; Pradhan, A.; Malhotra, R.; Banerjee, R.; Srivastava, R.; De, A. *Nano Letters* **2015**, *15*, 842.

(29) Wang, S.; Teng, Z.; Huang, P.; Liu, D.; Liu, Y.; Tian, Y.; Sun, J.; Li, Y.; Ju, H.; Chen, X.; Lu, G. *Small* **2015**, *11*, 1738.

(30) Zhu, M.-Q.; Wang, L.-Q.; Exarhos, G. J.; Li, A. D. Q. *Journal of the American Chemical Society* **2004**, *126*, 2656.

(31) Kim, D.; Park, S.; Jae, H. L.; Yong, Y. J.; Jon, S. *Journal of the American Chemical Society* **2007**, *129*, 7661.

(32) Fustin, C.-A.; Colard, C.; Filali, M.; Guillet, P.; Duwez, A.-S.; Meier, M. A. R.; Schubert, U. S.; Gohy, J.-F. *Langmuir* **2006**, *22*, 6690.

(33) Du, B.; Zhao, B.; Tao, P.; Yin, K.; Lei, P.; Wang, Q. *Colloids and Surfaces A: Physicochemical and Engineering Aspects* **2008**, *317*, 194.

(34) Barhoumi, A.; Wang, W.; Zurakowski, D.; Langer, R. S.; Kohane, D. S. *Nano Letters* **2014**.

(35) Lee, P.-W.; Hsu, S.-H.; Wang, J.-J.; Tsai, J.-S.; Lin, K.-J.; Wey, S.-P.; Chen, F.-R.; Lai, C.-H.; Yen, T.-C.; Sung, H.-W. *Biomaterials* **2010**, *31*, 1316.

(36) Gautier, J.; Munnier, E.; Paillard, A.; Hervé, K.; Douziech-Eyrolles, L.; Soucé, M.; Dubois, P.; Chourpa, I. *International Journal of Pharmaceutics* **2012**, *423*, 16.

(37) Ito, A.; Shinkai, M.; Honda, H.; Kobayashi, T. *Journal of Bioscience and Bioengineering* **2005**, *100*, 1.

(38) Kievit, F. M.; Wang, F. Y.; Fang, C.; Mok, H.; Wang, K.; Silber, J. R.; Ellenbogen, R. G.; Zhang, M. *Journal of Controlled Release* **2011**, *152*, 76.

(39) Huang, C.; Tang, Z.; Zhou, Y.; Zhou, X.; Jin, Y.; Li, D.; Yang, Y.; Zhou, S. *International Journal of Pharmaceutics* **2012**, *429*, 113.

(40) Wadajkar, A. S.; Bhavsar, Z.; Ko, C.-Y.; Koppolu, B.; Cui, W.; Tang, L.; Nguyen, K. T. *Acta Biomaterialia* **2012**, *8*, 2996.

(41) Koppolu, B.; Rahimi, M.; Nattama, S.; Wadajkar, A.; Nguyen, K. T. *Nanomedicine : nanotechnology, biology, and medicine* **2010**, *6*, 355.

(42) Bütün, V.; Billingham, N. C.; Armes, S. P. *Chemical Communications* **1997**, 671.

(43) Mitsukami, Y.; Donovan, M. S.; Lowe, A. B.; McCormick, C. L. *Macromolecules* **2001**, *34*, 2248.

(44) Koňák, Č.; Helmstedt, M. *Macromolecules* **2001**, *34*, 6131.

(45)   Imae, T.; Tabuchi, H.; Funayama, K.; Sato, A.; Nakamura, T.; Amaya, N. *Colloids and Surfaces A: Physicochemical and Engineering Aspects* **2000**, *167*, 73.

(46)   Sakuma, S.; Suita, M.; Yamamoto, T.; Masaoka, Y.; Kataoka, M.; Yamashita, S.; Nakajima, N.; Shinkai, N.; Yamauchi, H.; Hiwatari, K.-i.; Hashizume, A.; Tachikawa, H.; Kimura, R.; Ishimaru, Y.; Kasai, A.; Maeda, S. *European Journal of Pharmaceutics and Biopharmaceutics* **2012**, *81*, 64.

(47)   Hoffman, A. S. *Clinical Chemistry* **2000**, *46*, 1478.

(48)   McDaniel, J. R.; MacEwan, S. R.; Li, X.; Radford, D. C.; Landon, C. D.; Dewhirst, M.; Chilkoti, A. *Nano Letters* **2014**.

(49)   Abulateefeh, S. R.; Spain, S. G.; Thurecht, K. J.; Aylott, J. W.; Chan, W. C.; Garnett, M. C.; Alexander, C. *Biomaterials Science* **2013**.

(50)   Fujishige, S.; Kubota, K.; Ando, I. *The Journal of Physical Chemistry* **1989**, *93*, 3311.

(51)   Pelton, R. *Advances in Colloid and Interface Science* **2000**, *85*, 1.

(52)   Gil, E. S.; Hudson, S. M. *Progress in Polymer Science* **2004**, *29*, 1173.

(53)   Kotsuchibashi, Y.; Ebara, M.; Idota, N.; Narain, R.; Aoyagi, T. *Polymer Chemistry* **2012**, *3*, 1150.

(54)   Li, G.; Guo, L.; Meng, Y.; Zhang, T. *Chemical Engineering Journal* **2011**, *174*, 199.

(55)   Vihola, H.; Laukkanen, A.; Valtola, L.; Tenhu, H.; Hirvonen, J. *Biomaterials* **2005**, *26*, 3055.

(56)   Kujawa, P.; Segui, F.; Shaban, S.; Diab, C.; Okada, Y.; Tanaka, F.; Winnik, F. M. *Macromolecules* **2006**, *39*, 341.

(57)   Wang, X.; Qiu, X.; Wu, C. *Macromolecules* **1998**, *31*, 2972.

(58)   Wei, Z.; Yu, Q.; Gan, Z. *Macromolecular Research* **2012**, *20*, 313.

(59)   Dimitrov, I.; Trzebicka, B.; Müller, A. H. E.; Dworak, A.; Tsvetanov, C. B. *Progress in Polymer Science* **2007**, *32*, 1275.

(60)   Lutz, J.-F.; Akdemir, Ö.; Hoth, A. *Journal of the American Chemical Society* **2006**, *128*, 13046.

(61)   Özgür, A.; Nezha, B.; Sebastian, P.; Zoya, Z.; André, L.; Erik, W.; Jean-François, L. In *Controlled/Living Radical Polymerization: Progress in ATRP*; American Chemical Society: 2009; Vol. 1023, p 189.

(62)   Lu, Y.; Zhou, K.; Ding, Y.; Zhang, G.; Wu, C. *Physical Chemistry Chemical Physics* **2010**, *12*, 3188.

(63)   Lutz, J.-F. *Advanced Materials* **2011**, *23*, 2237.

(64)   Gao, X.; Kučerka, N.; Nieh, M.-P.; Katsaras, J.; Zhu, S.; Brash, J. L.; Sheardown, H. *Langmuir* **2009**, *25*, 10271.

(65)   Hyun, J.; Ma, H.; Zhang, Z.; Beebe Jr, T. P.; Chilkoti, A. *Advanced Materials* **2003**, *15*, 576.

(66)   Ma, H.; Hyun, J.; Stiller, P.; Chilkoti, A. *Advanced Materials* **2004**, *16*, 338.

(67)   Lee, H.-i.; Ah Lee, J.; Poon, Z.; Hammond, P. T. *Chemical Communications* **2008**, 3726.

(68)   Pasparakis, G.; Alexander, C. *Angewandte Chemie International Edition* **2008**, *47*, 4847.

(69)   Leung, M. K. M.; Such, G. K.; Johnston, A. P. R.; Biswas, D. P.; Zhu, Z.; Yan, Y.; Lutz, J.-F.; Caruso, F. *Small* **2011**, *7*, 1075.

(70)   Knop, K.; Pretzel, D.; Urbanek, A.; Rudolph, T.; Scharf, D. H.; Schallon, A.; Wagner, M.; Schubert, S.; Kiehntopf, M.; Brakhage, A. A.; Schacher, F. H.; Schubert, U. S. *Biomacromolecules* **2013**, *14*, 2536.

(71)   Ulasan, M.; Yavuz, E.; Bagriacik, E. U.; Cengeloglu, Y.; Yavuz, M. S. *Journal of Biomedical Materials Research Part A* **2015**, *103*, 243.

(72)   Stubbs, M.; McSheehy, P. M. J.; Griffiths, J. R.; Bashford, C. L. *Molecular medicine today* **2000**, *6*, 15.

(73)   Ojugo, A. S. E.; McSheehy, P. M. J.; Stubbs, M.; Alder, G.; Bashford, C. L.; Maxwell, R. J.; Leach, M. O.; Judson, I. R.; Griffiths, J. R. *Br J Cancer* **1998**, *77*, 873.

(74)   Jones, D. P.; Carlson, J. L.; Samiec, P. S.; Sternberg Jr, P.; Mody Jr, V. C.; Reed, R. L.; Brown, L. A. S. *Clinica Chimica Acta* **1998**, *275*, 175.

(75)   Chan, Y.; Wong, T.; Byrne, F.; Kavallaris, M.; Bulmus, V. *Biomacromolecules* **2008**, *9*, 1826.

(76)   Jackson, A. W.; Fulton, D. A. *Macromolecules* **2012**, *45*, 2699.

(77)   Guo, Q.; Luo, P.; Luo, Y.; Du, F.; Lu, W.; Liu, S.; Huang, J.; Yu, J. *Colloids and Surfaces B: Biointerfaces* **2012**, *100*, 138.

(78)   Jiang, X.; Li, L.; Liu, J.; Hennink, W. E.; Zhuo, R. *Macromolecular Bioscience* **2012**, *12*, 703.

(79)   Cui, Y.; Dong, H.; Cai, X.; Wang, D.; Li, Y. *ACS Applied Materials & Interfaces* **2012**, *4*, 3177.

(80)   Sun, H.; Guo, B.; Cheng, R.; Meng, F.; Liu, H.; Zhong, Z. *Journal of Controlled Release* **2011**, *152, Supplement 1*, e84.

(81)   Burdick, M. M.; Chu, J. T.; Godar, S.; Sackstein, R. *Journal of Biological Chemistry* **2006**, *281*, 13899.

(82)   Lapčík, L.; De Smedt, S.; Demeester, J.; Chabreček, P. *Chemical Reviews* **1998**, *98*, 2663.

(83)   Luo, Y.; Prestwich, G. D. *Bioconjugate Chemistry* **1999**, *10*, 755.

(84)   Moriyama, K.; Ooya, T.; Yui, N. *Journal of Controlled Release* **1999**, *59*, 77.

(85)   Avila, L. Z.; Gianolio, D. A.; Konowicz, P. A.; Philbrook, M.; Santos, M. R.; Miller, R. J. In *Carbohydrate Chemistry, Biology and Medical Applications*; Hari, G. G., Mary, K. C., Charles A. HalesA2 - Hari G. Garg, M. K. C., Charles, A. H., Eds.; Elsevier: Oxford, 2008, p 333.

(86)   Jeong, Y.-I.; Kim, D. H.; Chung, C.-W.; Yoo, J. J.; Choi, K. H.; Kim, C. H.; Ha, S. H.; Kang, D. H. *Colloids and Surfaces B: Biointerfaces* **2012**, *90*, 28.

(87)   Gaumet, M.; Vargas, A.; Gurny, R.; Delie, F. *European Journal of Pharmaceutics and Biopharmaceutics* **2008**, *69*, 1.

(88)   Brattain, M. G.; Fine, W. D.; Khaled, F. M.; Thompson, J.; Brattain, D. E. *Cancer Research* **1981**, *41*, 1751.

(89)   Choi, K. Y.; Jeon, E. J.; Yoon, H. Y.; Lee, B. S.; Na, J. H.; Min, K. H.; Kim, S. Y.; Myung, S.-J.; Lee, S.; Chen, X.; Kwon, I. C.; Choi, K.; Jeong, S. Y.; Kim, K.; Park, J. H. *Biomaterials* **2012**, *33*, 6186.

(90)   Choi, K. Y.; Min, K. H.; Na, J. H.; Choi, K.; Kim, K.; Park, J. H.; Kwon, I. C.; Jeong, S. Y. *Journal of Materials Chemistry* **2009**, *19*, 4102.

(91)   Choi, K. Y.; Chung, H.; Min, K. H.; Yoon, H. Y.; Kim, K.; Park, J. H.; Kwon, I. C.; Jeong, S. Y. *Biomaterials* **2010**, *31*, 106.

(92)   Rembacken, B. J.; Fujii, T.; Cairns, A.; Dixon, M. F.; Yoshida, S.; Chalmers, D. M.; Axon, A. T. R. *The Lancet* **2000**, *355*, 1211.

(93)   Hegde, S. R.; Sun, W.; Lynch, J. P. *Expert Review of Gastroenterology & Hepatology* **2008**, *2*, 135.

(94)   Kamen, B. A.; Capdevila, A. *Proceedings of the National Academy of Sciences* **1986**, *83*, 5983.

(95)   Leamon, C. P.; Reddy, J. A. *Advanced Drug Delivery Reviews* **2004**, *56*, 1127.

(96)   Campbell, I. G.; Jones, T. A.; Foulkes, W. D.; Trowsdale, J. *Cancer Research* **1991**, *51*, 5329.

(97)   Konda, S. D.; Aref, M.; Brechbiel, M.; Wiener, E. C. *Investigative Radiology* **2000**, *35*, 50.

(98)   Lee, J. W.; Lu, J. Y.; Low, P. S.; Fuchs, P. L. *Bioorganic & Medicinal Chemistry* **2002**, *10*, 2397.

(99)   Rui, Y.; Wang, S.; Low, P. S.; Thompson, D. H. *Journal of the American Chemical Society* **1998**, *120*, 11213.

(100)   Zhao, P.; Wang, H.; Yu, M.; Liao, Z.; Wang, X.; Zhang, F.; Ji, W.; Wu, B.; Han, J.; Zhang, H.; Wang, H.; Chang, J.; Niu, R. *European Journal of Pharmaceutics and Biopharmaceutics* **2012**, *81*, 248.

(101)   Shen, M.; Huang, Y.; Han, L.; Qin, J.; Fang, X.; Wang, J.; Yang, V. C. *Journal of Controlled Release* **2012**, *161*, 884.

(102)   Li, X.; Zhou, H.; Yang, L.; Du, G.; Pai-Panandiker, A. S.; Huang, X.; Yan, B. *Biomaterials* **2011**, *32*, 2540.

(103)   Bhattacharyya, S.; Khan, J. A.; Curran, G. L.; Robertson, J. D.; Bhattacharya, R.; Mukherjee, P. *Advanced Materials* **2011**, *23*, 5034.

(104)   Pillai, G. *SOJ Pharm Pharm Sci* **2014**, *1*, 1.

(105)   La-Beck, N.; Zamboni, B.; Gabizon, A.; Schmeeda, H.; Amantea, M.; Gehrig, P.; Zamboni, W. *Cancer Chemother Pharmacol* **2012**, *69*, 43.

(106)   Needham, D. In *Biomaterials for Cancer Therapeutics*; Park, K., Ed.; Woodhead Publishing: 2013, p 270.

(107)   Hrkach, J.; Von Hoff, D.; Ali, M. M.; Andrianova, E.; Auer, J.; Campbell, T.; De Witt, D.; Figa, M.; Figueiredo, M.; Horhota, A.; Low, S.; McDonnell, K.; Peeke, E.; Retnarajan, B.; Sabnis, A.; Schnipper, E.; Song, J. J.; Song, Y. H.; Summa, J.; Tompsett, D.; Troiano, G.; Van Geen Hoven, T.; Wright, J.; LoRusso, P.; Kantoff, P. W.; Bander, N. H.; Sweeney, C.; Farokhzad, O. C.; Langer, R.; Zale, S. *Science Translational Medicine* **2012**, *4*, 128ra39.

(108)   Rajasekaran, A. K.; Anilkumar, G.; Christiansen, J. J. *American Journal of Physiology - Cell Physiology* **2005**, *288*, C975.

(109)   http://bindtherapeutics.com/pipeline/BIND014.html September 2015.

(110)   Wang, A. Z.; Langer, R.; Farokhzad, O. C. *Annual Review of Medicine* **2012**, *63*, 185.

(111)   Bian, Q.; Xiao, Y.; Lang, M. *Polymer* **2012**, *53*, 1684.

(112) Summers, M. J.; Phillips, D. J.; Gibson, M. I. *Chemical Communications* **2013**.

(113) Gao, Y.; Zhao, T.; Wang, W. *RSC Advances* **2014**, *4*, 61687.

(114) Weiss, J.; Laschewsky, A. *Macromolecules* **2012**, *45*, 4158.

(115) www.sciencedirect.com 2015.

(116) Degée, P.; Dubois, P.; Jérǒme, R.; Jacobsen, S.; Fritz, H.-G. *Macromolecular Symposia* **1999**, *144*, 289.

(117) Kricheldorf, H. R.; Kreiser-Saunders, I.; Boettcher, C. *Polymer* **1995**, *36*, 1253.

(118) Kricheldorf, H. R. *Macromolecular Symposia* **2000**, *153*, 55.

(119) Ryner, M.; Stridsberg, K.; Albertsson, A.-C.; von Schenck, H.; Svensson, M. *Macromolecules* **2001**, *34*, 3877.

(120) Ravazzolo, E.; Salmaso, S.; Mastrotto, F.; Bersani, S.; Gallon, E.; Caliceti, P. *European Journal of Pharmaceutics and Biopharmaceutics* **2013**, *83*, 346.

(121) Majewski, A. P.; Schallon, A.; Jérôme, V.; Freitag, R.; Müller, A. H. E.; Schmalz, H. *Biomacromolecules* **2012**, *13*, 857.

(122) Kipping, M.; Krahl, F.; Döring, A.; Adler, H.-J. P.; Kuckling, D. *European Polymer Journal* **2010**, *46*, 313.

(123) Zhu, B.; Lu, D.; Ge, J.; Liu, Z. *Acta Biomaterialia* **2011**, *7*, 2131.

(124) Tian, K.; Zeng, J.; Zhao, X.; Liu, L.; Jia, X.; Liu, P. *Colloids and Surfaces B: Biointerfaces* **2015**, *134*, 188.

(125) Jakubowski, W.; Matyjaszewski, K. *Macromolecules* **2005**, *38*, 4139.

(126) Danhier, F.; Ansorena, E.; Silva, J. M.; Coco, R.; Le Breton, A.; Préat, V. *Journal of Controlled Release* **2012**, *161*, 505.

(127) Abulateefeh, S. R.; Saeed, A. O.; Aylott, J. W.; Chan, W. C.; Garnett, M. C.; Saunders, B. R.; Alexander, C. *Chemical Communications* **2009**, 6068.

(128) Kamber, N. E.; Jeong, W.; Waymouth, R. M.; Pratt, R. C.; Lohmeijer, B. G. G.; Hedrick, J. L. *Chemical Reviews* **2007**, *107*, 5813.

(129) Pratt, R. C.; Lohmeijer, B. G. G.; Long, D. A.; Waymouth, R. M.; Hedrick, J. L. *Journal of the American Chemical Society* **2006**, *128*, 4556.

(130) Chuma, A.; Horn, H. W.; Swope, W. C.; Pratt, R. C.; Zhang, L.; Lohmeijer, B. G. G.; Wade, C. G.; Waymouth, R. M.; Hedrick, J. L.; Rice, J. E. *Journal of the American Chemical Society* **2008**, *130*, 6749.

(131) Pratt, R. C.; Lohmeijer, B. G. G.; Long, D. A.; Lundberg, P. N. P.; Dove, A. P.; Li, H.; Wade, C. G.; Waymouth, R. M.; Hedrick, J. L. *Macromolecules* **2006**, *39*, 7863.

(132) Pounder, R. J.; Dove, A. P. *Biomacromolecules* **2010**, *11*, 1930.

(133) Magnusson, J. P.; Khan, A.; Pasparakis, G.; Saeed, A. O.; Wang, W.; Alexander, C. *Journal of the American Chemical Society* **2008**, *130*, 10852.

(134) Du, H.; Wickramasinghe, R.; Qian, X. *The Journal of Physical Chemistry B* **2010**, *114*, 16594.

(135) Cowie, J. M. G.; Arrighi, V. *Polymers : chemistry and physics of modern materials / J.M.G. Cowie, Valeria Arrighi*; CRC Press: Boca Raton, FL, 2008.

(136)   Fessi, H.; Puisieux, F.; Devissaguet, J. P.; Ammoury, N.; Benita, S. *International Journal of Pharmaceutics* **1989**, *55*, R1.

(137)   Govender, T.; Stolnik, S.; Garnett, M. C.; Illum, L.; Davis, S. S. *Journal of Controlled Release* **1999**, *57*, 171.

(138)   Yen, B. K. H.; Stott, N. E.; Jensen, K. F.; Bawendi, M. G. *Advanced Materials* **2003**, *15*, 1858.

(139)   *Lab on a Chip* **2004**, *4*, 11N.

(140)   Shestopalov, I.; Tice, J. D.; Ismagilov, R. F. *Lab on a Chip* **2004**, *4*, 316.

(141)   Karnik, R.; Gu, F.; Basto, P.; Cannizzaro, C.; Dean, L.; Kyei-Manu, W.; Langer, R.; Farokhzad, O. C. *Nano Letters* **2008**, *8*, 2906.

(142)   Valencia, P. M.; Hanewich-Hollatz, M. H.; Gao, W.; Karim, F.; Langer, R.; Karnik, R.; Farokhzad, O. C. *Biomaterials* **2011**, *32*, 6226.

(143)   Valencia, P. M.; Pridgen, E. M.; Rhee, M.; Langer, R.; Farokhzad, O. C.; Karnik, R. *ACS Nano* **2013**, *7*, 10671.

(144)   Lim, J.-M.; Bertrand, N.; Valencia, P. M.; Rhee, M.; Langer, R.; Jon, S.; Farokhzad, O. C.; Karnik, R. *Nanomedicine: Nanotechnology, Biology and Medicine* **2014**, *10*, 401.

(145)   Jain, A. K.; Goyal, A. K.; Gupta, P. N.; Khatri, K.; Mishra, N.; Mehta, A.; Mangal, S.; Vyas, S. P. *Journal of Controlled Release* **2009**, *136*, 161.

(146)   Gref, R.; Lück, M.; Quellec, P.; Marchand, M.; Dellacherie, E.; Harnisch, S.; Blunk, T.; Müller, R. H. *Colloids and Surfaces B: Biointerfaces* **2000**, *18*, 301.

(147)   Bazile, D. *J. Pharm. Sci.* **1995**, *84*, 493.

(148)   Owens, D. E.; Peppas, N. A. *Int. J. Pharm.* **2006**, *307*, 93.

(149)   Peracchia, M. T. *Biomaterials* **1999**, *20*, 1269.

(150)   Gref, R.; Minamitake, Y.; Peracchia, M.; Trubetskoy, V.; Torchilin, V.; Langer, R. *Science* **1994**, *263*, 1600.

(151)   Moghimi, S. M.; Hedeman, H.; Muir, I. S.; Illum, L.; Davis, S. S. *Biochim Biophys Acta* **1993**, *1157*, 233.

(152)   Porter, C. J. H.; Moghimi, S. M.; Illum, L.; Davis, S. S. *FEBS Letters* **1992**, *305*, 62.

(153)   Whitesides, G. M. *Nature* **2006**, *442*, 368.

(154)   Maeda, H.; Nakamura, H.; Fang, J. *Advanced Drug Delivery Reviews* **2013**, *65*, 71.

(155)   Sirsi, S. R.; Hernandez, S. L.; Zielinski, L.; Blomback, H.; Koubaa, A.; Synder, M.; Homma, S.; Kandel, J. J.; Yamashiro, D. J.; Borden, M. A. *Journal of Controlled Release* **2012**, *157*, 224.

(156)   Park, H.; Yang, J.; Lee, J.; Haam, S.; Choi, I.-H.; Yoo, K.-H. *ACS Nano* **2009**, *3*, 2919.

(157)   Lin, L. Y.; Lee, N. S.; Zhu, J.; Nyström, A. M.; Pochan, D. J.; Dorshow, R. B.; Wooley, K. L. *Journal of Controlled Release* **2011**, *152*, 37.

(158)   http://www.cancerresearchuk.org/about-cancer/cancers-in-general/treatment/cancer-drugs/doxorubicin 2015.

(159)   Kamimura, M.; Furukawa, T.; Akiyama, S.-i.; Nagasaki, Y. *Biomaterials Science* **2013**.

(160)   Zhang, C. Y.; Yang, Y. Q.; Huang, T. X.; Zhao, B.; Guo, X. D.; Wang, J. F.; Zhang, L. J. *Biomaterials* **2012**, *33*, 6273.

(161)   Li, W.; Li, J.; Gao, J.; Li, B.; Xia, Y.; Meng, Y.; Yu, Y.; Chen, H.; Dai, J.; Wang, H.; Guo, Y. *Biomaterials* **2011**, *32*, 3832.

(162)   Gibson, M. I.; O'Reilly, R. K. *Chemical Society Reviews* **2013**, *42*, 7204.

(163)   Phillips, D. J.; Patterson, J. P.; O'Reilly, R. K.; Gibson, M. I. *Polymer Chemistry* **2014**, *5*, 126.

(164)   Wang, H.; Yang, J.; Li, Y.; Sun, L.; Liu, W. *Journal of Materials Chemistry B* **2013**.

(165)   Cheng, R.; Meng, F.; Deng, C.; Klok, H.-A.; Zhong, Z. *Biomaterials* **2013**, *34*, 3647.

(166)   Louguet, S.; Rousseau, B.; Epherre, R.; Guidolin, N.; Goglio, G.; Mornet, S.; Duguet, E.; Lecommandoux, S.; Schatz, C. *Polymer Chemistry* **2012**, *3*, 1408.

(167)   Elsabahy, M.; Wooley, K. L. *Chemical Society Reviews* **2012**, *41*, 2545.

(168)   Mastrotto, F.; Caliceti, P.; Amendola, V.; Bersani, S.; Magnusson, J. P.; Meneghetti, M.; Mantovani, G.; Alexander, C.; Salmaso, S. *Chemical Communications* **2011**, *47*, 9846.

(169)   Ringsdorf, H.; Simon, J.; Winnik, F. M. *MACROMOLECULES* **1992**, *25*, 7306.

(170)   Rebelo, L. P. N.; Visak, Z. P.; De Sousa, H. C.; Szydlowski, J.; De Azevedo, R. G.; Ramos, A. M.; Najdanovic-Visak, V.; Da Ponte, M. N.; Klein, J. *MACROMOLECULES* **2002**, *35*, 1887.

(171)   Monopoli, M. P.; Aberg, C.; Salvati, A.; Dawson, K. A. *Nature Nanotechnology* **2012**, *7*, 779.

(172)   Hassouneh, W.; Fischer, K.; MacEwan, S. R.; Branscheid, R.; Fu, C. L.; Liu, R.; Schmidt, M.; Chilkoti, A. *Biomacromolecules* **2012**, *13*, 1598.

(173)   McDaniel, J. R.; MacEwan, S. R.; Dewhirst, M.; Chilkoti, A. *Journal of Controlled Release* **2012**, *159*, 362.

(174)   Fernandez-Trillo, F.; van Hest, J. C. M.; Thies, J. C.; Michon, T.; Weberskirch, R.; Cameron, N. R. *Chemical Communications* **2008**, 2230.

(175)   Fernandez-Trillo, F.; Dureault, A.; Bayley, J. P. M.; van Hest, J. C. M.; Thies, J. C.; Michon, T.; Weberskirch, R.; Cameron, N. R. *Macromolecules* **2007**, *40*, 6094.

(176)   Buller, J.; Laschewsky, A.; Lutz, J.-F.; Wischerhoff, E. *Polymer Chemistry* **2011**, *2*, 1486.

(177)   Ieong, N. S.; Hasan, M.; Phillips, D. J.; Saaka, Y.; O'Reilly, R. K.; Gibson, M. I. *Polymer Chemistry* **2012**, *3*, 794.

(178)   Phillips, D. J.; Gibson, M. I. *Polymer Chemistry* **2015**, *6*, 1033.

(179)   Lesniak, A.; Salvati, A.; Santos-Martinez, M. J.; Radomski, M. W.; Dawson, K. A.; Aberg, C. *J Am Chem Soc* **2013**, *135*, 1438.

(180)   Abulateefeh, S. R.; Saeed, A. O.; Aylott, J. W.; Chan, W. C.; Garnett, M. C.; Saunders, B. R.; Alexander, C. *Chemical Communications* **2009**, 6068

(181)   Han, S.; Hagiwara, M.; Ishizone, T. *Macromolecules* **2003**, *36*, 8312.

(182)   Gibson, M. I.; Paripovic, D.; Klok, H.-A. *Advanced Materials* **2010**, *22*, 4721.

(183)   París, R.; Liras, M.; Quijada-Garrido, I. *Macromolecular Chemistry and Physics* **2011**, *212*, 1859.

(184)   Matsumura, Y.; Maeda, H. *Cancer Res.* **1986**, *46*, 6387.

(185)   Noguchi, Y.; Wu, J.; Duncan, R.; Strohalm, J.; Ulbrich, K.; Akaike, T.; Maeda, H. *Japanese Journal of Cancer Research* **1998**, *89*, 307.

(186)   http://www.accessdata.fda.gov/scripts/cder/drugsatfda/index.cfm Accessed July 2015.

(187)   *http://celsion.com/docs/technology_thermodox*   **September 2015**.

(188)   Weitman, S. D.; Lark, R. H.; Coney, L. R.; Fort, D. W.; Frasca, V.; Zurawski, V. R.; Kamen, B. A. *Cancer Research* **1992**, *52*, 3396.

(189)   Hami, Z.; Amini, M.; Ghazi-Khansari, M.; Rezayat, S. M.; Gilani, K. *Colloids and Surfaces B: Biointerfaces* **2014**, *116*, 309.

(190)   Yang, C.; Chen, H.; Zhao, J.; Pang, X.; Xi, Y.; Zhai, G. *Colloids and Surfaces B: Biointerfaces* **2014**, *121*, 206.

(191)   Li, L.; Kim, J. K.; Huh, K. M.; Lee, Y.-k.; Kim, S. Y. *Carbohydrate Polymers* **2012**, *87*, 2120.

(192)   Werner, M. E.; Karve, S.; Sukumar, R.; Cummings, N. D.; Copp, J. A.; Chen, R. C.; Zhang, T.; Wang, A. Z. *Biomaterials* **2011**, *32*, 8548.

(193)   Li, L.; Yang, Q.; Zhou, Z.; Zhong, J.; Huang, Y. *Biomaterials* **2014**, *35*, 5171.

(194)   Reddy, J. A.; Abburi, C.; Hofland, H.; Howard, S. J.; Vlahov, I.; Wils, P.; Leamon, C. P. *Gene Ther* **2002**, *9*, 1542.

(195)   Gabizon, A.; Horowitz, A. T.; Goren, D.; Tzemach, D.; Mandelbaum-Shavit, F.; Qazen, M. M.; Zalipsky, S. *Bioconjugate Chemistry* **1999**, *10*, 289.

(196)   Hilgenbrink, A. R.; Low, P. S. *Journal of Pharmaceutical Sciences* **2005**, *94*, 2135.

(197)   Han, X.; Gelein, R.; Corson, N.; Wade-Mercer, P.; Jiang, J.; Biswas, P.; Finkelstein, J. N.; Elder, A.; Oberdörster, G. *Toxicology* **2011**, *287*, 99.

(198)   Chithrani, B. D.; Chan, W. C. W. *Nano Letters* **2007**, *7*, 1542.

(199)   Panyam, J.; Labhasetwar, V. *Pharmaceutical Research* **2003**, *20*, 212.

(200)   Kim, Y.; Pourgholami, M. H.; Morris, D. L.; Lu, H.; Stenzel, M. H. *Biomaterials Science* **2013**.

(201)   Kumar, M.; Singh, G.; Arora, V.; Mewar, S.; Sharma, U.; Jagannathan, N. R.; Sapra, S.; Dinda, A. K.; Kharbanda, S.; Singh, H. *International Journal of Nanomedicine* **2012**, *7*, 3503.

(202)   Duan, J.; Liu, M.; Zhang, Y.; Zhao, J.; Pan, Y.; Yang, X. *J Nanopart Res* **2012**, *14*, 1.

(203)   Doherty, G. J.; McMahon, H. T. *Annu. Rev. Biochem.* **2009**, *78*, 857.

(204)   Herd, H.; Daum, N.; Jones, A. T.; Huwer, H.; Ghandehari, H.; Lehr, C.-M. *ACS Nano* **2013**, *7*, 1961.

(205)   Tian, Z.; Yang, C.; Wang, W.; Yuan, Z. *ACS Applied Materials & Interfaces* **2014**, *6*, 17865.

(206)   Barhoumi, A.; Wang, W.; Zurakowski, D.; Langer, R. S.; Kohane, D. S. *Nano Letters* **2014**, *14*, 3697.

(207)   Sanoj Rejinold, N.; Muthunarayanan, M.; Divyarani, V. V.; Sreerekha, P. R.; Chennazhi, K. P.; Nair, S. V.; Tamura, H.; Jayakumar, R. *Journal of Colloid and Interface Science* **2011**, *360*, 39.

(208)   Nakamura, H.; Fang, J.; Gahininath, B.; Tsukigawa, K.; Maeda, H. *Journal of Controlled Release* **2011**, *155*, 367.

(209)   Dong, S.; Cho, H. J.; Lee, Y. W.; Roman, M. *Biomacromolecules* **2014**, *15*, 1560.

(210)   Low, P. S.; Henne, W. A.; Doorneweerd, D. D. *Acc. Chem. Res.* **2008**, *41*, 120.